



Universiteit
Leiden
The Netherlands

Near-infrared image guidance in cancer surgery

Schaafsma, B.E.

Citation

Schaafsma, B. E. (2017, April 19). *Near-infrared image guidance in cancer surgery*. Retrieved from <https://hdl.handle.net/1887/48097>

Version: Not Applicable (or Unknown)

License: [Licence agreement concerning inclusion of doctoral thesis in the Institutional Repository of the University of Leiden](#)

Downloaded from: <https://hdl.handle.net/1887/48097>

Note: To cite this publication please use the final published version (if applicable).

Cover Page



Universiteit Leiden



The handle <http://hdl.handle.net/1887/48097> holds various files of this Leiden University dissertation.

Author: Schaafsma , B.E.

Title: Near-infrared image guidance in cancer surgery

Issue Date: 2017-04-19

Near-Infrared Image Guidance in Cancer Surgery

B.E. Schaafsma

© B.E. Schaafsma 2017
ISBN/EAN: 978-94-6332-163-1

Printed by: GVO drukkers & vormgevers B.V. | Ponsen & Looijen, Ede

The research described in this thesis was financially supported by the Dutch Cancer Society (UL 2010-4732), the Center for Translational Molecular Medicine (CTMM, DeCoDe and MUSIS projects).

Financial support by Karl Storz, ChipSoft, Guerbet, Zeiss, Applied Medical, ERBE, TEVA farmachemie, ARA, Olympus, Bontius stichting, Pfizer, Sysmex, Nederlandse Vereniging voor Gastroenterologie for the printing of this thesis is gratefully acknowledged.

Near-Infrared Image Guidance in Cancer Surgery

Proefschrift

ter verkrijging van
de graad van Doctor aan de Universiteit Leiden
op gezag van de Rector Magnificus prof.mr C.J.J.M. Stolker,
volgens besluit van het College voor Promoties
te verdedigen op woensdag 19 april 2017
klokke 16.15 uur

door

Boudewijn Ewout Schaafsma

geboren te Leiden in 1985

Promotor: Prof. dr. C.J.H. van de Velde
Co-promotor: Dr. A.L. Vahrmeijer

Leden promotiecommissie:

Prof. dr. ir. B.P.F. Lelieveldt
Prof. dr. C.W.G.M. Löwik (Erasmus Universiteit)
Prof. dr. G.L. Beets (Antoni van Leeuwenhoek)
Prof. dr. V.T.H.B.M. Smit
Prof. dr. L.F. de Geus-Oei

Contents

Chapter 1.	The clinical use of near-infrared fluorescence imaging for image-guided oncologic procedure or treatment evaluation	7
------------	---	---

Part I: Clinical translation of image-guided surgery in sentinel lymph node mapping

Chapter 2.	Near-infrared fluorescence sentinel lymph node biopsy in vulvar cancer: a randomized comparison of lymphatic tracers	27
Chapter 3.	Randomized comparison of near-infrared fluorescence lymphatic tracers for sentinel lymph node mapping of cervical cancer	39
Chapter 4.	Combined radio- and fluorescence-guided sentinel lymph node biopsy in breast cancer	51
Chapter 5.	Ex vivo sentinel node mapping in colon cancer combining blue dye staining and fluorescence imaging	65

Part II: Clinical translation of optical tumor imaging

Chapter 6.	Optical mammography using diffuse optical spectroscopy for monitoring tumor response to neoadjuvant chemotherapy in women with locally advanced breast cancer	79
Chapter 7.	Near-infrared fluorescence-guided resection of otherwise undetectable colorectal cancer metastases in liver	97

Summary

Chapter 8.	Summary and future perspectives	111
	Nederlandse samenvatting	119
	List of publications	125
	Curriculum vitae	129
	Dankwoord	131

Chapter 1

Introduction: The clinical use of near-infrared fluorescence imaging for image-guided oncologic procedure or treatment evaluation

Adapted from

Schaafsma BE, Mieog JS, Hutteman M, van der Vorst JR, Kuppen PJ, Löwik CW, Frangioni JV, van de Velde CJ, Vahrmeijer AL

Journal of Surgical Oncology 2011;104:323-332

INTRODUCTION

The identification of structures that need to be resected (e.g. tumour tissue, lymph nodes) and structures that need to be spared (e.g. nerves, ureters, bile ducts) is of paramount importance in daily oncologic surgery. However, at present, surgeons mainly rely on palpation and visual inspection. Therefore, tumour positive resection margins and surgical morbidity as result of damage to vital structures are not uncommon. Thus, there is a unmet need for new intraoperative imaging modalities that can provide real-time assessment of tumour borders and affected lymph nodes, while eliminating the risk of damaging vital structures.

Optical imaging using near-infrared (NIR) fluorescence is a new technique that can be used to visualise structures in real-time during surgery. Advantages of NIR fluorescent light (700-900 nm) include high tissue penetration (millimetres to centimetres deep) and low autofluorescence, thereby providing sufficient contrast.¹ Because the human eye is insensitive to NIR wavelengths, the use of NIR light does not alter the surgical field. Recently developed intraoperative imaging systems are able to provide simultaneous acquisition of surgical anatomy (white light, colour video) and NIR fluorescence signal.²⁻⁴ Therefore, the use of NIR fluorescence imaging could potentially be of great value in the intraoperative detection of critical anatomical structures and oncologic targets.

In addition to NIR fluorescence imaging systems, exogenous NIR fluorescent contrast agents are necessary to visualise specific tissues. Ideally, tumour cells are labelled by targeted contrast agents. However, the only fluorescent contrast agents currently registered by the FDA and EMA for clinical applications are indocyanine green (ICG; peak emission \approx 820 nm), methylene blue (peak emission \approx 700 nm) and fluorescein (peak emission \approx 520 nm, below NIR spectrum). This thesis is mainly focused on the clinical use of ICG, due to its preferable fluorescent characteristics and widespread use in clinical research. ICG provides a higher signal-to-background ratio because of lower autofluorescence and increased tissue penetration at 820 nm compared to lower wavelengths and has a greater “brightness” (quantum yield) compared to methylene blue.⁵

ICG is currently utilised in NIR fluorescence image-guided surgery for multiple indications. NIR fluorescence imaging has the potential to improve sentinel lymph node (SLN) mapping in multiple types of cancer, by real-time transcutaneous and intraoperative visualisation of lymphatic channels and subsequent detection of the SLN.^{3,4,6-29} Additionally, ICG NIR fluorescence is used for endoscopic marking of colorectal tumours and intraoperative identification of certain solid tumours after intravenous injection.³⁰⁻³³ Moreover, NIR fluorescence angiography using ICG can be used in intraoperative assessment of tissue perfusion in reconstructive surgery for ablative defects following oncologic surgery³⁴ and to lower the risk of anastomotic dehescence during various procedures.

This introduction provides a review on clinical studies using ICG in NIR fluorescence-guided cancer surgery in order to understand current applications, limitations, and future prospects, which will be further explored in this thesis.

Table I. Clinically available imaging systems

Imaging system	Excitation source	Working distance	Field of view	White light illumination of surgical field	NIR-colour overlay
PDE	LED 805 nm, power NS	15 - 25 cm	NS	No	No
SPY	Laser 806 nm, 2.0 W	30 cm	56 cm ²	No	No
Fluobeam*	Laser 780 nm, 10mW/cm ²	22 cm	80 cm ²	Yes	No
HyperEye	LED 760 nm, power NS	30 - 50 cm	78.5 cm ²	Yes	Yes
FLARETM	LED 745-779 nm, 14 mW/cm ²	45 cm	3.7 cm ² - 169.5 cm ²	Yes	Yes
Mini-FLARETM	LED 760 nm, 8.6 mW/cm ²	30 cm	100 cm ²	Yes	Yes
FDPM imager	Laser Diode 785 nm \pm 10 nm, <1.9 mW/cm ²	<76.2 cm	Max 900 cm ²	No	No
Artemis camera system	Laser 400-1000nm, 4 mW/cm ²	1.5 - 25	60	Yes	Yes
Karl Storz high definition fluorescence laparoscope	760 nm	laparoscopy	laparoscopy	Yes	No
Firefly for robotic surgery	NA	laparoscopy	laparoscopy	Yes	No
Munich / SurgOptix prototype camera system	Laser 750 nm, 300 mW	21 cm	1,5 cm ² - 107 cm ²	Yes	Yes

PDE, Photodynamic Eye; LED, Light emitting diode; NS, not specified; FLARE, Fluorescence-Assisted Resection and Exploration; FDPM, Frequency Domain Photon Migration

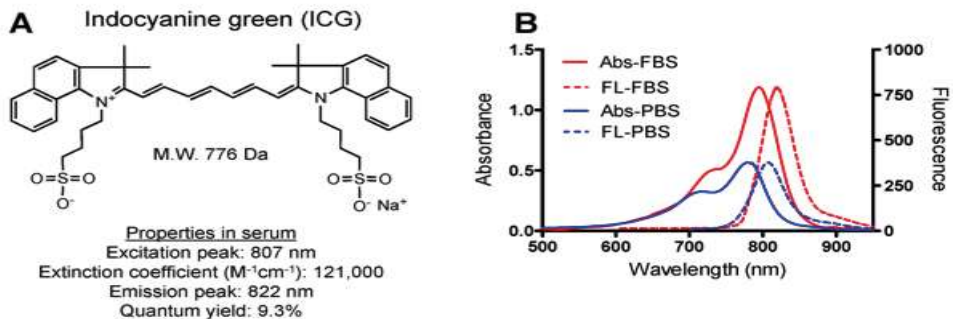


Fig. 1. Chemical and optical characteristics of ICG: **A.** Chemical structure and key optical properties (in serum). **B.** Absorption and emission of 10 mM ICG dissolved in phosphate-buffered saline (PBS) and fetal bovine serum (FBS).

NIR FLUORESCENCE IMAGING

Clinically available NIR imaging systems

Several NIR fluorescence imaging systems have been described for intraoperative clinical use (reviewed in Gioux et al.³⁵). Although differing in their technical specifications, all of these systems provide the surgeon with an image of the NIR fluorescence signal that would otherwise be invisible to the human eye (Table I). The majority of clinical studies published to date use the commercially available Photodynamic Eye (PDE, Hamamatsu Photonics, Hamamatsu, Japan) imaging camera system¹⁸. Other commercially available systems are the SPY system (Novadaq Technologies, Concord, ON, Canada), the Fluobeam® (Fluoptics, Grenoble, France), Artemis (Quest Medical Imaging, Middenmeer, The Netherlands)⁹¹, Karl Storz high definition fluorescence laparoscope (Karl Storz, Tuttlingen, Germany) and integrated in the DaVinci Firefly system (Intuitive Surgical, Sunnyvale, CA, USA). Several others imaging systems have been used in clinical studies but are not commercially available: HyperEye² (Kochi Medical School, Kochi, Japan), the FLARE™ and Mini-FLARE™³ (Beth Israel Deaconess Hospital, Boston, MA, USA), the FDPIM imager³⁶ (Texas Medical Center, Houston, TX, USA), and a prototype camera system from Munich⁴ (Technical University Munich, Munich, Germany and SurgOptix Inc., Redwood Shores, CA, USA).

Indocyanine green

ICG is a negatively charged, amphiphilic, water-soluble, tricarbocyanine with a molecular mass of 776 Da.^{37,38} ICG has been registered for several decades to determine cardiac output, hepatic function, and ophthalmic perfusion. Rapid registration was attributable to favourable characteristics such as the confinement to the vascular compartment by binding to plasma proteins, the fast and almost exclusive excretion into the bile, and the very low toxicity of ICG.^{39,40} ICG is safe to use, as the number of allergic reactions is very low (1: 10 000, as reported by manufacturer). The dose used for standard diagnostic procedures lies between 0.1 and 0.5 mg/kg. Above 0.5 mg/kg, the incidence of immediate allergic reactions increases.⁴¹

In plasma, ICG has an absorption peak around 807 nm and an emission peak around 822 nm, which is within the NIR window (Fig. 1). After intravenous administration, ICG has a short half-time of 150-180 seconds and is cleared exclusively by the liver.⁴² ICG molecules bind rapidly and almost completely to serum proteins. The binding to relative large serum proteins prevents the unwanted interaction between the ICG molecules and thereby improves its brightness (quantum yield increases 3.5x) and increases its hydrodynamic diameter.^{39,43-45} Hydrodynamic diameter has

important implications for distribution and transport of ICG for tumour visualisation and retention in the SLN as will be discussed below.^{6,46,47}

SENTINEL LYMPH NODE MAPPING

NIR fluorescence imaging provides new opportunities to improve and extend the indications of the SLN procedure. Gamma ray-emitting radiotracers and blue dyes are currently used as standard of care in clinical practice. However, the use of gamma ray-emitting radiotracers requires involvement of a nuclear medicine physician, localisation of the SLN can be difficult using a handheld gamma probe, and preoperative access to the injection site is required. Blue dyes cannot be easily seen through the skin and fatty tissue. Additionally, the learning curve for the standard SLN procedure using these techniques is estimated to be 60 required cases for technical proficiency when working with breast cancer patients.⁴⁸

NIR fluorescence imaging using ICG has been shown to visualise superficial lymphatic channels transcutaneously.¹⁴ Thereby, it could potentially reduce time of surgery and improve localisation of the SLN so that a small incision can be made, while maintaining a high identification rate. Moreover, the NIR fluorescence signal could aid the pathologist in both preparing and analysing the tissue specimen.^{13,18} It should be noted, however, that NIR fluorescence detection is in the millimetre to centimetre range, far less than radioactive tracers, which requires caution when examining thick tissues.

ICG has been used as lymphatic tracer in SLN procedures in breast, skin, gastro-intestinal, non-small cell lung, oropharyngeal and gynaecological cancer.^{3,4,7-29} Differences in imaging systems, ICG doses and injection sites prevent direct comparison of the results. In the next sections, the results will be discussed for each tumour type separately.

Breast cancer

Most studies using ICG as NIR fluorescent SLN tracer have been in breast cancer patients.^{3,12-21} Before the introduction of NIR fluorescence imaging systems, Motomura et al.⁴⁹ used only the intrinsic green colour of ICG and identified the SLN in 73.8% of the patients. After the introduction of intraoperative NIR fluorescence imaging systems, higher identification rates of 87.5% to 100% (aggregate 98.6%) were obtained and an average of 3.4 (range 1.5 to 5.4) SLNs were identified.^{3,12-21} Two studies performed an axillary dissection irrespective of the SLN status and found an aggregate false-negative rate of 7.7% in 39 patients with a negative SLN.^{12,14} Additionally, as a result of the capability of NIR fluorescence light to penetrate tissue, ICG offers non-invasive imaging of lymphatic flow (Fig. 2). Upon injection of ICG, travel time to the axilla

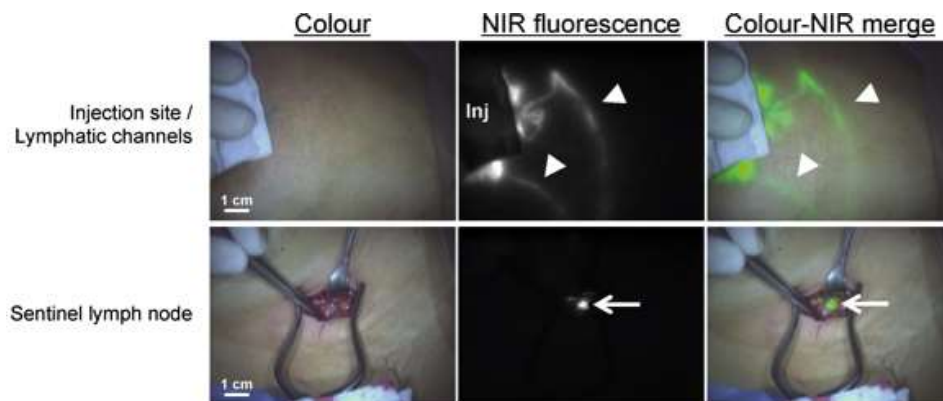


Fig. 2. Near-infrared fluorescence sentinel lymph node mapping: SLN mapping after injection of 600 mM ICG adsorbed to human serum albumin (ICG:HSA) in a breast cancer patient. Images acquired using the Mini-FLARETM imaging system (Frangioni laboratory, Boston, MA). Shown are colour images (left), NIR fluorescence images (middle), and pseudo-coloured (lime green) merge of the two images (right). In the upper panel, the periareolar injection site (Inj) of ICG:HSA is shown. In the NIR fluorescence image, the injection site (partially covered) and lymphatic channels (arrowheads) of the breast running into the axilla are clearly visualised. In the lower panel, identification of the SLN (arrow) with NIR fluorescence imaging is demonstrated. Camera exposure times were 67 msec (top row) and 20 msec (bottom row). Scale bars = 1 cm.

is one to ten minutes.^{13,16} The small size of the ICG particle is probably responsible for this relatively high velocity, which has logistical advantages compared to relatively larger gamma ray-emitting radiotracers. Hojo et al.¹⁵ compared ICG to patent blue in 113 patients and showed that ICG had a higher identification rate (100%) than patent blue (93%). Three studies compared the method of SLN detection by ICG fluorescence (71 out of 73 nodes) and the radiotracer (70 out of 73 nodes).^{12,15,17} Though both identification rates were similar, as both techniques are used simultaneously in all studies, no comparison can be made whether one is superior to the other.

Several factors influence the success of the SLN procedure using ICG. In the reported clinical trials, various doses of ICG have been used ranging from 0.01 mM to 6.4 mM. Sevic-Muraca et al.¹⁶ found that a minimal dose of 0.01 mM ICG is required for successful SLN mapping. Mieog et al.¹⁷ allocated patients in groups of escalating ICG concentrations from 0.05 mM to 1.0 mM diluted in albumin and obtained the highest brightness of the SLN using a concentration between 0.4 mM to 0.8 mM ICG (1.6 ml injection volume). Additionally, because of its relatively small hydrodynamic diameter, ICG is able to pass through the sentinel node to second-tier nodes and eventually spread through the subcutaneous tissue.¹⁸ To surpass this effect, imaging should to be performed shortly after ICG administration. Furthermore, as a result of the limited tissue penetration of the fluorescent signal, visualisation is limited once ICG has reached the axillary fossa, particularly in patients with a high body mass index.^{13,19,50}

Skin cancer

ICG has successfully been introduced as an NIR fluorescent lymphatic tracer in the SLN procedure in skin cancer patients.^{22-25,93} The NIR fluorescence-guided SLN procedure resulted in identification of at least one SLN in over 97% of the patients (total number of SLNs identified was not reported).^{22-25,93} This is concordant with recent trials using conventional techniques, which showed a 93% to 100% identification rate.^{51,52} Upon intradermal injection, ICG enables easy visualisation of the subcutaneous lymphatic drainage, which takes approximately 15 minutes after injection to reach the SLN and stays visible for at least three hours.²² The results of these studies are promising. However, larger trials are needed to assess patient benefit.

Gastro-intestinal cancer

Nodal status is one of the most important prognostic factors in gastric and colorectal cancer. It is hypothesised that the SLN procedure in gastro-intestinal cancer patients can improve nodal staging.⁵³ Currently, prophylactic lymphadenectomy is considered standard-of-care in these patients. Several studies have assessed the use of the SLN procedure using radiotracers or blue dye, or both.⁵³⁻⁵⁵ However, these studies show varying lymphatic drainage patterns and report high rates of skip metastases, preventing the introduction of the SLN procedure in general clinical practice.

In early gastric cancer, multiple studies reported the use of ICG as NIR fluorescent lymphatic tracer in the SLN procedure.²⁶⁻²⁹ ICG was injected during surgery or at one to three days before surgery. After both preoperative subserosal and preoperative submucosal injection of ICG, lymphatic vessels draining the tumour could be visualised.²⁶⁻²⁹ The identification rates ranged from 90.9% to 96.4% (aggregate 94.9%) with an average number of SLNs identified of 3.0 to 7.5.²⁶⁻²⁹ The false-negative rates reported in these studies ranged from 14.3% to 33.3% in T1 tumours, which increased with tumour stage up to 75% in T3 gastric tumours.^{26,28,29} However, the number of patients in these tumour stages with tumour positive lymph nodes is small (range 3-10).

Several factors influence the success of SLN procedure in gastric cancer. Frequent leakage was observed from lacerated lymphatic vessels during the SLN mapping in patients with intraoperative ICG injection.²⁸ Preoperative endoscopic ICG injection results in a higher number of fluorescent lymph nodes and lower false negative rate compared to intraoperative injection.²⁸ Due to the longer interval between injection and imaging, it is expected that ICG passes through the SLN to the higher-tier nodes. Additionally, next to fluorescence imaging, absorption by ICG can be used for SLN detection in early gastric cancer by infrared ray electronic endoscopy.^{27,55-58} Miyashiro et al.²⁷ compared both fluorescent imaging and infrared ray imaging in 3 patients after

laparotomy and was able to visualize the individual nodes more clearly by fluorescent imaging.

In colorectal cancer, the use of ICG as an NIR fluorescent lymphatic tracer resulted in an identification rate of 88.5% and 92%, with an average number of identified SLNs of 2.1 and 2.6.^{7,26} The false negative rate in these studies was relatively high (44%) in patients with tumour positive lymph nodes.

When the SLN procedure is used for nodal staging to determine prognosis and possible adjuvant therapy, as has been suggested for colorectal cancer, an ex vivo approach can be considered.⁵⁹ Using an ex vivo approach, more optimised NIR fluorescent dyes can be used, which are not yet approved for in vivo administration, such as IRDye 800CW (LI-COR, Lincoln, NE, USA). These dyes can be coupled to albumin or nanocolloid to increase lymph node retention.^{43,60} This ex vivo strategy was successfully applied in a recent clinical study.⁶

Conclusions sentinel lymph node mapping

NIR fluorescence SLN mapping has shown excellent results to date in breast and skin cancer. Therefore, the use of ICG should be particularly attractive to hospitals unable to work with radioactive isotopes as an adjunct or possible replacement to the use of blue dye alone.^{15,17} Though, lack of studies in which a direct comparison between ICG fluorescence and radiotracers is made prohibits drawing conclusions between these two methods. In gastro-intestinal cancer, SLN procedures using ICG obtain high identification rates, although the high false negative rates in the small patient samples require further assessment. Additionally, the feasibility of NIR fluorescence SLN mapping using ICG has also been assessed in single studies in cervical, vulvar, anal, oropharyngeal and non-small cell lung cancer.^{4,8-11}

As the available data on ICG fluorescence in the sentinel lymph node procedure is relatively limited, conclusion on direct patient benefit and clinical outcome cannot yet be drawn. Currently, several groups are performing clinical trials using NIR fluorescence imaging and ICG in the SLN procedure in multiple malignancies.

TUMOUR IMAGING

The main goal of cancer surgery is the complete and 'en-bloc' excision of tumours with adequate tumour-free margins while minimising surgical morbidity. Presently, though, intraoperative assessment of tumour margins relies on palpation and visual inspection. NIR fluorescence imaging is a promising technique for intraoperative tumour identification. NIR fluorescent probes that specifically target tumour cells could aid the surgeon in determining resection margins and possibly reduce the risk of locoregional recurrence.^{62,63} Although ICG is a non-targeted probe, it can provide

NIR fluorescence tumour localisation in a limited number of hepatobiliary cancer patients^{31,64-67}, either due to physiological uptake in well-differentiated tumours or rim uptake as a result of leakage and retention in poorly-differentiated tumours and colorectal metastases.^{32,68}

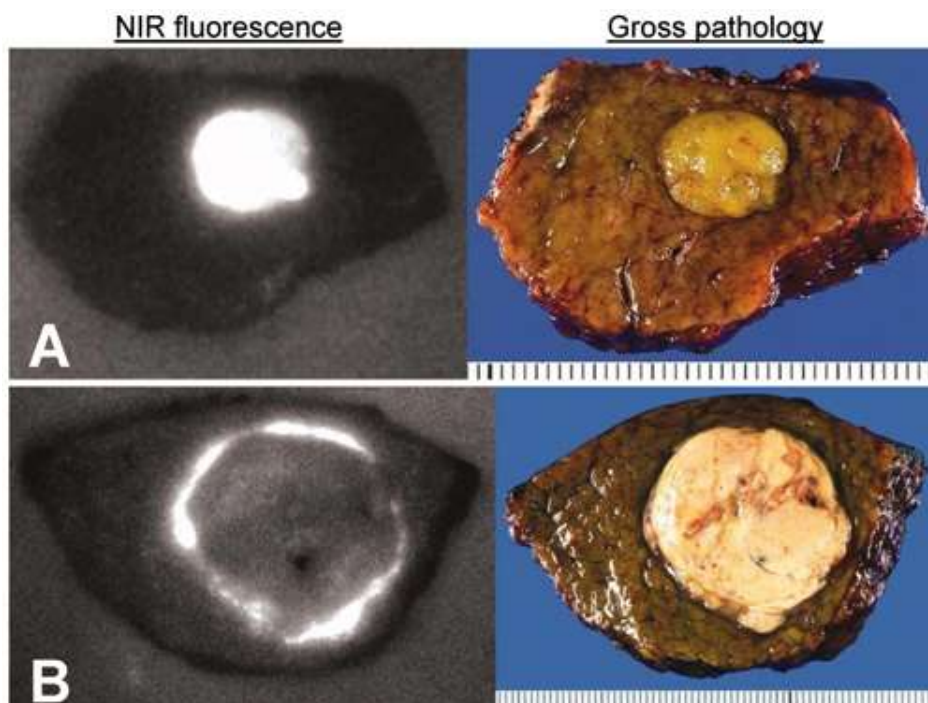


Fig. 3. ICG uptake and retention in liver tumours: Patterns of nearinfrared fluorescence of liver cancers in surgical specimens using the PDE (Hamamatsu Photonics, Hamamatsu, Japan) (left) and their gross appearances (right). A. Well-differentiated hepatocellular carcinoma, 7 mm in diameter, displaying uniform fluorescence. B. Poorly differentiated hepatocellular carcinoma, 30 mm in diameter, displaying rim fluorescence. Adapted from Ishizawa et al. (200915) and reprinted with permission from John Wiley & Sons, Inc.

Imaging of hepatobiliary cancer

Liver resection is the only curative option in the treatment of hepatobiliary cancer. Intrahepatic recurrence rates after resection of colorectal cancer metastases range from 11% to 37.5% and the majority of these recurrences appear within two year after resection.⁶⁹⁻⁷³ A possible explanation for this high intrahepatic recurrence rate is that these hepatic metastases were present at time of resection of the liver metastases but were undetected by preoperative imaging and intraoperative ultrasound. NIR fluorescence detection is a new technique to intraoperatively visualise hepatobiliary cancer.

ICG is excreted exclusively into the bile, which allows real-time NIR fluorescence cholangiography of biliary anatomy during cholecystectomy and other hepatobiliary surgery.⁷⁴⁻⁷⁶ This technique provides a reliable roadmap of the biliary

tree, which enables the surgeon to avoid injuring the bile duct.⁷⁴ In hepatobiliary cancer, it is hypothesised that the NIR fluorescent signal in or around the tumour is caused by passive accumulation due to hampered biliary excretion, which, in the case of a colorectal liver metastasis, results in a fluorescent rim around the tumour (Fig. 3).³¹ Several studies have reported the use of ICG in NIR fluorescence imaging of hepatobiliary cancer including colorectal metastasis, hepatocellular carcinoma and cholangiocarcinoma.^{31,64-67} To identify liver tumours, the best time window is beyond 24 hours after injection, when most ICG is washed out of the healthy liver parenchyma and is still present in and around the tumour tissue.³¹

In patients with hepatocellular carcinoma or colorectal liver metastases, 98.1% to 100% of the lesions were detected using NIR fluorescence in the resection tissue specimen.^{31,65,67} However, due to limited penetration of the NIR fluorescent signal, intraoperative detection of deeper located tumours was not possible (Ishizawa et al.³¹ reported a maximal detection depth of 8 mm). Tumours located at the liver surface provide a bright fluorescent signal and are easily detected, which is especially useful for colorectal liver metastases as these are mostly located on the surface of the liver parenchyma. In these studies this resulted in detection of new small superficial lesions by NIR fluorescence imaging that could not be detected by intraoperative ultrasonography or by visual inspection.^{31,67}

In the case of cholangiocarcinoma, Harada et al.⁶⁶ showed ICG fluorescence on the liver surface in the regions of liver with cholestasis caused by bile duct tumour invasion or thrombi. Although the tumour itself was not fluorescent, the information provided by NIR fluorescence imaging can help to estimate the extent of the bile duct tumour infiltration.

In conclusion, ICG fluorescence might be of value during hepatobiliary surgery when used as an adjunct to intraoperative ultrasound, and could be particularly useful in the intraoperative identification of small superficially located liver tumours. However, to identify deeper tumours, intraoperative ultrasound imaging is still required. Additionally, ICG fluorescence can aid in the identification of tumour lesions during pathological examination.

Marking tumours

Endoscopic marking of intestinal lesions is essential in laparoscopic surgery or when difficulty in locating the lesion during resection is anticipated.^{30,68} India ink is a frequently used dye, but is associated with complications and side effects and alters the surgical field.⁶⁸ ICG could be a more suitable dye for tattooing, because of fewer side effects, relatively long absorption time (up to 14 days), and potential increased detection using NIR fluorescence compared to macroscopic colour perception.^{30,77,78}

Watanabe et al.³⁰ and Handgraaf et al.⁹² showed accurate and clear NIR fluorescence tumour localization after preoperative and intraoperative peritumoural injection of ICG. In all patients, the NIR fluorescence signal was detected in the colon or rectal tumour and could be visualised clearly. In the preoperative injected patients the signal was visible for at least 72 to 120 hours, whereas the marked location detection based on the intrinsic green colour of ICG was possible in only two patients. Moreover, this technique allows for simultaneous SLN mapping.^{33,92}

Other solid tumours

It has been proposed that ICG can be used in intraoperative imaging of solid tumours other than hepatobiliary cancer. The “enhanced permeability and retention” (EPR) effect can potentially be used for tumour imaging. Due to newly formed, more porous blood vessels, molecules can passively accumulate in tumour tissue. Furthermore, a poorly developed tumoural lymphatic system results in increased retention.⁷⁹⁻⁸²

Exploiting the EPR effect, multiple clinical studies with breast tumours used ICG for tumour identification in an outpatient, mammography-like setting.^{32,82-86} These studies used optical tomography, which has higher depth penetration and potentially higher specificity, albeit with much lower resolution. During the first 10 minutes, ICG was retained in the breast tumour tissue and provided contrast to the surrounding healthy tissue.^{82,83} Hagen et al.³² and Poellinger et al.⁸⁶ used a prototype fluorescence mammographic imaging system and showed the ability to discriminate between malignant and benign lesions after intravenous administration of ICG. However, in an intraoperative setting a higher tumour-to-background ratio would be needed to provide sufficient tumour demarcation.

Additionally, ICG can be useful as a diagnostic tool to estimate the invasiveness of early gastric cancer during endoscopy. Multiple Japanese studies used NIR fluorescence endoscopy using ICG as contrast agent to differentiate between mucosal and submucosal or more invasive tumours, and obtained a diagnostic accuracy of 85 % up to 93 %.⁸⁷⁻⁹⁰ The NIR fluorescence signal was visible up to 3 minutes in tumour tissue compared to several seconds in healthy tissue.⁸⁷ Therefore, ICG might be useful to distinguish mucosal cancer from submucosal and deeper cancers, which is a risk factor for lymph node metastasis. However, the short duration of the signal limits its use in a surgical setting. Therefore, the lack of direct tumour targeting properties prevents the introduction of ICG as NIR fluorescent probe in most tumour types in an intraoperative setting.

CONCLUSION AND OUTLINE OF THE THESIS

The recent introduction of NIR fluorescence image guidance provides new opportunities for cancer surgery. Currently, ICG and methylene blue are the only clinically available NIR fluorescent probes. Clinical experience with ICG for intraoperative NIR fluorescence imaging is rather extensive and shows a favourable safety profile. Though, conclusions on direct patient benefit and clinical outcome cannot yet be drawn. This thesis further explores the possibilities of NIR imaging for SLN mapping and tumour and is divided in two parts: Part I focuses on the optimization and exploration of added value of NIR fluorescence imaging for SLN mapping, Part II describes the use of NIR imaging for tumour identification.

Part I, chapter 2 and 3 explore whether premixing with human serum albumin is indeed beneficial for SLN mapping in a randomized controlled trial in patients with vulvar and cervical cancer. In chapter 4 the added value of NIR fluorescence SLN mapping in breast cancer is explored using a novel hybrid radioactive and fluorescent ICG-based SLN tracer. In chapter 5 the additional value of human serum albumin linked to fluorescent tracer 800CW is evaluated for SLN mapping in patients with colon cancer and compared to results obtained with blue dye.

In Part II, chapter 6 the use of NIR light without NIR contrast agents is explored for tumour detection and neoadjuvant treatment monitoring by diffuse optical spectroscopy in patients with locally advanced breast cancer. In chapter 7, the optimal dose and timing of administration of ICG is assessed for the NIR fluorescence detection of liver metastases from colorectal cancer and the added value of ICG is evaluated.

REFERENCES

1. Frangioni JV: New technologies for human cancer imaging. *J Clin Oncol* 2008;26:4012-21.
2. Handa T, Katare RG, Nishimori H et al.: New device for intraoperative graft assessment: HyperEye charge-coupled device camera system. *Gen Thorac Cardiovasc Surg* 2010;58:68-77.
3. Troyan SL, Kianzad V, Gibbs-Strauss SL et al.: The FLARE Intraoperative Near-Infrared Fluorescence Imaging System: A First-in-Human Clinical Trial in Breast Cancer Sentinel Lymph Node Mapping. *Ann Surg Oncol* 2009;16:2943-52.
4. Crane LM, Themelis G, Pleijhuis RG et al.: Intraoperative Multispectral Fluorescence Imaging for the Detection of the Sentinel Lymph Node in Cervical Cancer: A Novel Concept. *Mol Imaging Biol* 2010.
5. Matsui A, Tanaka E, Choi HS et al.: Real-time intra-operative near-infrared fluorescence identification of the extrahepatic bile ducts using clinically available contrast agents. *Surgery* 2010;148:87-95.
6. Tanaka E, Choi HS, Fujii H et al.: Image-guided oncologic surgery using invisible light: completed pre-clinical development for sentinel lymph node mapping. *Ann Surg Oncol* 2006;13:1671-81.
7. Noura S, Ohue M, Seki Y et al.: Feasibility of a lateral region sentinel node biopsy of lower rectal cancer guided by indocyanine green using a near-infrared camera system. *Ann Surg Oncol* 2010;17:144-51.
8. Crane LM, Themelis G, Arts HJ et al.: Intraoperative near-infrared fluorescence imaging for sentinel lymph node detection in vulvar cancer: First clinical results. *Gynecol Oncol* 2010.
9. Bredell MG: Sentinel lymph node mapping by indocyanin green fluorescence imaging in oropharyngeal cancer - preliminary experience. *Head Neck Oncol* 2010;2:31.
10. Yamashita SI, Tokushima K, Anami K et al.: Video-assisted thoracoscopic indocyanine green fluorescence imaging system shows sentinel lymph nodes in non-small-cell lung cancer. *J Thorac Cardiovasc Surg* 2010.
11. Hirche C, Dresel S, Krempien R et al.: Sentinel node biopsy by indocyanine green retention fluorescence detection for inguinal lymph node staging of anal cancer: preliminary experience. *Ann Surg Oncol* 2010;17:2357-62.
12. Murawa D, Hirche C, Dresel S et al.: Sentinel lymph node biopsy in breast cancer guided by indocyanine green fluorescence. *Br J Surg* 2009;96:1289-94.
13. Kitai T, Inomoto T, Miwa M et al.: Fluorescence navigation with indocyanine green for detecting sentinel lymph nodes in breast cancer. *Breast Cancer* 2005;12:211-5.
14. Hirche C, Murawa D, Mohr Z et al.: ICG fluorescence-guided sentinel node biopsy for axillary nodal staging in breast cancer. *Breast Cancer Res Treat* 2010;121:373-8.
15. Hojo T, Nagao T, Kikuyama M et al.: Evaluation of sentinel node biopsy by combined fluorescent and dye method and lymph flow for breast cancer. *Breast* 2010;19:210-3.
16. Sevic-Muraca EM, Sharma R, Rasmussen JC et al.: Imaging of lymph flow in breast cancer patients after microdose administration of a near-infrared fluorophore: feasibility study. *Radiology* 2008;246:734-41.
17. Micog JSD, Troyan SL, Hutteman M et al.: Towards Optimization of Imaging System and Lymphatic Tracer for Near-Infrared Fluorescent Sentinel Lymph Node Mapping in Breast Cancer. *Ann Surg Oncol* 2011.
18. Tagaya N, Yamazaki R, Nakagawa A et al.: Intraoperative identification of sentinel lymph nodes by near-infrared fluorescence imaging in patients with breast cancer. *Am J Surg* 2008;195:850-3.
19. Ogasawara Y, Ikeda H, Takahashi M et al.: Evaluation of breast lymphatic pathways with indocyanine green fluorescence imaging in patients with breast cancer. *World J Surg* 2008;32:1924-9.
20. Tagaya N, Nakagawa A, Abe A et al.: Non-invasive identification of sentinel lymph node using indocyanine green fluorescence imaging in patient with breast cancer. *The Open Surgical Oncology Journal* 2010;2:71-4.
21. Tagaya N, Aoyagi H, Nakagawa A et al.: A novel approach for sentinel lymph node identification using fluorescence imaging and image overlay navigation surgery in patients with breast cancer. *World J Surg* 2011;35:154-8.

22. Fujiwara M, Mizukami T, Suzuki A et al.: Sentinel lymph node detection in skin cancer patients using real-time fluorescence navigation with indocyanine green: preliminary experience. *J Plast Reconstr Aesthet Surg* 2009;62:e373-e378.
23. Mizukami T, Fujiwara M, Suzuki A et al.: Sentinel lymph node detection by indocyanine green fluorescence imaging in skin cancer patients: technical refinement. *The Open Surgical Oncology Journal* 2010;2:57-61.
24. Tanaka R, Nakashima K, Fujimoto W: Sentinel lymph node detection in skin cancer using fluorescence navigation with indocyanine green. *J Dermatol* 2009;36:468-70.
25. Tsujino Y, Mizumoto K, Matsuzaka Y et al.: Fluorescence navigation with indocyanine green for detecting sentinel nodes in extramammary Paget's disease and squamous cell carcinoma. *J Dermatol* 2009;36:90-4.
26. Kusano M, Tajima Y, Yamazaki K et al.: Sentinel node mapping guided by indocyanine green fluorescence imaging: a new method for sentinel node navigation surgery in gastrointestinal cancer. *Dig Surg* 2008;25:103-8.
27. Miyashiro I, Miyoshi N, Hiratsuka M et al.: Detection of sentinel node in gastric cancer surgery by indocyanine green fluorescence imaging: comparison with infrared imaging. *Ann Surg Oncol* 2008;15:1640-3.
28. Tajima Y, Yamazaki K, Masuda Y et al.: Sentinel node mapping guided by indocyanine green fluorescence imaging in gastric cancer. *Ann Surg* 2009;249:58-62.
29. Tajima Y, Murakami M, Yamazaki K et al.: Sentinel node mapping guided by indocyanine green fluorescence imaging during laparoscopic surgery in gastric cancer. *Ann Surg Oncol* 2010;17:1787-93.
30. Watanabe M, Tsunoda A, Narita K et al.: Colonic tattooing using fluorescence imaging with light-emitting diode-activated indocyanine green: a feasibility study. *Surg Today* 2009;39:214-8.
31. Ishizawa T, Fukushima N, Shibahara J et al.: Real-time identification of liver cancers by using indocyanine green fluorescent imaging. *Cancer* 2009;115:2491-504.
32. Hagen A, Grosenick D, Macdonald R et al.: Late-fluorescence mammography assesses tumor capillary permeability and differentiates malignant from benign lesions. *Opt Express* 2009;17:17016-33.
33. Handgraaf HJ, Boogerd LS, Verbeek FP et al.: Intraoperative fluorescence imaging to localize tumors and sentinel lymph nodes in rectal cancer. *Minim Invasive Ther Allied Technol* 2015;7:1-6.
34. Lee BT, Matsui A, Hutteman M et al.: Intraoperative near-infrared fluorescence imaging in perforator flap reconstruction: current research and early clinical experience. *J Reconstr Microsurg* 2010;26:59-65.
35. Gioux S, Choi HS, Frangioni JV: Image-guided surgery using invisible near-infrared light: fundamentals of clinical translation. *Mol Imaging* 2010;9:237-55.
36. Marshall MV, Rasmussen JC, Tan I et al.: Near-infrared fluorescence imaging in humans with indocyanine green: a review and update. *The Open Surgical Oncology Journal* 2010;2:12-25.
37. Moody ED, Viskari PJ, Colyer CL: Non-covalent labeling of human serum albumin with indocyanine green: a study by capillary electrophoresis with diode laser-induced fluorescence detection. *J Chromatogr B Biomed Sci Appl* 1999;729:55-64.
38. Ogawa M, Kosaka N, Choyke PL et al.: In vivo molecular imaging of cancer with a quenching near-infrared fluorescent probe using conjugates of monoclonal antibodies and indocyanine green. *Cancer Res* 2009;69:1268-72.
39. Landsman ML, Kwant G, Mook GA et al.: Light-absorbing properties, stability, and spectral stabilization of indocyanine green. *J Appl Physiol* 1976;40:575-83.
40. Alford R, Simpson HM, Duberman J et al.: Toxicity of organic fluorophores used in molecular imaging: literature review. *Mol Imaging* 2009;8:341-54.
41. Speich R, Saessli B, Hoffmann U et al.: Anaphylactoid reactions after indocyanine-green administration. *Ann Intern Med* 1988;109:345-6.
42. Shimizu S, Kamiike W, Hatanaka N et al.: New method for measuring ICG Rmax with a clearance meter. *World J Surg* 1995;19:113-8.
43. Ohnishi S, Lomnes SJ, Laurence RG et al.: Organic alternatives to quantum dots for intraoperative near-infrared fluorescent sentinel lymph node mapping. *Mol Imaging* 2005;4:172-81.

44. Yoneya S, Saito T, Komatsu Y et al.: Binding properties of indocyanine green in human blood. *Invest Ophthalmol Vis Sci* 1998;39:1286-90.
45. Philip R, Penzkofer A, Bäuml W et al.: Absorption and fluorescence spectroscopic investigation of indocyanine green. *Journal of Photochemistry and Photobiology A: Chemistry* 1996;137-48.
46. Dreher MR, Liu W, Michelich CR et al.: Tumor vascular permeability, accumulation, and penetration of macromolecular drug carriers. *J Natl Cancer Inst* 2006;98:335-44.
47. Nakajima M, Takeda M, Kobayashi M et al.: Nano-sized fluorescent particles as new tracers for sentinel node detection: experimental model for decision of appropriate size and wavelength. *Cancer Sci* 2005;96:353-6.
48. Mariani G, Moresco L, Viale G et al.: Radioguided sentinel lymph node biopsy in breast cancer surgery. *J Nucl Med* 2001;42:1198-215.
49. Motomura K, Inaji H, Komoike Y et al.: Sentinel node biopsy guided by indocyanine green dye in breast cancer patients. *Jpn J Clin Oncol* 1999;29:604-7.
50. Murawa D, Hirche C, Dresel S et al.: Authors' reply: Sentinel lymph node biopsy in breast cancer guided by indocyanine green fluorescence (*Br J Surg* 2009; 96: 1289-1294). *Br J Surg* 2010;97:455-6.
51. van Akkooi AC, de Wilt JH, Verhoef C et al.: High positive sentinel node identification rate by EORTC melanoma group protocol. Prognostic indicators of metastatic patterns after sentinel node biopsy in melanoma. *Eur J Cancer* 2006;42:372-80.
52. Clary BM, Brady MS, Lewis JJ et al.: Sentinel lymph node biopsy in the management of patients with primary cutaneous melanoma: review of a large single-institutional experience with an emphasis on recurrence. *Ann Surg* 2001;233:250-8.
53. Bembenek A, Gretscher S, Schlag PM: Sentinel lymph node biopsy for gastrointestinal cancers. *J Surg Oncol* 2007;96:342-52.
54. Ichikura T, Sugawara H, Sakamoto N et al.: Limited gastrectomy with dissection of sentinel node stations for early gastric cancer with negative sentinel node biopsy. *Ann Surg* 2009;249:942-7.
55. Ohdaira H, Nimura H, Mitsumori N et al.: Validity of modified gastrectomy combined with sentinel node navigation surgery for early gastric cancer. *Gastric Cancer* 2007;10:117-22.
56. Kelder W, Nimura H, Takahashi N et al.: Sentinel node mapping with indocyanine green (ICG) and infrared ray detection in early gastric cancer: an accurate method that enables a limited lymphadenectomy. *Eur J Surg Oncol* 2010;36:552-8.
57. Ishikawa K, Yasuda K, Shiromizu A et al.: Laparoscopic sentinel node navigation achieved by infrared ray electronic endoscopy system in patients with gastric cancer. *Surg Endosc* 2007;21:1131-4.
58. Ohdaira H, Nimura H, Takahashi N et al.: The possibility of performing a limited resection and a lymphadenectomy for proximal gastric carcinoma based on sentinel node navigation. *Surg Today* 2009;39:1026-31.
59. Markl B, Arnholdt HM, Jahnig H et al.: A new concept for the role of ex vivo sentinel lymph nodes in node-negative colorectal cancer. *Ann Surg Oncol* 2010;17:2647-55.
60. Buckle T, van Leeuwen AC, Chin PT et al.: A self-assembled multimodal complex for combined pre- and intraoperative imaging of the sentinel lymph node. *Nanotechnology* 2010;21:355101.
61. Hutteman M, Choi HS, Mieog JS et al.: Clinical Translation of Ex Vivo Sentinel Lymph Node Mapping for Colorectal Cancer Using Invisible Near-Infrared Fluorescence Light. *Ann Surg Oncol* 2010.
62. Mieog JS, Hutteman M, van der Vorst JR et al.: Image-guided tumor resection using real-time near-infrared fluorescence in a syngeneic rat model of primary breast cancer. *Breast Cancer Res Treat* 2010.
63. Pleijhuis RG, Graafland M, de VJ et al.: Obtaining adequate surgical margins in breast-conserving therapy for patients with early-stage breast cancer: current modalities and future directions. *Ann Surg Oncol* 2009;16:2717-30.
64. Ishizawa T, Bandai Y, Harada N et al.: Indocyanine green-fluorescent imaging of hepatocellular carcinoma during laparoscopic hepatectomy: An initial experience. *Asian J Endosc Surg* 2010;3:42-5.
65. Uchiyama K, Ueno M, Ozawa S et al.: Combined use of contrast-enhanced intraoperative ultrasonography and a fluorescence navigation system for identifying hepatic metastases. *World J Surg* 2010;34:2953-9.

66. Harada N, Ishizawa T, Muraoka A et al.: Fluorescence navigation hepatectomy by visualization of localized cholestasis from bile duct tumor infiltration. *J Am Coll Surg* 2010;210:e2-e6.
67. Gotoh K, Yamada T, Ishikawa O et al.: A novel image-guided surgery of hepatocellular carcinoma by indocyanine green fluorescence imaging navigation. *J Surg Oncol* 2009;100:75-9.
68. Miyoshi N, Ohue M, Noura S et al.: Surgical usefulness of indocyanine green as an alternative to India ink for endoscopic marking. *Surg Endosc* 2009;23:347-51.
69. Fong Y, Cohen AM, Fortner JG et al.: Liver resection for colorectal metastases. *J Clin Oncol* 1997;15:938-46.
70. Abdalla EK, Vauthey JN, Ellis LM et al.: Recurrence and outcomes following hepatic resection, radiofrequency ablation, and combined resection/ablation for colorectal liver metastases. *Ann Surg* 2004;239:818-25.
71. Wei AC, Greig PD, Grant D et al.: Survival after hepatic resection for colorectal metastases: a 10-year experience. *Ann Surg Oncol* 2006;13:668-76.
72. Pawlik TM, Scoggins CR, Zorzi D et al.: Effect of surgical margin status on survival and site of recurrence after hepatic resection for colorectal metastases. *Ann Surg* 2005;241:715-22.
73. Karanjia ND, Lordan JT, Fawcett WJ et al.: Survival and recurrence after neo-adjuvant chemotherapy and liver resection for colorectal metastases: a ten year study. *Eur J Surg Oncol* 2009;35:838-43.
74. Ishizawa T, Bandai Y, Ijichi M et al.: Fluorescent cholangiography illuminating the biliary tree during laparoscopic cholecystectomy. *Br J Surg* 2010;97:1369-77.
75. Aoki T, Murakami M, Yasuda D et al.: Intraoperative fluorescent imaging using indocyanine green for liver mapping and cholangiography. *J Hepatobiliary Pancreat Sci* 2010;17:590-4.
76. Mitsuhashi N, Kimura F, Shimizu H et al.: Usefulness of intraoperative fluorescence imaging to evaluate local anatomy in hepatobiliary surgery. *J Hepatobiliary Pancreat Surg* 2008;15:508-14.
77. Askin MP, Wayne JD, Fiedler L et al.: Tattoo of colonic neoplasms in 113 patients with a new sterile carbon compound. *Gastrointest Endosc* 2002;56:339-42.
78. Lee JG, Low AH, Leung JW: Randomized comparative study of indocyanine green and India ink for colonic tattooing: an animal survival study. *J Clin Gastroenterol* 2000;31:233-6.
79. Maeda H, Wu J, Sawa T et al.: Tumor vascular permeability and the EPR effect in macromolecular therapeutics: a review. *J Control Release* 2000;65:271-84.
80. Weinberg AW: "The Biology of Cancer." New York: Garland Science, Taylor & Francis Group, LLC, 2007.
81. Makino A, Kizaka-Kondoh S, Yamahara R et al.: Near-infrared fluorescence tumor imaging using nanocarrier composed of poly(L-lactic acid)-block-poly(sarcosine) amphiphilic polydepsipeptide. *Biomaterials* 2009;30:5156-60.
82. Intes X, Ripoll J, Chen Y et al.: In vivo continuous-wave optical breast imaging enhanced with Indocyanine Green. *Med Phys* 2003;30:1039-47.
83. Ntzichristos V, Yodh AG, Schnall M et al.: Concurrent MRI and diffuse optical tomography of breast after indocyanine green enhancement. *Proc Natl Acad Sci U S A* 2000;97:2767-72.
84. Alacam B, Yazici B, Intes X et al.: Pharmacokinetic-rate images of indocyanine green for breast tumors using near-infrared optical methods. *Phys Med Biol* 2008;53:837-59.
85. Corlu A, Choe R, Durduran T et al.: Three-dimensional in vivo fluorescence diffuse optical tomography of breast cancer in humans. *Opt Express* 2007;15:6696-716.
86. Poellinger A, Burock S, Grosenick D et al.: Breast Cancer: Early- and Late-Fluorescence Near-Infrared Imaging with Indocyanine Green--A Preliminary Study. *Radiology* 2010.
87. Kimura T, Muguruma N, Ito S et al.: Infrared fluorescence endoscopy for the diagnosis of superficial gastric tumors. *Gastrointest Endosc* 2007;66:37-43.
88. Iseki K, Tatsuta M, Iishi H et al.: Effectiveness of the near-infrared electronic endoscope for diagnosis of the depth of involvement of gastric cancers. *Gastrointest Endosc* 2000;52:755-62.
89. Matakai N, Nagao S, Kawaguchi A: Clinical usefulness of a new infra-red videoendoscope system for diagnosis of early stage gastric cancer. *Gastrointest Endosc* 2003;57:336-42.
90. Ishihara R, Uedo N, Ishii H: Recent development and usefulness of infrared endoscopic system for diagnosis of gastric cancer. *Dig Endosc* 2006;18:45-8.
91. van Driel PB, van de Giessen M, Boonstra MC, et al.: Characterization and evaluation of the Artemis Camera for fluorescence-guided cancer surgery. *Mol Imaging Biol* 2015;17:413-23

92. Handgraaf HJ, Boogerd LS, Verbeek FP, et al.: Intraoperative fluorescence imaging to localize tumors and sentinel lymph nodes in rectal cancer. *Minim Invasive Ther Allied Technol* 2015;7:1-6
93. van den Berg NS, Brouwer OR, Schaafsma BE, et al.: Multimodal surgical guidance during sentinel node biopsy for melanoma: combined gamma tracing and fluorescence imaging of the sentinel node through use of the hybrid tracer indocyanine green-(99m)tc-nanocolloid. *Radiology* 2015;275:521-9

PART I

**Clinical translation of image-guided
surgery in sentinel lymph node mapping**



Chapter 2

Near-infrared fluorescence sentinel lymph node biopsy in vulvar cancer: a randomized comparison of lymphatic tracers

Schaafsma BE¹, Verbeek FPR¹, Peters AAW, van der Vorst JR, de Kroon CD, van Poelgeest MIE, Trimbos JBMZ, van de Velde CJH, Frangioni JV, Vahrmeijer AL, Gaarenstroom KN

¹ Shared first authorship

British Journal of Obstetrics and Gynaecology 2013;120:758-764

ABSTRACT

This study aims to confirm feasibility of near-infrared (NIR) fluorescence imaging for sentinel lymph node (SLN) biopsy in vulvar cancer and to compare the tracer indocyanine green (ICG) bound to human serum albumin (HSA) versus ICG alone. Patients received ^{99m}Tc -nanocolloid and patent blue for SLN detection. Subsequently, women randomly received ICG:HSA or ICG alone. In 24 women, 35 SLNs were intraoperatively detected. All SLNs detected were radioactive and NIR fluorescent and 27 (77%) were blue. No significant difference was found between ICG:HSA and ICG alone. This trial confirms the feasibility of NIR fluorescence imaging for SLN mapping in vulvar cancer.

INTRODUCTION

Lymph node status is the most significant prognostic factor for survival in women with vulvar cancer.^{1,2} Therefore, lymphadenectomy plays a major role in the surgical treatment and staging of vulvar cancer. However, approximately 70% of women undergo unnecessary lymphadenectomy, which is associated with high morbidity and prolonged hospitalization.³⁻⁵ The introduction of sentinel lymph node (SLN) biopsy has provided a less invasive technique for nodal staging.⁶⁻⁸ SLN biopsy in early-stage vulvar cancer is considered accurate and safe without compromising groin recurrence or survival rates.^{3,9}

Currently, radioactive colloids, blue dyes, or a combination of both are used for SLN detection and offer high identification rates and low false-negative rates.⁹ ¹⁰ Recently, near-infrared (NIR) fluorescence optical imaging for SLN detection has been introduced. This technique uses the clinically available NIR fluorescent tracer indocyanine green (ICG).¹¹ The use of NIR light (700-900 nm) has several characteristics that can be advantageous in SLN biopsy as it offers relatively high tissue penetration (several millimeters) compared to blue dye and detection of low concentrations of tracer.¹²⁻¹⁴ Furthermore, NIR fluorescence imaging outperformed blue dye for SLN detection in multiple clinical studies.¹⁴⁻¹⁶ In vulvar cancer, two pilot studies demonstrated feasibility of NIR fluorescence for SLN biopsy.^{17,18} Hutteman et al. used ICG adsorbed to human serum albumin (HSA, complex ICG:HSA) and Crane et al. used ICG alone for SLN mapping in women with vulvar cancer.^{17,18} In vitro studies demonstrated that adsorption of ICG to HSA, by simple mixing, increases its fluorescence intensity (by threefold) and hydrodynamic diameter, which possibly results in better retention in the SLN.¹⁹ However, lymphatic vessels contain high concentrations of HSA and other proteins, which would make adsorption of ICG to HSA before injection redundant. Therefore, clinical assessment and comparison of these two lymphatic tracers is essential.

The aim of this double-blind randomized trial was to confirm feasibility of NIR fluorescence imaging for SLN biopsy in vulvar cancer and to assess whether ICG alone could render the same fluorescence intensity in the SLNs as ICG:HSA.

MATERIALS AND METHODS

Tracer Preparation

ICG (25-mg vials, Pulsion Medical Systems, Munich, Germany) was resuspended in 10 cc of sterile water. To obtain 500 μ M, 7.8 mL of the 3.2-mM ICG solution was diluted in 42.8 mL of sterile water or 42.8 mL of Cealb (20% human serum albumin, Sanquin, Amsterdam, The Netherlands) for the preparation of ICG alone or ICG:HSA,

respectively. A dose of 500 μM was chosen based on previous dose optimization studies.^{18, 20}

Clinical Trial

This double-blind, randomized, non-inferiority trial comparing ICG:HSA with ICG alone was approved by the Medical Ethics Committee of the Leiden University Medical Center and was performed in accordance with the ethical standards of the Helsinki Declaration of 1975. Inclusion criteria were a clinically FIGO stage I vulvar cancer with an unifocal squamous cell carcinoma measuring less than 4cm in diameter, not encroaching the vagina, anus, or urethra and with negative inguinofemoral nodes as determined by palpation and ultrasonography.⁵ However, four participants with a tumour >4cm were scheduled to undergo SLN biopsy of the inguinofemoral nodes outside this protocol, because of other co-morbidity or age > 80. Exclusion criteria were pregnancy, lactation, or an allergy to iodine or ICG. All women gave informed consent and were anonymized. Randomization was performed by the Department of Clinical Pharmacy by block randomization.

Women received the standard-of-care SLN procedure by gynecologic oncologists experienced with SLN biopsy.^{3,18} For our institution, this implied peritumoural injections of 60-100 MBq 99mtechnetium-nanocolloid the day before, or the morning prior to surgery. Prior to surgery, 1 mL of patent blue V (Guerbet, France) was injected at 4 sites peritumourally intracutaneously or around the excision scar, in cases of earlier excision biopsy. Subsequently, 1.6 mL total of ICG:HSA or ICG alone was injected as 4 injections at the same location as the blue dye injections. SLN mapping was performed using the Mini-Fluorescence-Assisted Resection and Exploration (Mini-FLARE™) image-guided surgery system as described previously.^{18, 20} The NIR fluorescence signal was measured percutaneously prior to skin incision, and continuously during the surgical procedure. Relative brightness of the SLNs was determined by measuring signal-to-background ratios (SBR). Both the surgeon and the assessor of the Mini-FLARE™ data were blinded to the treatment allocation. A SLN was defined as a lymph node on a direct lymphatic drainage pathway from the primary tumour as detected preoperatively by lymphoscintigraphy.²¹ Intraoperatively, lymph nodes with a gamma count of 10% or more compared to the most radioactive SLN, were also designated as SLNs. A SLN exhibiting a $\text{SBR} \geq 1.1$ in situ was considered positive by NIR fluorescence.

Excised SLNs were routinely analyzed by histopathological frozen section analysis. SLNs were fixed in formalin and embedded in paraffin for hematoxylin, eosin, and immunohistopathological staining for AE1/AE3 at multiple levels, with an interval of 250 μm , according to the GROningen International Study on Sentinel nodes in Vulvar cancer (GROINSS-V) study protocol.³ A full inguinofemoral

lymphadenectomy was performed in cases of tumour positive frozen sections of the SLN showing macrometastases 2 mm or larger or when the SLN could not be identified intraoperatively.

Power Calculation and Statistical Analysis

The power calculation is based on previous data, in which a SBR of 12.8 ± 4.5 was observed during SLN detection.¹⁸ These data revealed that 24 women are needed to achieve at least 90% power to detect non-inferiority using a one-sided, 2-sample t test ($\alpha = 0.025$) with a margin of equivalence of 6.4 while assuming no difference between the SBR of ICG:HSA and ICG alone. For statistical analysis, SPSS statistical software (Version 16.0, Chicago, IL) was used. To compare the SBR and the number of SLNs identified between ICG:HSA and ICG alone, a 1-sided, 2-sample t test was performed. $P < 0.05$ was considered significant.

RESULTS

Characteristics of participants

Twenty-four consecutive women with vulvar cancer undergoing SLN biopsy were included in this study (Fig. 1). Participant and tumour characteristics and previous treatment are presented in Table 1 and were equally distributed over the treatment groups. Three women underwent previous groin surgery due to varicose veins and SLN biopsy related to a previous vulvar cancer. The two treatment groups included each a total of 12 women.

Table 1. Patient and tumour characteristics

Characteristic	ICG:HSA (n = 12)	ICG alone (n = 12)	P
Age (median, range)	63 (36 - 83)	73 (47 - 87)	.10
Body mass index (median, range)	28 (21 - 35)	30 (24 - 40)	.37
Average tumour size (mm) \pm SD	22 \pm 15	22 \pm 17	.98
Average tumour infiltration depth (mm) \pm SD	3.6 \pm 4.1	6.2 \pm 8.3	.37
Previous groin surgery	1 (8%)	2 (17%)	.54

ICG:HSA, indocyanine green (ICG) adsorbed to human serum albumin (HSA)

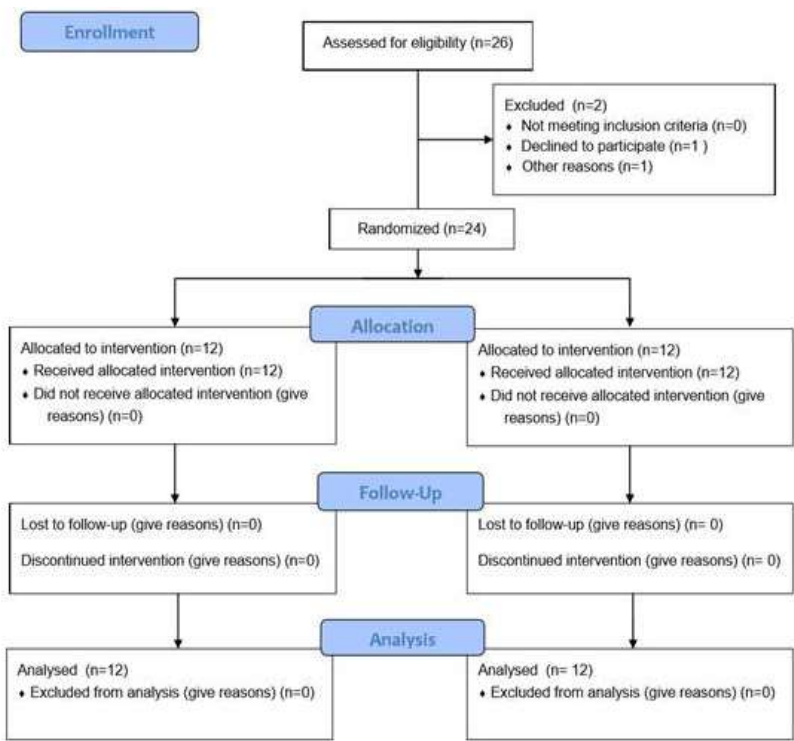


Fig 1. Patient enrollment

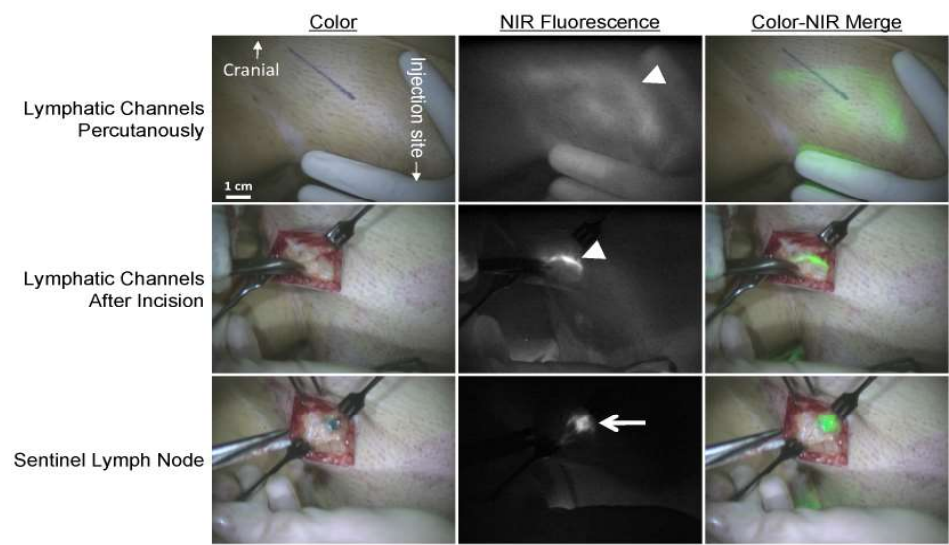


Fig 2. NIR Fluorescence-Based SLN Mapping. NIR fluorescence SLN mapping in a woman with early-stage vulvar cancer. Upper panel: Percutaneous visualization of the lymphatic vessels (arrowhead). Marker line presents planned incision before NIR fluorescence imaging. Middle panel: Identification of the lymphatic vessel (arrowhead) after incision. Lower panel: Identification of the radioactive, NIR fluorescent and blue SLN (ar-row). Camera exposure times were 250 msec (upper panel), 60 msec (middle panel), and 10 msec (lower panel). Scale bars = 1 cm.

Sentinel lymph node detection

Preoperative lymphoscintigraphy identified at least one SLN in each woman. The SLN was located unilaterally in 14 women and bilateral SLNs were identified in 10 women. In eight women (33%) lymphatic vessels were percutaneously visible using NIR fluorescence, which could assist in the location of the incision (Fig. 2). Average time between skin incision and detection of the first SLN was 10 ± 8 min. Intraoperatively, on average 1.5 ± 1.2 SLNs per participant were identified (Supplementary Video). Of the 35 SLNs identified 35 (100%) were radioactive, 35 (100%) were fluorescent and 27 (77%) were blue. In all women, the NIR fluorescence signal in the SLN was detected before patent blue. In 19 out of the 24 women at least one SLN was detected during surgery. In 25 out of the 34 groins in which a SLN was detected by lymphoscintigraphy at least one SLN was detected. In two women, in whom no SLN could be located intraoperatively, a fluorescent node could be detected in the resection specimen of the inguinofemoral lymphadenectomy following the SLN procedure. Histological analysis showed lymph node metastases in seven out of 24 women of whom four women had macrometastases (> 2 mm) and three had micrometastases (≤ 2 mm). In all women with lymph node metastases at least one of the tumour positive lymph nodes was appointed SLN. No adverse reactions associated with the use of ICG or ICG:HSA occurred.

Comparison between treatment groups

The average SBR of ICG:HSA (10.3 ± 2.5) and ICG alone (11.2 ± 6.0) were not significantly different ($P = 0.65$) (Table 2). No significant difference was observed in the average number of in vivo identified fluorescent SLNs per groin between ICG:HSA and ICG alone (1.9 ± 1.4 vs. 1.0 ± 0.7 , $P = 0.06$). Similarly, there was no significant difference in intraoperative detection rate ($P = 0.27$).

COMMENT

The present study confirmed feasibility of NIR fluorescence for optical guidance for intraoperative SLN biopsy using ICG in women with vulvar cancer. All SLNs that were detected by radio guidance could also be detected by NIR fluorescence, however not all SLNs were detected by blue dye staining. This double-blind randomized trial did not show any advantages of ICG:HSA over ICG alone in SBR and average number of intraoperative detected fluorescent SLNs.

NIR fluorescence was of added value during SLN detection, as all SLNs detected could be identified by the direct optical guidance of NIR fluorescence, but only 77% by blue dye staining. Moreover, the NIR fluorescence signal in the SLN could be detected

Table 2. SLN Identification Results

Characteristic	Total (24 subjects)		ICG:HSA (12 subjects)		ICG alone (12 subjects)		P
	N	%	N	%	N	%	
SLNs detected by lymphoscintigraphy							.41
Unilateral	14	42	6	50	8	67	
Bilateral	10	58	6	50	4	33	
Intraoperative detection rate*							
Per patient	19	79	10	83	9	75	.61
Per groin† (34 groins)	25	74	15	83	10	63	.17
Average number of intraoperative identified SLNs per patient ± SD	1.5 ± 1.2		1.9 ± 1.4		1.0 ± 0.7		.06
Number of SLNs identified	35		23		12		
Method of SLN detection							
Radioactive	35	100	23	100	12	100	
Fluorescence	35	100	23	100	12	100	
Blue dye	27	77	16	70	11	92	.09
Signal-to-background ratio	10.7 ± 4.4		10.3 ± 2.5		11.2 ± 6.0		.65
Average time between injection and skin incision ± SD (min)	17 ± 6		18 ± 6		16 ± 6		.39
Average time between skin incision and first SLN detection ± SD (min)	10 ± 9		10 ± 9		11 ± 8		.75
Histology							.50
negative	17	71	8	67	9	75	
ITC/micrometastasis	3	13	1	8	2	17	
macrometastasis	4	16	3	25	1	8	

ICG:HSA, indocyanine green (ICG) adsorbed to human serum albumin (HSA); SLN, sentinel lymph node; ITC, isolated tumour cells

*Detection rate combining NIR fluorescence imaging, the gamma probe, and blue dye staining

†Groins with SLN localization by preoperative lymphoscintigraphy (N=18 ICG:HSA, N=16 ICG alone)

before patent blue in all cases. Blue dye staining and NIR fluorescence both provide real-time optical guidance. Tissue penetration of NIR fluorescent light is significantly higher than penetration of visible light, which enables deeper and earlier visualization of signal by NIR fluorescence. This can assist to determine the location of the incision and provide improved optical guidance during SLN localization. Furthermore, since ICG is diluted to levels invisible to the human eye after injection, no discoloration of the surgical field occurs. It can therefore be questioned whether blue dye can be

omitted when NIR fluorescence is used.²² Moreover, compared to radioactive lymphatic tracers, NIR fluorescence is not hampered by high background signals of the injection site by the gamma probe, which can interfere SLN detection using the gamma probe. However, due to the limited penetration depth of NIR fluorescence imaging (several mm), radioactive SLN tracers remain necessary for preoperative surgical planning and to detect deeper located SLNs. Therefore, a combination of a radiocolloid tracer for preoperative planning and guidance of deeper located nodes and a NIR fluorescence tracer for real-time optical guidance is advocated.^{23,24}

This study is one out of three simultaneously initiated clinical studies to directly compare the lymphatic tracers ICG:HSA and ICG alone.^{15,25} In concordance with these studies, no significant difference in SBR and average number of identified SLNs between the lymphatic tracers ICG:HSA and ICG alone was found in vulvar cancer. Since lymph fluids consist of a high protein levels,²⁶ a potential explanation for the lack of difference between ICG:HSA and ICG alone is that ICG rapidly binds to these endogenous proteins when drained in the lymphatic system, eliminating the need for premixing ICG and HSA. Together, the three clinical studies demonstrate no difference between ICG:HSA and ICG alone for the SLN identification in a large heterogeneous group of women, with different anatomical locations (breast cancer, cervical cancer, and vulvar cancer) and different times from injection to imaging.^{15,25}

All SLNs identified intraoperatively could be detected by both radio guidance and NIR fluorescence. Although a high concordance between detection by NIR fluorescence and radio guidance was found, the intraoperative detection rate of the SLN (19 out of 24 women) in this study is relatively low compared to other studies.¹⁰ A possible explanation could be that two women underwent previous groin surgery for varicose veins and one underwent a SLN procedure previously. Moreover, in two women fluorescent SLNs could be detected in the lymphadenectomy specimen *ex vivo*, which if detected intraoperatively would have increased the intraoperative detection rate considerably. Nevertheless, in all women with lymph node metastases, the SLN containing tumour cells could be identified intraoperatively.

In conclusion, this double-blind, randomized trial showed no advantage of using ICG:HSA in comparison to ICG alone and shows the added value of NIR fluorescence for SLN biopsy in vulvar cancer.

ACKNOWLEDGMENTS

The authors thank Margriet J.G. Löwik and Dorien M.A. Berends-van der Meer for their assistance during the participant inclusion process and Lindsey Gendall for editing. This work was supported in part by NIH grants R01-CA-115296 and R21-CA-130297 and the Dutch Cancer Society grant UL2010-4732. This research was performed within the framework of CTMM, the Center for Translational Molecular Medicine, project MUSIS (grant 03O-202). Joost van der Vorst is an MD-medical research trainee funded by The Netherlands Organisation for Health Research and Development (grant 92003593).

REFERENCES

1. Beller U, Quinn MA, Benedet JL, et al. Carcinoma of the vulva FIGO 26th Annual Report on the Results of Treatment in Gynecological Cancer. *Int J Gynaecol Obstet* 2006; 95(Suppl 1):S7–27.
2. Burger MP, Hollema H, Emanuels AG, et al. The importance of the groin node status for the survival of T1 and T2 vulval carcinoma patients. *Gynecol Oncol* 1995; 57:327–34.
3. Van Der Zee AG, Oonk MH, De Hullu JA, et al. Sentinel node dissection is safe in the treatment of early-stage vulvar cancer. *J Clin Oncol* 2008; 26:884–9.
4. Johann S, Klaeser B, Krause T, et al. Comparison of outcome and recurrence-free survival after sentinel lymph node biopsy and lymphadenectomy in vulvar cancer. *Gynecol Oncol* 2008; 110:324–8.
5. Oonk MH, van Hemel BM, Hollema H, et al. Size of sentinel-node metastasis and chances of non-sentinel-node involvement and survival in early stage vulvar cancer: results from GROINSS-V, a multicentre observational study. *Lancet Oncol* 2010; 11:646–52.
6. Morton DL, Wen DR, Wong JH, et al. Technical details of intraoperative lymphatic mapping for early stage melanoma. *Arch Surg* 1992; 127:392–9.
7. Dhar KK, Woolas RP. Lymphatic mapping and sentinel node biopsy in early vulvar cancer. *BJOG* 2005; 112:696–702.
8. Levenback C, Burke TW, Gershenson DM, et al. Intraoperative lymphatic mapping for vulvar cancer. *Obstet Gynecol* 1994; 84:163–7.
9. Devaja O, Mehra G, Coutts M, et al. A prospective study of sentinel lymph node detection in vulval carcinoma: is it time for a change in clinical practice? *Int J Gynecol Cancer* 2011; 21:559–64.
10. Van Oostrum NH, Makar AP, Van Den Broecke R. Sentinel node procedures in gynecologic cancers: an overview. *Acta Obstet Gynecol Scand* 2012; 91:174–81.
11. Schaafsma BE, Mieog JS, Hutteman M, et al. The clinical use of indocyanine green as a near-infrared fluorescent contrast agent for image-guided oncologic surgery. *J Surg Oncol* 2011; 104:323–32.
12. Murawa D, Hirche C, Dresel S, et al. Sentinel lymph node biopsy in breast cancer guided by indocyanine green fluorescence. *Br J Surg* 2009; 96:1289–94.
13. Frangioni JV. In vivo near-infrared fluorescence imaging. *Curr Opin Chem Biol* 2003; 7:626–34.
14. Fujisawa Y, Nakamura Y, Kawachi Y, et al. Indocyanine green fluorescence-navigated sentinel node biopsy showed higher sensitivity than the radioisotope or blue dye method, which may help to reduce false-negative cases in skin cancer. *J Surg Oncol* 2012; 106:41–5.
15. Hutteman M, Mieog JS, van der Vorst JR, et al. Randomized, double-blind comparison of indocyanine green with or without albumin premixing for near-infrared fluorescence imaging of sentinel lymph nodes in breast cancer patients. *Breast Cancer Res Treat* 2011; 127:163–70.
16. Hojo T, Nagao T, Kikuyama M, et al. Evaluation of sentinel node biopsy by combined fluorescent and dye method and lymph flow for breast cancer. *Breast* 2010; 19:210–3.
17. Crane LM, Themelis G, Arts HJ, et al. Intraoperative near-infrared fluorescence imaging for sentinel lymph node detection in vulvar cancer: first clinical results. *Gynecol Oncol* 2011; 120:291–5.
18. Hutteman M, van der Vorst JR, Gaarenstroom KN, et al. Optimization of near-infrared fluorescent sentinel lymph node mapping for vulvar cancer. *Am J Obstet Gynecol* 2012; 206:89–95.
19. Ohnishi S, Lomnes SJ, Laurence RG, et al. Organic alternatives to quantum dots for intraoperative near-infrared fluorescent sentinel lymph node mapping. *Mol Imaging* 2005; 4:172–81.
20. Mieog JS, Troyan SL, Hutteman M, et al. Toward optimization of imaging system and lymphatic tracer for near-infrared fluorescent sentinel lymph node mapping in breast cancer. *Ann Surg Oncol* 2011; 18:2483–91.
21. Nieweg OE, Tanis PJ, Kroon BB. The definition of a sentinel node. *Ann Surg Oncol* 2001; 8:538–41.
22. van der Vorst JR, Schaafsma BE, Verbeek FP, et al. Randomized comparison of near-infrared fluorescence imaging using Indocyanine Green and 99(m)technetium with or without patent

- blue for the sentinel lymph node procedure in breast cancer patients. *Ann Surg Oncol* 2012; 19:4104–11.
23. van der Poel HG, Buckle T, Brouwer OR, et al. Intraoperative laparoscopic fluorescence guidance to the sentinel lymph node in prostate cancer patients: clinical proof of concept of an integrated functional imaging approach using a multimodal tracer. *Eur Urol* 2011; 60:826–33.
 24. Brouwer OR, Buckle T, Vermeeren L, et al. Comparing the hybrid fluorescent-radioactive tracer indocyanine green-99mTc-nanocolloid with 99mTc-nanocolloid for sentinel node identification: a validation study using lymphoscintigraphy and SPECT/CT. *J Nucl Med* 2012; 53:1034–40.
 25. Schaafsma BE, van der Vorst JR, Gaarenstroom KN, et al. Randomized comparison of nearinfrared fluorescence lymphatic tracers for sentinel lymph node mapping of cervical cancer. *Gynecol Oncol* 2012; 127:126–30.
 26. Cherrick GR, Stein SW, Leevy CM, et al. Indocyanine green: observations on its physical properties, plasma decay, and hepatic extraction. *J Clin Invest* 1960; 39:592–600.

Chapter 3

Randomized comparison of near-infrared fluorescence lymphatic tracers for sentinel lymph node mapping of cervical cancer

Schaafsma BE¹, van der Vorst JR¹, Gaarenstroom KN, Peters AAW, Verbeek FPR, de Kroon CD, Trimbos JBMZ, van Poelgeest MIE, Frangioni JV, van de Velde CJH, Vahrmeijer AL

¹ Shared first authorship

Gynecologic Oncology 2012;127:126-130

ABSTRACT

Objective

Near-infrared fluorescence imaging using indocyanine green (ICG) has recently been introduced as a novel technique for sentinel lymph node (SLN) mapping in early-stage cervical cancer. Although preclinical research has shown that ICG adsorbed to human serum albumin (ICG:HSA) improves its performance, the need for HSA has not yet been confirmed in cervical cancer patients. The current randomized study aims to determine whether ICG:HSA offers advantages over using ICG alone.

Methods

Eighteen consecutive early-stage cervical cancer patients scheduled to undergo pelvic lymphadenectomy were included. Prior to surgery, 1.6 mL of 500 μ M ICG:HSA or 500 μ M ICG alone was injected transvaginally in 4 quadrants around the tumour. The Mini-FLARE imaging system was used for intraoperative NIR fluorescence detection and quantitation.

Results

SLNs were identified intraoperatively in 78% of the patients. Patient and tumour characteristics were equally distributed over both treatment groups. No significant difference in signal-to-background ratio (9.3 vs. 10.1, $P = .72$) or average number of detected SLNs (2.9 vs 2.7, $P = .84$) was found between the ICG:HSA group and the ICG alone group, respectively.

Conclusions

In conclusion, this double-blind, randomized trial showed no advantage of ICG:HSA over ICG alone for the SLN procedure in early-stage cervical cancer. Further optimization is required to improve the intraoperative detection rate.

INTRODUCTION

As part of surgical management in early-stage cervical cancer, bilateral pelvic lymphadenectomy is considered standard of care. However, pelvic lymphadenectomy is associated with complications, such as lymphedema, the risk of nerve injury, and lymphocyst formation.¹ Because lymph node involvement occurs in approximately 12% to 22% of early-stage cervical cancer patients, the majority of patients do not benefit from a pelvic lymphadenectomy, but may suffer from its complications.^{2,3} Over the last decades, the sentinel lymph node (SLN) concept has proven to be feasible and safe in vulvar cancer, melanoma, and breast cancer for selecting patients who would benefit from lymphadenectomy. In addition, the SLN can be used for ultra staging to aid in the identification of micrometastases.⁴ However, due to the bilateral multifarious drainage pattern of the cervix, the SLN procedure is more challenging in cervical cancer patients than in breast cancer patients, for example. SLN biopsy in early-stage cervical cancer patients has been extensively described using blue dye, a radiocolloid, or a combination of both, with various results.⁵

Intraoperative near-infrared (NIR) fluorescence imaging using indocyanine green (ICG) has emerged as a novel technique for SLN detection in cervical cancer patients.⁶⁻¹⁰ NIR fluorescence imaging has several advantages, such as a relatively high tissue penetration and low autofluorescence. ICG is currently the only clinically available NIR lymphatic tracer. However, due to its relatively low fluorescence brightness (quantum yield) and its small hydrodynamic diameter, it is not an optimal lymphatic tracer. Preclinical work has demonstrated that adsorption of ICG to human serum albumin (HSA, complex is ICG:HSA), by simply mixing it, increases the fluorescence intensity (a threefold) and hydrodynamic diameter.¹¹ These advantages could provide improved detection and retention of the tracer in the SLN. On the other hand, the use of albumin adds cost and complexity to the procedure. Moreover, the use of human blood products, such as HSA, poses regulatory hurdles in certain countries, such as the United States.

The aim of this double-blind randomized trial was to confirm feasibility of NIR fluorescence imaging for SLN mapping in cervical cancer and to assess whether ICG alone could render the same fluorescence intensity in the SLNs as ICG:HSA.

METHODS

Preparation of Indocyanine Green adsorbed to Human Serum Albumin

Indocyanine green (25-mg vials) was purchased from Pulsion Medical Systems (Munich, Germany) and was resuspended in 10 cc of sterile water. To obtain a 500 μ M final concentration, 7.8 mL of the 3.2-mM ICG solution was diluted in 42.8

mL of sterile water for injection or 42.8 ml of Cealb (20% human serum albumin, Sanquin, Amsterdam, The Netherlands) for the preparation of ICG alone or ICG:HSA, respectively. A dose of 500 μ M was chosen based on previous studies that showed that the optimal dose of ICG:HSA lies between 400 and 800 μ M and has the benefit of minimal manipulation of ICG and albumin volumes.^{6,12}

Intraoperative Near-Infrared Imaging System (Mini-FLARE)

SLN mapping was performed using the Mini-Fluorescence-Assisted Resection and Exploration (Mini-FLARE) image-guided surgery system as described previously.¹² Briefly, the system consists of 2 wavelength isolated light sources: a “white” light source, generating 26,600 lx of 400-650 nm light, and a “near-infrared” light source, generating 7.7 mW/cm² of 760 nm light. Color video and NIR fluorescence images are simultaneously acquired and displayed in real time using custom optics and software that separate the color video and NIR fluorescence images. A pseudo-colored (lime green) merged image of the color video and NIR fluorescence images is also displayed. The imaging head is attached to a flexible gooseneck arm, which permits positioning of the imaging head at extreme angles virtually anywhere over the surgical field. For intraoperative use, the imaging head and imaging system pole stand are wrapped in a sterile shield and drape (Medical Technique Inc., Tucson, AZ).

Clinical Trial

The double-blind, randomized, noninferiority trial comparing ICG:HSA with ICG alone was approved by the Medical Ethics Committee of the Leiden University Medical Center and was performed in accordance with the ethical standards of the Helsinki Declaration of 1975. All patients planning to undergo a total pelvic lymphadenectomy for early stage cervical cancer were eligible for participation in the study. Exclusion criteria were pregnancy, lactation, or an allergy to iodine, shellfish, or indocyanine green. All patients gave informed consent and were anonymized. Patients were randomized by the Department of Clinical Pharmacy. Treatment allocation was performed by block randomization. Before the start of surgery, 1.6 mL of 500 μ M ICG:HSA or ICG alone was transvaginally injected by the surgeon submucosally in 4 quadrants of the cervix. Directly after injection, following surgical scrub and sterile covering of the operation field, a laparotomy was performed.

Prior to the systematic pelvic lymphadenectomy, all standard locations (along the external iliac vessels and the hypogastric artery, the common iliac artery, the obturator fossa and the lateral parametrium) were examined for NIR fluorescence using the Mini-FLARE imaging system. Both the surgeon and the Mini-FLARE operator, who was responsible for analyzing the data, were blinded to the treatment allocation. All

fluorescent hotspots, containing one or more lymph nodes, were denominated as SLNs and were subsequently resected and measured for fluorescence *ex vivo*. Subsequently, the standard systemic pelvic lymphadenectomy was performed and all resected lymph nodes were also measured for fluorescence *ex vivo*. Lymphadenectomy consisted of removal of all lymph node-bearing fatty tissue along the external iliac vessels, the common iliac artery, the hypogastric artery, and from the obturator fossa.¹³ Also, the area lateral to and underneath the superior vesical arteries (lateral parametrium) was cleared from the lymphatic tissue. The radical hysterectomy or abdominal trachelectomy were performed according to the standard procedure. Afterwards, all resected lymph nodes were examined by routine histopathological analysis; lymph nodes were fixed in formalin and embedded in paraffin for routine hematoxylin and eosin staining. SLNs and non-SLNs were examined separately. Additionally, a substantial part of the SLNs and clinical suspected nodes were subsequently examined using a cytokeratin staining.

Power Calculation and Statistical Analysis

The power calculation is based on data from previous studies, in which *in vitro* a threefold difference in fluorescent brightness (quantum yield) was reported between ICG alone and ICG:HSA and *in vivo* signal-to-background ratio of 10.1 ± 1.2 was observed during SLN detection by ICG:HSA.^{6,11} These data revealed that 18 patients are needed to achieve 91% power to detect non-inferiority using a one-sided, 2-sample t test ($\alpha = 0.025$) with a margin of equivalence of 5.0 while assuming no difference between the signal-to-background ratio (SBR) of ICG:HSA and ICG alone. For statistical analysis, SPSS statistical software package (Version 16.0, Chicago, IL) was used. To compare the SBR and the number of SLNs identified between ICG:HSA and ICG alone, a 1-sided, 2-sample t test was performed. $P < 0.05$ was considered significant.

RESULTS

Patient characteristics

Eighteen consecutive early-stage cervical cancer patients scheduled to undergo a pelvic lymphadenectomy were randomized to ICG:HSA or ICG alone for NIR fluorescence SLN imaging. All patients were clinically staged as FIGO stage IB1 cervical cancer. Of these 18 patients, the median age was 40 years (range, 28-67), median body mass index was 25 (21-38), and median tumour size was 1.6 cm (range, 0.3-5.0 cm). In one patient in whom preoperative pathology was not conclusive (either cervical cancer or endometrial cancer), postoperative pathological evaluation showed endometrial

cancer. In all patients a complete bilateral pelvic lymphadenectomy was performed, except for one case. In this case the surgeon did not complete the lymphadenectomy, due to pathologically proven metastatic lymphatic disease by intraoperative frozen section and excessive blood loss during surgery. Patient and tumour characteristics and previous treatment were equally distributed over the treatment groups (Table 1).

Table 1. Patient and Tumour Characteristics

Characteristic	ICG:HSA (N = 9)		ICG alone (N = 9)		P
	N	%	N	%	
Age (median, range)	40 (28 - 67)		40 (30 - 50)		.86
Body mass index (median, range)	25 (22 - 38)		23 (21 - 34)		.13
Previous procedures					
No local treatment	3	33	3	33	.77
Local excision	2	23	2	23	
Conization	3	33	4	44	
Local excision + Neoadjuvant chemotherapy	1	11	0	0	
Histological type					
Squamous cell carcinoma	4	44.5	5	56.5	.57
Adenocarcinoma	4	44.5	4	44.5	
Endometroid adenocarcinoma	1	11	0	0	
Type of tumour excision					
Radical hysterectomy	6	67	8	89	.26
Radical trachelectomy	3	33	1	11	
Type of lymphadenectomy					
Complete bilateral lymphadenectomy	8	89	9	100	.30
Incomplete bilateral lymphadenectomy	1	11	0	0	
Tumour size (median, range)	1.4 (0.6 - 5.0)		1.8 (0.3 - 3.6)		.88

NIR Fluorescence Imaging

The results of the NIR fluorescence detection of SLNs are presented in Table 2. During surgery, NIR fluorescence imaging enabled identification of 1 or more fluorescent hotspots in 14 out of 18 (78%) patients (Figure 1). In 11 patients (61%) fluorescent hotspots were identified bilaterally, whereas in 3 patients (17%) hotspots were identified unilaterally. In 4 patients (22%) no fluorescent hotspots were detected intraoperatively. Average time between injection of ICG:HSA or ICG alone and imaging was 43 ± 14 min and did not lengthen the standard of care surgery. On average, 2.8 ± 2.2 hotspots were detected intraoperatively by NIR fluorescence, yielding an average of 4.2 ± 3.7 SLNs per patient at pathological examination. An average of 24.5 (range, 9-46) lymph nodes per patient were harvested when a complete bilateral lymphadenectomy was performed.

In addition, all lymph nodes were examined for fluorescence ex vivo directly after surgical resection in the operating room. In 11 of 18 patients, a total of 29 additional fluorescent hotspots could be identified, which were not identified during

in vivo NIR fluorescence imaging. When the ex vivo detected fluorescent hotspots and the in vivo detected fluorescent hotspots were combined, NIR fluorescence imaging enabled identification of 1 or more fluorescent hotspots in 16 out of 18 (89%) patients, thus in 2 more patients compared to in vivo identification alone. In 13 patients (72%) these were identified bilaterally, in 3 patients (17%) unilaterally, and in 2 patients (11%) there were no fluorescent hotspots detected in vivo or ex vivo.

Histological analysis showed lymph node metastases in 6 out of 18 patients of whom 4 patients had macrometastases (> 2 mm) and 2 patients had micrometastases (≤ 2 mm).¹⁴ In 5 of 6 patients with lymph node metastases, one or more tumour positive nodes were fluorescent. Though, in 2 of these 6 patients, the fluorescent nodes were only detected ex vivo. Furthermore, in 1 patient, the resection specimen contained a nonfluorescent fibrotic nodule with mature fat cells, some lymphoid infiltration, and a micrometastatic lesion. No metastases were found in this patient's fluorescent nodes.

Table 2. SLN Identification Results

Characteristic	Total (18 subjects)		ICG:HSA (9 subjects)		ICG alone (9 subjects)		P
	N	%	N	%	N	%	
Intraoperative detection rate							
Bilateral	11	61	5	56	6	67	.13
Unilateral	3	17	3	33	0	0	
None	4	22	1	11	3	33	
Average number of intraoperative NIR hotspots \pm SD	2.8 \pm 2.2		2.9 \pm 1.7		2.7 \pm 2.6		.84
Signal-to-background ratio	9.7 \pm 3.9		9.3 \pm 3.6		10.1 \pm 4.5		.72
Average lymph nodes in lymphadenectomy \pm SD	24.5 \pm 8.8		23.4 \pm 4.3		25.6 \pm 11.6		.62
Average number of additional hotspots ex vivo \pm SD	1.6 \pm 2.0		1.0 \pm 1.3		2.2 \pm 2.4		.21
Presence of fluorescent nodes							
Bilateral	13	72	6	67	7	78	.82
Unilateral	3	17	2	22	1	11	
None	2	11	1	11	1	11	
Histology							
Negative	12	67	7	78	5	56	.51
ITC/micrometastasis	2	11	1	11	1	11	
Macrometastasis	4	22	1	11	3	33	
False negative rate							
Intraoperatively detected nodes	3/6		1/2		2/4		
All fluorescent nodes	1/6		1/2		0/4		

ICG:HSA, indocyanine green adsorbed to human serum albumin; ITC, isolated tumour cells

Comparison between treatment groups

The primary endpoint of this study was the average brightness of the SLN, expressed in SBR. The average SBR of ICG:HSA (9.3 ± 3.6) and ICG alone (10.1 ± 4.5) were not significantly different ($P = .72$). No significant difference was observed in the average number of in vivo identified fluorescent hotspots between ICG:HSA and ICG alone (2.9 ± 1.7 vs 2.7 ± 2.6 , $P = .84$). Similarly, there was no significant difference in intraoperative detection rate ($P = .13$) or presence of fluorescent nodes after ex vivo inspection ($P = .82$).

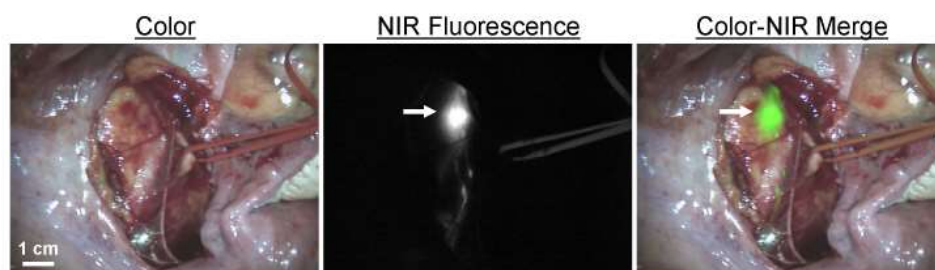


Fig 1. NIR Fluorescence-Based SLN Mapping using ICG:HSA and Mini-FLARE: Identification of a SLN (arrow), located along the right iliac vessels, with NIR fluorescence imaging is demonstrated in a cervical cancer patient after administration of 500 μ M ICG:HSA.

DISCUSSION

The current 18-patient clinical study confirmed the feasibility of the SLN procedure in early-stage cervical cancer using NIR fluorescence imaging with ICG. The overall intraoperative detection rate was 78%, and in 61% of all patients fluorescent nodes could be identified bilaterally. This double-blind randomized trial did not show any advantages of ICG:HSA over ICG alone in SBR, average number of intraoperatively detected fluorescent hotspots, or percentage of patients in whom fluorescent nodes could be detected.

The recent introduction of NIR fluorescence imaging has provided new opportunities in the field of SLN mapping. Preclinical studies indicated that adsorption of ICG to HSA increases the fluorescence intensity and the hydrodynamic diameter, thereby providing improved detection and better retention in the SLN.¹¹ In the current study, ICG:HSA performed equally well as ICG alone. This is in concordance with a previous study performed by our group in which no differences were found between the use of ICG:HSA and ICG alone in SLN mapping in breast cancer patients.¹⁵ In lymph fluids a high protein constitution is found.¹⁶ A potential explanation for the lack of difference between ICG:HSA and ICG alone is that ICG rapidly binds to endogenous proteins when drained in the lymphatic system, eliminating the need for premixing ICG and HSA.

The detection rate in this study is in concordance with previously reported detection rates in studies using NIR fluorescence for SLN mapping in early-stage cervical cancer, which vary from 60% to 100%.⁶⁻⁹ Large studies in early-stage cervical cancer patients using radiocolloid tracers reported higher detection rates varying from 88% to 99%.¹⁷⁻²³ Possible explanations for the lower detection rate observed in this study could be the inclusions of patients with larger tumours (>2 cm) and, especially, the learning curve associated with cervical injection of the tracer and the intraoperatively exposure of tissue to maximize NIR fluorescence detection.^{17,24} Unlike the present study, our initial 9-patient study of NIR fluorescence SLN mapping in cervical cancer utilized two clinicians for all NIR lymphatic tracer injections. Although the learning curve could be of significant effect on the intraoperative identification rate and time needed to identify the SLN, it is unlikely that the learning curve interferes with the SBR, which was used to power the present trial and to test difference between ICG alone and ICG:HSA. Assessment of the learning curve will be essential before NIR fluorescence can be compared to conventional techniques using radiocolloid tracers in a sufficient powered study.

After resection, additional fluorescent lymph nodes, which were missed during intraoperative inspection with the Mini-FLARE, were identified in the resection specimens of 11 out of the 18 patients. Intraoperative detection of these additional fluorescent nodes would have considerably improved the detection rate and the false negative rate. Difficulty in the intraoperative detection of these nodes could be based on the relatively limited tissue penetration of NIR light (several millimeters) compared to radiocolloid tracers, or the learning curve associated with positioning tissue intraoperatively to maximize NIR fluorescence detection. Moreover, radiocolloid tracers permit preoperative localization of the SLN, which assists surgical planning. Still, radiocolloids have the disadvantage that there is no real-time visualization during the operation, and detection is hampered if the SLNs are located near the point of the tracer injection. NIR fluorescence imaging is suitable for real-time identification and detection of SLNs located in the vicinity of the injection site. In addition, NIR fluorescence has as a much better tissue penetration when compared to blue dyes. Therefore, a combination of a radiocolloid and a NIR fluorescence tracer might be preferable. In a recent study, van der Poel et al. reported the successful use of such a multimodal tracer combining radioactivity and NIR fluorescence in sentinel lymph node mapping in prostate cancer patients using a NIR fluorescence laparoscope.²⁵

In conclusion, this double-blind, randomized trial showed no advantage of ICG:HSA in comparison to ICG alone for the SLN procedure in early-stage cervical cancer. Further optimization of NIR fluorescence imaging is required to improve the intraoperative detection rate to permit this technique to compete with radiocolloid tracers.

ACKNOWLEDGMENTS

The authors thank Margriet J.G. Löwik and Dorien M.A. Berends-van der Meer for their assistance during the patient inclusion process and Lindsey Gendall for editing. This work was supported in part by NIH grants R01-CA-115296 and R21-CA-130297 and the Dutch Cancer Society grant UL2010-4732. This research was performed within the framework of CTMM, the Center for Translational Molecular Medicine, project MUSIS (grant 03O-202).

REFERENCES

1. Kashima K, Yahata T, Fujita K, et al. Analysis of the complications after radical hysterectomy for stage IB, IIA and IIB uterine cervical cancer patients. *J Obstet Gynaecol Res* 2010; 36:555–9.
2. Sakuragi N. Up-to-date management of lymph node metastasis and the role of tailored lymphadenectomy in cervical cancer. *Int J Clin Oncol* 2007; 12:165–75.
3. Delgado G, Bundy BN, Fowler Jr WC, et al. A prospective surgical pathological study of stage I squamous carcinoma of the cervix: a Gynecologic Oncology Group Study. *Gynecol Oncol* 1989; 35: 314–20.
4. Gortzak-Uzan L, Jimenez W, Nofech-Mozes S, et al. Sentinel lymph node biopsy vs. pelvic lymphadenectomy in early stage cervical cancer: is it time to change the gold standard? *Gynecol Oncol* 2010; 116: 28–32.
5. Eiriksson L, Covens A. Sentinel lymph node mapping in cervical cancer: the future? *BJOG* 2012; 119:129–33.
6. van der Vorst JR, Hutteman M, Gaarenstroom KN, et al. Optimization of near-infrared fluorescent sentinel lymph node mapping in cervical cancer patients. *Int J Gynecol Cancer* 2011; 21:1472–8.
7. Furukawa N, Oi H, Yoshida S, et al. The usefulness of photodynamic eye for sentinel lymph node identification in patients with cervical cancer. *Tumori* 2010; 96:936–40.
8. Crane LM, Themelis G, Pleijhuis RG, et al. Intraoperative multispectral fluorescence imaging for the detection of the sentinel lymph node in cervical cancer: a novel concept. *Mol Imaging Biol* 2011; 13: 1043–9.
9. Rossi EC, Ivanova A, Boggess JF. Robotically assisted fluorescence-guided lymph node mapping with ICG for gynecologic malignancies: a feasibility study. *Gynecol Oncol* 2012; 124(1):78–82.
10. Schaafsma BE, Mieog JS, Hutteman M, et al. The clinical use of indocyanine green as a near-infrared fluorescent contrast agent for image-guided oncologic surgery. *J Surg Oncol* 2011; 104:323–32.
11. Ohnishi S, Lomnes SJ, Laurence RG, et al. Organic alternatives to quantum dots for intraoperative near-infrared fluorescent sentinel lymph node mapping. *Mol Imaging* 2005; 4:172–81.
12. Mieog JS, Troyan SL, Hutteman M, et al. Toward optimization of imaging system and lymphatic tracer for near-infrared fluorescent sentinel lymph node mapping in breast cancer. *Ann Surg Oncol* 2011; 18:2483–91.
13. Pieterse QD, Kenter GG, Gaarenstroom KN, et al. The number of pelvic lymph nodes in the quality control and prognosis of radical hysterectomy for the treatment of cervical cancer. *Eur J Surg Oncol* 2007; 33:216–21.
14. Hermanek P, Hutter RV, Sobin LH, et al. International Union Against Cancer. Classification of isolated tumor cells and micrometastasis. *Cancer* 1999; 86:2668–73.
15. Hutteman M, Mieog JS, van der Vorst JR, et al. Randomized, double-blind comparison of indocyanine green with or without albumin premixing for near-infrared fluorescence imaging of sentinel lymph nodes in breast cancer patients. *Breast Cancer Res Treat* 2011; 127:163–70.
16. Cherrick GR, Stein SW, Leevy CM, et al. Indocyanine green: observations on its physical properties, plasma decay, and hepatic extraction. *J Clin Invest* 1960; 39:592–600.
17. Altgassen C, Hertel H, Brandstadt A, et al. Multicenter validation study of the sentinel lymph node concept in cervical cancer: AGO Study Group. *J Clin Oncol* 2008; 26:2943–51.
18. Ogawa S, Kobayashi H, Amada S, et al. Sentinel node detection with (99m)Tc phytate alone is satisfactory for cervical cancer patients undergoing radical hysterectomy and pelvic lymphadenectomy. *Int J Clin Oncol* 2010; 15:52–8.
19. Darlin L, Persson J, Bossmar T, et al. The sentinel node concept in early cervical cancer performs well in tumors smaller than 2 cm. *Gynecol Oncol* 2010; 117:266–9.
20. Du XL, Sheng XG, Jiang T, et al. Sentinel lymph node biopsy as guidance for radical trachelectomy in young patients with early stage cervical cancer. *BMC Cancer* 2011; 11:157.
21. Diaz JP, Gemignani ML, Pandit-Taskar N, et al. Sentinel lymph node biopsy in the management of early-stage cervical carcinoma. *Gynecol Oncol* 2011; 120:347–52.
22. Roy M, Bouchard-Fortier G, Popa I, et al. Value of sentinel node mapping in cancer of the cervix. *Gynecol Oncol* 2011; 122:269–74.

23. Lecuru F, Mathevet P, Querleu D, et al. Bilateral negative sentinel nodes accurately predict absence of lymph node metastasis in early cervical cancer: results of the SENTICOL study. *J Clin Oncol* 2011; 29:1686–91.
24. Plante M, Renaud MC, Tetu B, et al. Laparoscopic sentinel node mapping in early-stage cervical cancer. *Gynecol Oncol* 2003; 91:494–503.
25. van der Poel HG, Buckle T, Brouwer OR, et al. Intraoperative laparoscopic fluorescence guidance to the sentinel lymph node in prostate cancer patients: clinical proof of concept of an integrated functional imaging approach using a multimodal tracer. *Eur Urol* 2011; 60:826–33.

Chapter 4

Clinical trial of combined radio- and fluorescence-guided sentinel lymph node biopsy in breast cancer

Schaafsma BE¹, Verbeek FPR¹, Rietbergen DDD, van der Hiel B, van der Vorst JR, Liefers GJ, Fragnioni JV, van de Velde CJH, van Leeuwen FWB, Vahrmeijer AL

¹ Shared first authorship

British Journal of Surgery 2013;100:1037-1044

ABSTRACT

Background

Combining radioactive colloids and a near-infrared (NIR) fluorophore permits preoperative planning and intraoperative localization of deeply located sentinel lymph nodes (SLNs) with direct optical guidance by a single lymphatic tracer. The aim of this clinical trial was to evaluate and optimize a hybrid NIR fluorescence and radioactive tracer for SLN detection in patients with breast cancer.

Methods

Patients with breast cancer undergoing SLN biopsy were enrolled. The day before surgery, a periareolar injection of indocyanine green (ICG)– ^{99m}Tc -radiolabelled nanocolloid was administered and a lymphoscintigram acquired. Blue dye was injected immediately before surgery. Intraoperative SLN localization was performed using a gamma probe and the Mini-FLARETM NIR fluorescence imaging system. Patients were divided into two dose groups, with one group receiving twice the particle density of ICG and nanocolloid, but the same dose of radioactive ^{99m}Tc .

Results

Thirty-two patients were enrolled in the trial. At least one SLN was identified before and during operation. All 48 axillary SLNs could be detected by gamma tracing and NIR fluorescence imaging, but only 42 of them stained blue. NIR fluorescence imaging permitted detection of lymphatic vessels draining to the SLN up to 29 h after injection. Doubling the particle density did not yield a difference in fluorescence intensity (median 255 (range 98–542) versus 284 (90–921) arbitrary units; $P = 0.590$) or signal-to-background ratio (median 5.4 (range 3.0–15.4) versus 4.9 (3.5–16.3); $P = 1.000$) of the SLN.

Conclusion

The hybrid NIR fluorescence and radioactive tracer permitted accurate preoperative and intraoperative detection of the SLNs in patients with breast cancer. Registration number: NTR3685 (Netherlands Trial Register; <http://www.trialregister.nl>).

INTRODUCTION

Sentinel lymph node (SLN) biopsy is the standard of care for nodal staging in patients with breast cancer and clinically negative axillary lymph nodes.¹ To locate the SLNs, a combination of radioactive lymphatic tracers and blue dye staining is often preferred.^{2–5} Radioactive tracers permit preoperative planning and retention in the first-echelon nodes, whereas blue dye allows direct intraoperative visualization of the lymphatics and SLNs.

Optical imaging using near-infrared (NIR; 700–900 nm) fluorescence has been tested extensively for SLN detection in breast cancer and in other cancers, such as melanoma.^{6–15} The fluorescent tracer indocyanine green (ICG) is used for detection of SLNs up to several millimetres deep in tissue.^{16–18} This tracer has outperformed blue dye staining for SLN identification in multiple clinical trials.^{7,8,18,19} Nevertheless, radioactive colloids are still considered the standard of care for preoperative planning. Radioactive colloids are essential for localization of more deeply located SLNs, for example in patients with a higher body mass index (BMI).^{8,20}

To combine radioactive and NIR fluorescence guidance in one ‘package’, the hybrid tracer ICG–^{99m}Tc-labelled nanocolloid (ICG–^{99m}Tc-nanocolloid) has been developed.²¹ The fluorescent label ICG and the radioactive label ^{99m}Tc are integrated into the same colloidal particle. Unlike ‘free’ ICG, this nanoparticle is retained in the SLN for an extended period.²² The feasibility and validity of use of this tracer has been shown in various tumour types.^{23–25} However, it has not been studied in SLN biopsy procedures in patients with breast cancer.

The aim of this study was to evaluate the hybrid tracer for SLN detection in patients with breast cancer, and to assess the effect of increasing the particle density of the tracer on its nodal accumulation and the fluorescent signal intensity in the SLN.

METHODS

This clinical trial was approved by the medical ethics committee of Leiden University Medical Centre and performed in accordance with the ethical standards of the Helsinki Declaration of 1975. All patients with breast cancer scheduled for SLN biopsy between August 2011 and July 2012 were eligible to participate in the study. Included patients had clinically negative axillary nodes as assessed by palpation and ultrasonography. Exclusion criteria were pregnancy, lactation, or an allergy to iodine or ICG. Informed consent was given by all included patients and the acquired data were anonymized.

Tracer preparation

^{99m}Tc -labelled nanocolloid was prepared by adding sodium pertechnetate (approximately 1000 MBq) in 2 ml saline to a vial containing 0.5 mg human serum albumin nanocolloid (GE Healthcare, Eindhoven, The Netherlands). After 30 min of incubation at room temperature, 50 μl 6.4 mmol/l (0.25 mg) ICG (Pulsion Medical Systems, Munich, Germany) was dissolved in water for injection to obtain ICG- ^{99m}Tc -nanocolloid at a final ICG concentration of 160 $\mu\text{mol/l}$ and pH of 6.0–7.0.^{24,25} To obtain a twofold higher concentration of ICG-nanocolloid, ^{99m}Tc -labelled nanocolloid was prepared by adding pertechnetate (approximately 500 MBq) in 1 ml saline to 0.5 mg nanocolloid, while the amount of ICG (0.25 mg) was kept the same, resulting in a final ICG concentration of 320 $\mu\text{mol/l}$. This preparation resulted in doubling of the ICG and nanocolloid concentration, without changing the dose of radioactivity (approximately 100 MBq). All procedures were performed under current good manufacturing practice and under supervision of the institution's pharmacist.

Study design

The day before surgery, a periareolar injection of ICG- ^{99m}Tc -nanocolloid was given intracutaneously in the quadrant in which the tumour was located (at one site in a total volume 0.2 ml; 100 MBq). Patients were divided into groups with a low and high ICG- ^{99m}Tc -nanocolloid particle density; the first consecutive half of the patients were assigned to the low dose, and the second half to receive a twofold higher dose. Anterior, lateral and anterior oblique planar images were obtained at 15 min and approximately 3 h after injection, by the detector of a single- or two-headed gamma camera (Symbia T6, Siemens, Erlangen, Germany; or Toshiba GCA-7200PI/7200DI/7100UI, Toshiba, Tokyo, Japan). The percentage of tracer in the SLN was calculated from the anterior oblique images by dividing the counts in the SLN(s) by the sum of counts at the injection site and all lymph nodes. Simultaneously with the gamma-camera images, percutaneous NIR fluorescence images were acquired using the Mini-FLARETM NIR fluorescence imaging system, as described previously.²⁶ A SLN was defined as a lymph node on a direct lymphatic drainage pathway from the primary tumour as detected by lymphoscintigraphy.²⁷ During surgery lymph nodes with a gamma count of 10 per cent or more compared with the most radioactive SLN were also designated as SLNs.²⁸

Directly before surgery, a total of 1 ml patent blue dye (Bleu Patenté V; Guerbet, Brussels, Belgium) was injected at multiple sites around the areola. Gentle pressure was applied to the injection site for 1 min. The surgical field was illuminated using the white light source of the Mini-FLARETM imaging system. During surgical exploration, the combined radioactive and fluorescence signature of the SLNs defined

before surgery was visualized by means of a hand-held gamma probe (Europrobe, Euromedical Instruments, Le Chesnay, France) and the Mini-FLARE™.

The primary endpoint of the study was the SLN identification rate. Secondary endpoints were the number of SLNs identified per patient, the percentage of tracer accumulated in the SLN based on scintigraphy, the fluorescence intensity, and the fluorescence signal-to-background ratio (SBR) of the SLNs. The SBR of the SLN was calculated by dividing the fluorescence intensity of the SLN by the fluorescence intensity of the fatty tissue directly surrounding the SLN. Blue dye staining was used to provide additional optical guidance.

SLNs were fixed in formalin and embedded in paraffin for routine haematoxylin and eosin staining, and immunohistopathological staining for cytokeratin (AE1/AE3). This was done at three levels, with an interval of 150–250 µm, according to the Dutch guidelines for SLN analysis in breast cancer.

Statistical analysis

For statistical analysis, SPSS statistical software package (Version 20.0, Chicago, IL) was used. To compare categorical characteristics between the two groups of patients, the Fisher's Exact test was used for binary data and the chi-square test for non-binary data. Continuous data was tested for normal distribution using the Shapiro-Wilk test. Normal distributed continuous data (age and tumour size) was tested using the independent-sample t- test and not normally distributed data was tested using the Mann-Whitney test. Continuous data is presented as median and range. $P < 0.05$ was considered significant.

RESULTS

Thirty-two consecutive patients with breast cancer undergoing SLN biopsy were included in the study (Fig. 1). The median age was 56 (34–82) years and median BMI was 24 (18–39) kg/m². The first 16 patients were assigned to the low dose of ICG-^{99m}Tc-nanocolloid and the following 16 received the twofold higher dose. There were no differences in patient, tumour and treatment characteristics between the two treatment groups (Table 1). The median time between injection of ICG-^{99m}Tc-nanocolloid and surgery was 24 (19–29) and 22 (20–25) h for the low- and high-dose treatment groups respectively. Similar to the use of 'free' ICG,^{7,8,26} no adverse reactions were associated with the use of ICG-^{99m}Tc-nanocolloid.

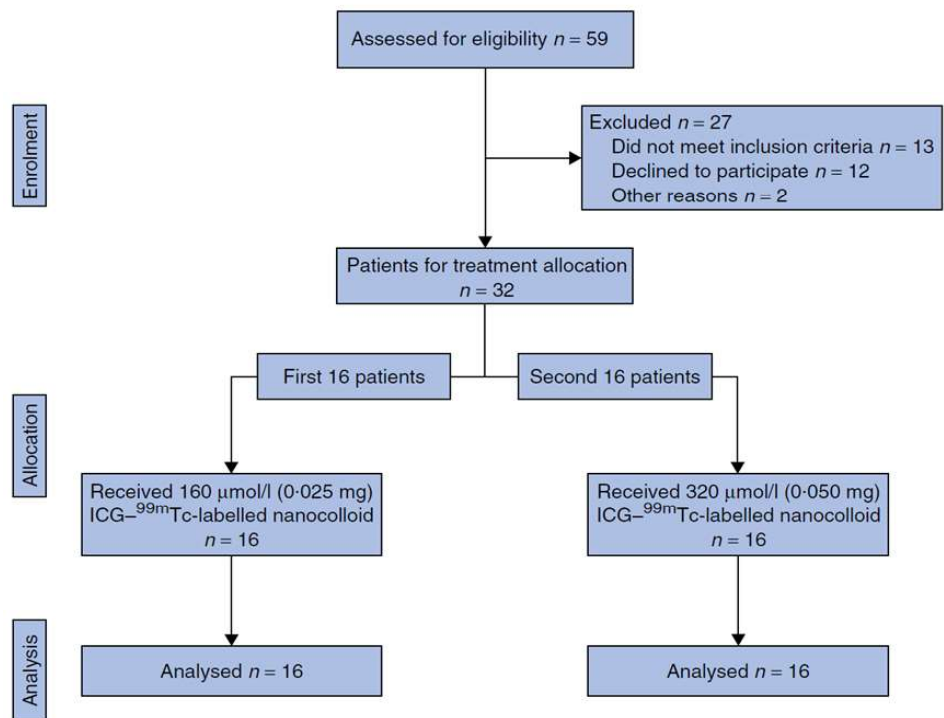


Fig. 1. Patient enrolment. ICG, indocyanine green

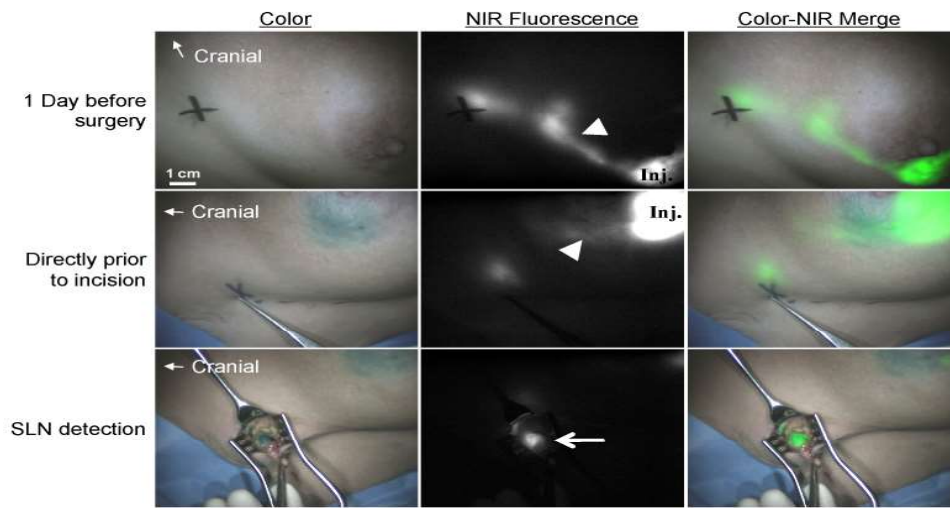


Fig. 2. Near-infrared (NIR) fluorescence imaging during sentinel lymph node (SLN) mapping in breast cancer. The periareolar injection site (inj.) and an afferent lymphatic channel (arrowhead) are clearly visualized the day before surgery (upper panel). Directly before surgery, patent blue is injected around the areola. The lymphatic channels (arrowhead) can still be visualized percutaneously using NIR fluorescence (middle panel). The SLN (arrow) is identified by NIR fluorescence and blue staining. The black cross indicates the presumed position of the SLN. Camera exposure times were 100 ms (upper and middle panels) and 40 ms (lower panel).

Table 1. Patient and tumour characteristics

Characteristic	Low-dose group (16 patients)	High-dose group (16 patients)	P
	N	N	
Age in years (median; range)	59 (44 – 82)	55 (34 – 77)	0.322
Body mass index, kg/m ² (median; range)	25 (21 – 39)	23 (18 – 37)	0.043
Previous breast procedure			0.635
Breast augmentation	1	1	
Lumpectomy	0	1	
Neoadjuvant hormonal / Chemotherapy	4	2	
Previous axillary surgery	0	0	
Multifocality	1	5	0.172
Type of Operation			0.458
Mastectomy	7	4	
Wide local excision	9	12	
Hours between injection and surgery (median; range)	24 (19 - 29)	22 (20 - 25)	0.196
Pathological tumour size in mm (median; range)	14 (3 – 34)	15 (4 – 30)	0.681
Histological type			0.717
Infiltrating ductal adenocarcinoma	13	13	
Infiltrating lobular adenocarcinoma	2	1	
Ductal Carcinoma In Situ (DCIS)	1	2	
Histological grade			0.058
I	2	3	
II	10	4	
III	1	7	
No grading possible (DCIS)	3	2	

Sentinel lymph node detection

Preoperative scintigraphy identified at least one SLN in all patients, with a median of 1 (1–2) per patient. All SLNs were located in the axilla. In 22 patients superficial lymph drainage could be at least partially visualized percutaneously by NIR fluorescence at the time of preoperative scintigraphy or before surgery (Fig. 2).

Surgical excision of the SLNs was guided by a combination of radioactivity and fluorescence. After initial guidance from the preoperative scintigram and the gamma probe, the axilla was explored using NIR fluorescence imaging. The gamma probe was used for additional intraoperative guidance only when NIR fluorescence did not directly point to the SLN. The results of the SLN biopsy procedures are summarized in Table 2. The NIR fluorescence-based detection of lymphatic vessels that drained to the SLN contributed to their identification (Fig. 3). At least one SLN was identified and resected in all patients. In addition to the SLNs detected by lymphoscintigraphy,

ten lymph nodes were considered as SLN during surgery, with a median of 1 (1–3) SLNs harvested from each patient. All 48 radioactive SLNs were detected by NIR fluorescence and the gamma probe, but only 42 of 48 SLNs stained blue. In all patients the NIR fluorescence signal in the SLN was detected before patent blue was visualized. Histological analysis of the SLNs showed lymph node metastases in 13 of 32 patients. Macrometastases (larger than 2 mm) were found in eight patients and isolated tumour cells or micrometastases (2 mm or smaller) in five.

Table 2. Results of sentinel lymph node identification

Characteristic	Total (32 patients)	Low-dose (16 patients)	High-dose (16 patients)	P
	N	N	N	
Preoperative SLN identification				
Identification rate	32 / 32	16 / 16	16 / 16	
Number of SLNs detected per patient (median; range)	1 (1 – 2)	1 (1 – 2)	1 (1 – 2)	0.564
Percutaneous fluorescence lymph drainage visualization	22 / 32	10 / 16	12 / 16	0.704
Intraoperative SLN identification				
Identification rate	32 / 32	16 / 16	16 / 16	
Total number of SLNs removed	48	21	27	
Method of intraoperative detection				
Radioactive	48 / 48	21 / 21	27 / 27	
Blue	42 / 48	17 / 21	25 / 27	0.383
Fluorescent	48 / 48	21 / 21	27 / 27	
Histology sentinel lymph node				0.686
Negative	19 / 32	10 / 16	9 / 16	
Micrometastases / ITC	5 / 32	3 / 16	2 / 16	
Macrometastases	8 / 32	3 / 16	5 / 16	

ITC; Isolated tumour cells, SLN; Sentinel lymph node

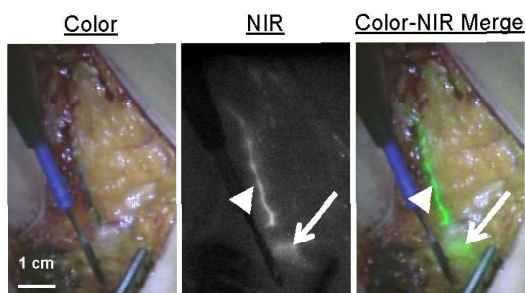


Fig. 3. Intraoperative detection of lymphatic vessels using near-infrared (NIR) fluorescence imaging. The lymphatic vessel (arrowhead) draining to the sentinel node (arrow) located more deeply in the tissue is clearly identified by NIR fluorescence

Comparison between treatment groups

The number of preoperative identified SLNs by radioscintigraphy was not different between the low dose group, median one (1 – 2), and high dose group, median one (1 – 2), $P = 0.564$. Despite doubling the particle density, the percentage of the amount of injected tracer accumulated in the SLN per patient based on the scintigraphy did not improve, median 1.7 (0.2 – 7.3) per cent vs. median 2.6 (0.4 – 30.4) per cent, $P = 0.402$. Nevertheless, the higher particle density group had SLNs that showed a higher accumulation of the tracer (Fig. 4). Between the groups no difference was observed in the amount of higher echelon nodes during lymphoscintigraphy.

Intraoperatively, the number of identified SLNs did not differ between the low dose group, median one (1 – 2), and high dose group, median one (1 – 3), $P = 0.323$. No significant difference was found for the fluorescence intensity, median 255 (98 – 542) vs. median 284 (90 – 921), $P = 0.590$ or signal-to-background ratio of the SLN, median 5.4 (3.0 – 15.4) vs. median 4.9 (3.5 – 16.3), $P = 1.000$, between the low dose group and higher dose group, respectively (Fig. 4).

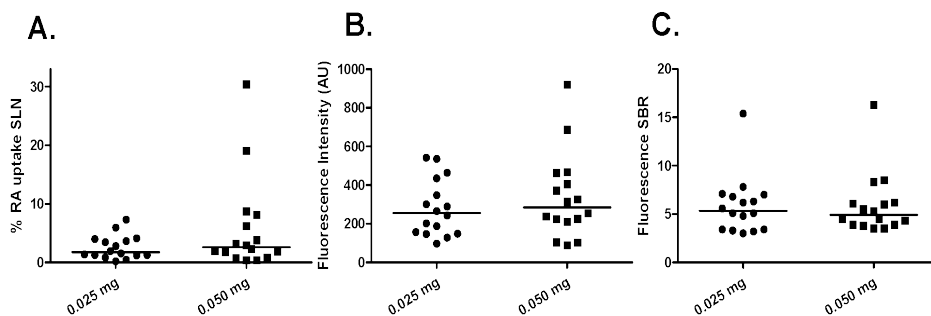


Fig. 4. Influence of indocyanine green-labelled nanocolloid dose on a percentage of radioactive injected dose of hybrid tracer in the sentinel lymph node (SLN) approximately 3 h after injection, b fluorescence intensity of the SLN measured during surgery and c fluorescence signal-to-background ratio (SBR) of the SLN during surgery. Circles represent individual patient values and the line indicates the median. AU, arbitrary units

DISCUSSION

The present study has shown that the use of ICG-^{99m}Tc-nanocolloid for SLN biopsy is feasible in patients with breast cancer. This tracer permits preoperative imaging and intraoperative guidance. By combining NIR fluorescence and radioactivity in a single tracer, discrepancies between the two imaging modalities used for SLN localization are less likely to occur. In the present study all SLNs could be detected surgically by both gamma radiation and NIR fluorescence imaging. Lymphatic vessels draining to the SLN were fluorescent the day after tracer administration and contributed to detection of the SLN.

In an attempt to optimize nodal accumulation of the tracer and the NIR fluorescence signal, a twofold higher particle density of ICG and nanocolloid was administered. In the higher-dose group, multiple outliers with greater accumulation of tracer in the SLN were observed, although there was no statistically significant increase in tracer accumulation. The results were similar for the fluorescence-based identification. In contrast to intratumoural tracer deposition²⁹, an increase in particle density does not appear to have a significant influence on SLN identification when periareolar administration is used. In the present study the dose of ^{99m}Tc was kept the same for both groups (100 MBq). Globally, different doses of ^{99m}Tc , varying from 10 to 370 MBq, are used for SLN detection.³⁰ As the lymphatic distribution of ICG- ^{99m}Tc -nanocolloid is mainly determined by the large nanocolloid particles, no significant differences in sensitivity of the fluorescence signal are to be expected when the amount of ^{99m}Tc is varied while maintaining the nanocolloid dose.

In previous studies using ICG alone, 25 times more ICG was injected during surgery.^{7,8} In addition, the volume of these injections was eight times higher, thereby increasing the interstitial fluid pressure and lymphatic drainage. These two factors contributed to a SBR of approximately nine.^{7,8} Here, a lower SBR (approximately six) was observed when ICG- ^{99m}Tc -nanocolloid was used. This decrease is relatively small because the lower dose and smaller injection volume of ICG was probably offset by the longer time between injection and imaging, which would have aided in the concentration of ICG in the SLN. Importantly, this decrease did not influence surgical guidance, as ICG- ^{99m}Tc -nanocolloid permitted accurate SLN identification during surgery in all these patients and lymphatic vessels were still clearly visible.

In the present study 42 of 48 SLNs stained blue, which is comparable to the identification rate of blue dye in large multicentre studies.³ NIR fluorescence identified more SLNs than blue dye staining and detected SLNs that were more deeply located in the tissue. Similar results were obtained in previous studies^{7,26}, and blue dye showed no benefit when NIR fluorescence imaging was used.⁸ When ICG- ^{99m}Tc -nanocolloid is used and blue dye omitted, no lymphatic tracer has to be injected directly before surgery; this, combined with the enhanced detection by NIR fluorescence compared with blue dyes, can improve logistics and reduce the duration of surgery.

Various techniques are being evaluated to improve the depth penetration of NIR fluorescence contrast agents^{31,32} and to study when radioactivity can be omitted.⁸ If in the future depth penetration of NIR fluorescence contrast agents can be increased, radioactive colloids may possibly be omitted, thereby improving logistics and costs. At present, NIR fluorescence is mainly used in addition to radioactive colloids. Widespread clinical dissemination of this technique requires a cost-effective approach. ICG- ^{99m}Tc -nanocolloid is based on a lymphatic tracer that is in regular use in Europe and only needs addition of a small amount (0.025 mg) of ICG, at a cost of

approximately €50–80 for 25 mg. A variety of relatively low-cost commercial camera systems are already available for clinical use.³³

The hybrid optical–nuclear agent ICG-^{99m}Tc-nanocolloid has been used successfully as a tracer for image-guided SLN biopsy in patients with breast cancer. Use of ICG-^{99m}Tc-nanocolloid provides fully integrated preoperative and intraoperative radioactive and NIR fluorescence guidance, with no need for an injection immediately before surgery, producing intraoperative findings comparable to those provided by use of ICG alone. As no difference was observed between the two ICG-^{99m}Tc-nanocolloid doses, a particle density of 160 µmol/l ICG-^{99m}Tc-nanocolloid injected in a volume of 200 µl the day before surgery could be recommended.

ACKNOWLEDGMENTS

The authors thank G. Ranke, E. Krol-Warmerdam (Breast Cancer Unit), K. Schimmel (Central Pharmacy) and H. Putter (Medical Statistics) for their contribution to this study, and D. Burrington Jr for editing.

This work was supported in part by National Institutes of Health (grants R01-CA-115296 and R21-CA-130297), the Dutch Cancer Society (grants UL2010-4732 and PGF 2009-4344), and a VIDI grant from the Dutch national research council (NWO-STW-11272). This research was performed within the framework of the Centre for Translational Molecular Medicine, project MUSIS (grant 03O-202). J.R.v.d.V. is an MD-medical research trainee funded by the Netherlands Organization for Health Research and Development (grant 92003593).

REFERENCES

1. Cox CE, Pendas S, Cox JM, et al. Guidelines for sentinel node biopsy and lymphatic mapping of patients with breast cancer. *Ann Surg* 1998; 227:645–651.
2. Goyal A, Newcombe RG, Chhabra A, et al. ALMANAC Trialists Group. Factors affecting failed localisation and false negative rates of sentinel node biopsy in breast cancer – results of the ALMANAC validation phase. *Breast Cancer Res Treat* 2006; 99: 203–208.
3. Krag DN, Anderson SJ, Julian TB, et al. National Surgical Adjuvant Breast and Bowel Project. Technical outcomes of sentinel-lymph-node resection and conventional axillary-lymph-node dissection in patients with clinically node-negative breast cancer: results from the NSABP B-32 randomised phase III trial. *Lancet Oncol* 2007; 8: 881–888.
4. Zavagno G, De Salvo GL, Scalco G, et al. GIVOM Trialists. A randomized clinical trial on sentinel lymph node biopsy versus axillary lymph node dissection in breast cancer: results of the Sentinella/GIVOM trial. *Ann Surg* 2008; 247: 207–213.
5. Straver ME, Meijnen P, van Tienhoven G, et al. Sentinel node identification rate and nodal involvement in the EORTC 10981–22023 AMAROS trial. *Ann Surg Oncol* 2010; 17: 1854–1861.
6. Schaafsma BE, Mieog JS, Hutteman M, et al. The clinical use of indocyanine green as a near-infrared fluorescent contrast agent for image-guided oncologic surgery. *J Surg Oncol* 2011; 104: 323–332.
7. Hutteman M, Mieog JS, van der Vorst JR, et al. Randomized, double-blind comparison of indocyanine green with or without albumin premixing for near-infrared fluorescence imaging of sentinel lymph nodes in breast cancer patients. *Breast Cancer Res Treat* 2011; 127: 163–170.
8. van der Vorst JR, Schaafsma BE, Verbeek FP, et al. Randomized comparison of near-infrared fluorescence imaging using indocyanine green and 99(m) technetium with or without patent blue for the sentinel lymph node procedure in breast cancer patients. *Ann Surg Oncol* 2012; 19: 4104–4111.
9. Abe H, Mori T, Umeda T, et al. Indocyanine green fluorescence imaging system for sentinel lymph node biopsies in early breast cancer patients. *Surg Today* 2011; 41: 197–202.
10. Kitai T, Kawashima M. Transcutaneous detection and direct approach to the sentinel node using axillary compression technique in ICG fluorescence-navigated sentinel node biopsy for breast cancer. *Breast Cancer* 2011; 19: 343–348.
11. Hirche C, Mohr Z, Kneif S, et al. High rate of solitary sentinel node metastases identification by fluorescence-guided lymphatic imaging in breast cancer. *J Surg Oncol* 2012; 105: 162–166.
12. Polom K, Murawa D, Nowaczyk P, et al. Breast cancer sentinel lymph node mapping using near infrared guided indocyanine green and indocyanine green–human serum albumin in comparison with gamma emitting radioactive colloid tracer. *Eur J Surg Oncol* 2012; 38: 137–142.
13. Hirano A, Kamimura M, Ogura K, et al. A comparison of indocyanine green fluorescence imaging plus blue dye and blue dye alone for sentinel node navigation surgery in breast cancer patients. *Ann Surg Oncol* 2012; 19: 4112–4116.
14. Wishart GC, Loh SW, Jones L, et al. A feasibility study (ICG-10) of indocyanine green (ICG) fluorescence mapping for sentinel lymph node detection in early breast cancer. *Eur J Surg Oncol* 2012; 38: 651–656.
15. Aoyama K, Kamio T, Ohchi T, et al. Sentinel lymph node biopsy for breast cancer patients using fluorescence navigation with indocyanine green. *World J Surg Oncol* 2011; 9: 157.
16. Murawa D, Hirche C, Dresel S, et al. Sentinel lymph node biopsy in breast cancer guided by indocyanine green fluorescence. *Br J Surg* 2009; 96: 1289–1294.
17. Frangioni JV. In vivo near-infrared fluorescence imaging. *Curr Opin Chem Biol* 2003; 7: 626–634.
18. Fujisawa Y, Nakamura Y, Kawachi Y, et al. Indocyanine green fluorescence-navigated sentinel node biopsy showed higher sensitivity than the radioisotope or blue dye method, which may help to reduce false-negative cases in skin cancer. *J Surg Oncol* 2012; 106: 41–45.
19. Hojo T, Nagao T, Kikuyama M, et al. Evaluation of sentinel node biopsy by combined fluorescent and dye method and lymph flow for breast cancer. *Breast* 2010; 19: 210–213.

20. Nos C, Freneaux P, Guilbert S, et al. Sentinel lymph node detection for breast cancer: which patients are best suited for the patent blue dye only method of identification? *Ann Surg Oncol* 2001; 8: 438–443.
21. Buckle T, van Leeuwen AC, Chin PT, et al. A self-assembled multimodal complex for combined pre- and intraoperative imaging of the sentinel lymph node. *Nanotechnology* 2010; 21: 355101.
22. van Leeuwen AC, Buckle T, Bendle G, et al. Tracer-cocktail injections for combined pre- and intraoperative multimodal imaging of lymph nodes in a spontaneous mouse prostate tumor model. *J Biomed Opt* 2011; 16: 016004.
23. van der Poel HG, Buckle T, Brouwer OR, et al. Intraoperative laparoscopic fluorescence guidance to the sentinel lymph node in prostate cancer patients: clinical proof of concept of an integrated functional imaging approach using a multimodal tracer. *Eur Urol* 2011; 60: 826–833.
24. Brouwer OR, Buckle T, Vermeeren L, et al. Comparing the hybrid fluorescent–radioactive tracer indocyanine green–^{99m}Tc-nanocolloid with ^{99m}Tc-nanocolloid for sentinel node identification: a validation study using lymphoscintigraphy and SPECT/CT. *J Nucl Med* 2012; 53:1034–1040.
25. Brouwer OR, KlopWM, Buckle T, et al. Feasibility of sentinel node biopsy in head and neck melanoma using a hybrid radioactive and fluorescent tracer. *Ann Surg Oncol* 2011; 19:1988–1994.
26. Mieog JS, Troyan SL, Hutteman M, et al. Toward optimization of imaging system and lymphatic tracer for near-infrared fluorescent sentinel lymph node mapping in breast cancer. *Ann Surg Oncol* 2011; 18: 2483–2491.
27. Nieweg OE, Tanis PJ, Kroon BB. The definition of a sentinel node. *Ann Surg Oncol* 2001; 8: 538–541.
28. Chung A, Yu J, Stempel M, Patil S, et al. Is the ‘10% rule’ equally valid for all subsets of sentinel-node-positive breast cancer patients? *Ann Surg Oncol* 2008; 15: 2728–2733.
29. Valdes Olmos RA, Tanis PJ, Hoefnagel CA, et al. Improved sentinel node visualization in breast cancer by optimizing the colloid particle concentration and tracer dosage. *Nucl Med Commun* 2001; 22: 579–586.
30. Mariani G, Erba P, Villa G, et al. Lymphoscintigraphic and intraoperative detection of the sentinel lymph node in breast cancer patients: the nuclear medicine perspective. *J Surg Oncol* 2004; 85: 112–122.
31. Kim C, Erpelding TN, Maslov K, et al. Handheld array-based photoacoustic probe for guiding needle biopsy of sentinel lymph nodes. *J Biomed Opt* 2010; 15: 046010.
32. Gioux S, Mazhar A, Cuccia DJ, et al. Three-dimensional surface profile intensity correction for spatially modulated imaging. *J Biomed Opt* 2009; 14: 034045.
33. van den Berg NS, van Leeuwen FW, van der Poel HG. Fluorescence guidance in urologic surgery. *Curr Opin Urol* 2012; 22: 109–120.

Chapter 5

Ex vivo sentinel node mapping in colon cancer combining blue dye staining and fluorescence imaging

Schaafsma BE, Verbeek FPR, van der Vorst JR, Hutteman M, Kuppen PJK, Frangioni JV, van de Velde CJH, Vahrmeijer AL

Journal of Surgical Research 2013;183:253-257

ABSTRACT

Background

The sentinel lymph node procedure has been proposed to improve nodal staging in colon cancer patients. The aim of this study was to assess the added value of near-infrared (NIR) fluorescence imaging to conventional blue dye staining for ex vivo sentinel lymph node mapping.

Materials and methods

We included 22 consecutive patients undergoing surgery for colon cancer. After tumour resection, we submucosally injected a premixed cocktail of the near-infrared lymphatic tracer HSA800 and blue dye around the tumour for detection of sentinel lymph nodes. We used the Mini-FLARE imaging system for fluorescence imaging.

Results

In 95% of patients, we identified at least one sentinel lymph node. Overall, a total of 77 sentinel lymph nodes were identified, 77 of which were fluorescent (100%) and 70 of which were blue (91%). Sentinel lymph nodes that were located deeper in the mesenteric fat could easily be located by NIR fluorescence. In four of five patients with lymph node metastases, tumour cells were present in at least one of the sentinel lymph nodes.

Conclusions

This study shows the successful use and added value of the NIR fluorescence tracer HSA800 to conventional blue dye for the ex vivo sentinel lymph node procedure in colon cancer.

INTRODUCTION

Colorectal cancer is the third most common cancer and remains a major public health issue because of its high prevalence, morbidity, and mortality.¹ Complete surgical removal with en bloc regional lymphadenectomy is pivotal for patient staging and prognosis. Lymph node status is of major importance in proper clinicopathologic staging and determines the need for adjuvant chemotherapy. Although surgery is often considered curative in node-negative disease, approximately 20%-30% of these patients will develop disease recurrence.^{1,2} This is most likely caused by understaging during the initial procedure.

Correct nodal staging depends on multiple factors, including number of examined nodes.³ Moreover, occult tumour cells and micrometastases are easily missed by conventional histopathologic examination. Various retrospective studies have shown poor prognosis for patients with micrometastases compared with patients without metastases.^{4,5} Multiple clinical trials are currently ongoing in which patients with micrometastatic disease are treated with adjuvant chemotherapy, which is currently not considered for this indication.⁶ However, detection of micrometastases often requires ultrastaging techniques for each lymph node using serial sectioning and additional immunohistochemistry or reverse transcriptase-polymerase chain reaction.^{7,8} However, this is currently beyond standard histopathologic analysis and is time consuming, and expensive. To overcome this disadvantage, the sentinel lymph node (SLN) procedure for colon cancer patients has been evaluated extensively.⁹

Sentinel lymph nodes are the first lymph nodes that receive lymphatic drainage from the tumour, and identification of the SLN and analysis for tumour involvement could predict the tumour status of the remaining lymph nodes. Therefore, the SLN procedure in colon cancer can be a useful tool to select the nodes for ultrastaging.⁴ In colon cancer patients, both blue dyes and radiotracers have been used as SLN tracers in an in vivo and ex vivo setting.⁹ However, both have disadvantages. The use of gamma ray emitting radiotracers requires involvement of a nuclear medicine physician, and localization requires a handheld gammaprobe, which does not permit real-time visualization. Also, preoperative access to the injection site is often required, which in colon cancer patients requires endoscopic injection. Blue dyes cannot be easily seen through fatty tissue and can easily diffuse through the true SLN to second- to third-tier nodes because of their small size.

Recently, optical imaging using near-infrared (NIR) fluorescence has been introduced for real-time visualization of structures during surgery. Advantages of NIR fluorescent (700-900 nm) light include high tissue penetration (several millimeters) and low autofluorescence of tissue in this wavelength region, thereby providing high contrast. To date, indocyanine green is the only clinically available NIR fluorescent tracer and has been used with success for the SLN procedure in several types of cancer including gastrointestinal cancer.¹⁰⁻¹⁸ However, because of relative low fluorescence

brightness (quantum yield) and poor SLN retention, indocyanine green is not an ideal SLN tracer.¹⁹ To improve retention of the NIR tracer in the SLN, conjugation of an NIR fluorescent dye, such as IRDye 800CW, to a larger molecule, such as human serum albumin (HSA; complex: HSA800) is recommended.¹⁹ However, because HSA800 is not yet clinically approved, it can only be used for ex vivo SLN mapping. Previously, our group used HSA800 successfully ex vivo in a feasibility study with patients with colon cancer, and we were able to identify SLNs in all patients.²⁰ However, in our earlier study we used no blue dye staining because blue dyes might interfere with NIR fluorescence imaging by absorbing the fluorescent light and thereby decreasing the identification rate. At present, blue dye staining is frequently used for the ex vivo SLN procedure, and blue dye staining also provides visual information, which could make it easier to identify and resect SLNs. The aims of this study were to assess the feasibility of the combined use of NIR fluorescence using HSA800 and blue dye staining, and to assess the added value of NIR fluorescence to blue dye staining for SLN mapping in colon cancer patients.

MATERIALS AND METHODS

Preparation of lymphatic tracers

The preparation of HSA800 (IRDye 800CW conjugated to HSA) has been described in detail previously.¹⁹ Briefly, after conjugation of CW800-NHS to albumin, we purified HSA800 using a 7K Zeba Spin Desalting Column (Thermo Scientific, Rockford, IL). The ratio of fluorophore (IRDye 800CW; Li-Cor, Lincoln, NE) to albumin (HSA) was 1.5:1, estimated using the extinction coefficients of HSA ($\epsilon_{280\text{nm}} = 32,900 \text{ mol/L}\cdot\text{1cm}^{-1}$) and CW800 ($\epsilon_{778\text{nm}} = 240,000 \text{ mol/L}\cdot\text{1cm}^{-1}$) in phosphate buffered saline, with a stock concentration of approximately 600 $\mu\text{mol/L}$. Peak absorbance and emission of HSA800 were 778 and 795 nm, respectively. To obtain a solution of 50 $\mu\text{mol/L}$ HSA800, we diluted 50 nmol HSA800 in 1 mL patent blue (Bleu Patente V; Guerbet, Brussels, Belgium) before injection.

Intraoperative NIR imaging system (Mini-FLARE)

We performed clinical SLN mapping using the Mini-FLARE imaging system, which has been described in detail elsewhere.^{21,22} Briefly, the system consists of two wavelength isolated light sources: a white light source, generating 26,600 lx of 400- to 650-nm light and an NIR light source, generating 7.7 mW/cm² of 760-nm light. Color video and NIR fluorescence images are simultaneously acquired and displayed in real time using custom optics and software that separate the color video and NIR fluorescence images. A pseudo-colored (lime green) merged image of the color video and NIR fluorescence

images is also displayed. The imaging head is attached to a flexible gooseneck arm, which permits positioning of the imaging head virtually anywhere over the surgical field and at extreme angles.

Table 1. Patient and tumour characteristics

Characteristic	N	%
Gender		
Male	12	55
Female	10	45
Age (median, range)	69 (41 – 88)	
Body mass index (median, range)	25 (20 – 40)	
Tumour size (cm; median, range)	3.7 (0.9 – 9.0)	
Tumour location		
Cecum	3	13
Ascending colon	9	41
Transverse colon	1	5
Sigmoid colon	9	41
Tumour differentiation		
Well	1	5
Moderately	17	77
Poorly	4	18
Tumour invasion		
T1	2	9
T2	7	32
T3	10	46
T4	3	13

Clinical trial

We enrolled 22 consecutive patients undergoing surgery with curative intent for colon cancer. Patients with known metastatic disease were excluded. The Leiden University Medical Center Medical Ethics Committee approved this study, which we performed in accordance with the Declaration of Helsinki. All known patients underwent a standard oncological resection including a segmental colonic resection and lymphadenectomy. Tumours were endoscopically marked before surgery when indicated. Directly after resection, the resection specimen was freshly delivered to the Department of Pathology, where the specimen was opened antimesenterically by the pathologist. Subsequently, 1 mL of 50 µmol/L HSA800 diluted in patent blue was injected submucosally circumferentially with a 5-mm margin around the tumour. The injection site was massaged for 5 min, which has been proven sufficient to secure drainage to the SLN in both an in vivo and ex vivo setting.²⁰ After 5 min, the specimen was inspected using the Mini-FLARE camera system and by visual inspection. We allocated all fluorescent hotspots as SLN and noted whether these nodes were stained blue. The SLNs were separately fixated in 2% buffered formalin for 24 h. After

fixation, we harvested all remaining lymph nodes from the specimen and paraffin-embedded all lymph nodes (sentinel and nonsentinel); 4-mm sections were stained with hematoxylin-eosin and subsequently analyzed microscopically for the presence of tumour cells.

Table 2. Results of sentinel lymph node procedure

Characteristic	N	%
Detection rate	21	95
SLNs detected per patient		
0	1	5
1	3	13
2	2	9
3	6	28
4	3	13
5	4	18
6	1	5
7	2	9
>7	0	0
Method of detection		
Fluorescence and blue staining	70	91
Fluorescence only	7	9
Number of total dissected nodes (median, range)	21 (11 – 38)	
Histology		
Negative	17	77
Positive	5	23
False negatives	1	20

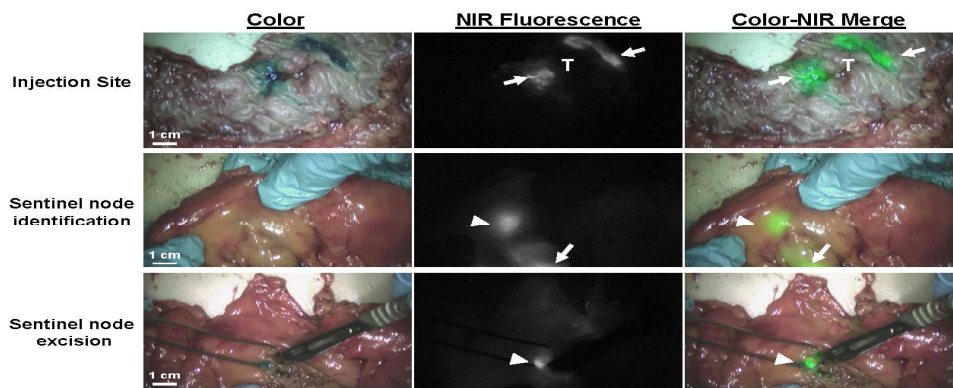


Fig. Sentinel lymph node mapping using NIR fluorescence and blue dye in colon cancer. (Upper) Peritumoural submucosal injection (arrows) of 1.0 mL of 50 μ mol/L HSA800 and patent blue. (Middle) Identification of the SLN (arrowheads) by NIR fluorescence located in the mesenteric fat near the injection site (arrows). The NIR fluorescence signal is scattered (i.e., blurred) by the mesenteric fat covering the node. (Lower) After incision of the mesentery by the pathologist, a clear blue and fluorescent SLN (arrowhead) can be identified. Camera exposure times were 25 ms (upper panel), 100 ms (middle panel), and 67 ms (lower panel). Scale bars = 1 cm.

RESULTS

We enrolled 22 consecutive patients undergoing surgery for colon cancer. Table 1 lists patient and tumour characteristics. Of these 22 patients, the median age was 69 y (range, 41-88 y); median body mass index was 25 kg/m² (range, 20-40 kg/m²). A total of 12 patients were male. Tumour invasion ranged from stage T1 to T4. The median tumour size was 3.7 cm (range, 0.9-9 cm). Four patients had a poorly differentiated tumour, 17 patients had a moderately differentiated tumour, and one had a well-differentiated tumour. Twelve patients received preoperative endoscopic tattooing of the tumour.

After administration of the lymphatic tracer cocktail, at least one SLN was identified in 21 of 22 patients (95%) (Table 2). Sentinel lymph nodes that were located deeper in the mesenteric fat could easily be located by NIR fluorescence but not with the blue dye. After the pathologist subsequently incised the mesentery, in most cases, blue staining of the lymph node was also detected, which provided the pathologist with direct visual support (Fig.). On average, 3.5 ± 1.9 SLNs/patient were identified. Overall, a total of 77 SLNs were identified, of which 77 (100%) were fluorescent and 70 (91%) were blue (Pearson's correlation coefficient, 0.94). In five patients, fluorescent SLNs were identified (average 1.4 ± 0.5 nodes/patient) that were not stained blue. A total (sentinel and nonsentinel) of 20.5 ± 8.1 nodes were harvested on average from each specimen. Standard histologic analysis showed that five of 22 patients had lymph node metastases. In all but one of these five patients, tumour cells were present in at least one of the SLNs. The false-negative (neither fluorescent nor blue) lymph node was almost completely filled with tumour cells and was easily detected by the pathologist.

DISCUSSION

Nodal status in colon cancer is the most important prognostic factor, which makes it crucial in deciding whether a patient should be considered for adjuvant treatment. Therefore, the main purpose of the SLN procedure in colon cancer patients is the selection of lymph nodes to be assessed by ultrastaging techniques. The current study shows the successful use of NIR fluorescence imaging in combination with blue dye during ex vivo SLN mapping in colon cancer. The NIR fluorescent tracer HSA800 permitted detection of the SLN located deeper into the mesenteric fat. The detection rate of 95% in this study is in concordance with previously reported detection rates in SLN mapping using radiotracers, blue dyes, or a combination of both.⁹

This is the first study in which an NIR fluorescent tracer is used in combination with conventional blue dye staining, which is most commonly used as lymphatic tracer, in the ex vivo SLN procedure. Because NIR fluorescence imaging is capable of penetrating millimeters into tissue, it allowed identification of small amounts of the lymphatic tracer deeper into the mesenteric fatty tissue. Moreover, owing to the high spatial resolution of NIR fluorescence, we observed no interference between the fluorescent signal of the injection site and SLNs. We premixed HSA800 with patent blue, and we therefore anticipated staining the same nodes NIR fluorescent and blue. Indeed, there was a high correlation between identification using fluorescence and identification using blue dye staining. However, several fluorescent nodes (9%) did not stain blue. Possible explanations could be the high sensitivity of NIR fluorescence imaging, which allows detection of low concentrations of the tracer, and dilution of the blue dye to concentrations not visible with the human eye.²³⁻²⁵ Because there appears to be little interference of blue dye with NIR fluorescence, in most cases blue staining could be used as complementary direct visual support to assist the pathologist in resecting the SLNs.

Preoperative tattooing of the tumour, which is mostly used for tumour localization during laparoscopic surgery, can result in staining of lymph nodes and has been suggested for SLN mapping.²⁶⁻²⁹ In the current study, multiple patients received preoperative endoscopic tattooing of the tumour, which resulted in multiple blue colored nodes before the SLN procedure. Because it appeared to be difficult to differentiate between staining by endoscopic tattooing and patent blue staining, the blue dye staining could be less reliable for detecting the first echelon nodes in the current study. Therefore, in patients who received preoperative endoscopic tattooing, the use of NIR fluorescence imaging could overcome these problems.

One false-negative case occurred out of five patients with nodal metastases, which is in concordance with other, earlier studies.^{9,30} In the current study, we identified the SLNs approximately 15 min after injection of HSA800, which adds extra time to the standard workup. In addition, identification of the SLN can be difficult, because not all lymph nodes can be exposed. Identification of SLNs after fixation would allow the pathologist to identify the SLN during routine practice. When SLN detection is performed several hours after injection, optimal retention of the lymphatic tracer in the SLN tracer is essential. However, HSA800 still migrates to higher-echelon lymph nodes, albeit slower than small molecules such as patent blue.¹⁹ When improved retention in the SLN is wanted, nanocolloidal albumin combined with fluorescence can be used, which provides optimal retention in the SLN because of its favorable large hydrodynamic diameter and charge.^{19,31-33} Moreover, rather than being only potentially useful for pathologic staging, in vivo SLN mapping has been suggested for patient-tailored extent of surgery.^{11,34,35} Clinical approval of HSA800 would also allow in vivo NIR fluorescence SLN mapping using this tracer.

This study demonstrated the successful use of a combination of an NIR fluorescence tracer and a conventional blue dye for the ex vivo SLN detection in colon cancer, which can be used as a tool to select the nodes for ultrastaging techniques to identify micrometastases and improve nodal staging. NIR fluorescence was of added value compared with blue dye staining, because NIR fluorescence allowed detection of additional SLNs and easy detection of SLNs located deeper into the mesenteric fat. Moreover, NIR fluorescence cannot be confused with blue nodal staining resulting from preoperative tattooing of the tumour.

ACKNOWLEDGMENTS

The authors thank Lindsey Gendall for editing. This work was supported in part by NIH Grants R01-CA-115296 and R21-CA-130297 and Dutch Cancer Society Grant UL2010-4732. This research was performed within the framework of the Center for Translational Molecular Medicine, project DeCoDe (Grant 03O-101). Joost van der Vorst is an MD-medical research trainee funded by The Netherlands Organisation for Health Research and Development (Grant 92003593).

REFERENCES

1. Iddings D, Ahmad A, Elashoff D, et al. The prognostic effect of micrometastases in previously staged lymph node negative (N0) colorectal carcinoma: a meta-analysis. *Ann Surg Oncol* 2006;13:1386.
2. Nicastrì DG, Doucette JT, Godfrey TE, et al. Is occult lymph node disease in colorectal cancer patients clinically significant? A review of the relevant literature. *J Mol Diagn* 2007;9:563.
3. Govindarajan A, Baxter NN. Lymph node evaluation in early stage colon cancer. *Clin Colorectal Cancer* 2008;7:240.
4. Sirop S, Kanaan M, Korant A, et al. Detection and prognostic impact of micrometastasis in colorectal cancer. *J Surg Oncol* 2011;103:534.
5. Doekhie FS, Mesker WE, Kuppen PJ, et al. Detailed examination of lymph nodes improves prognostication in colorectal cancer. *Int J Cancer* 2010;126:2644.
6. Lips DJ, Koebrugge B, Liefers GJ, et al. The influence of micrometastases on prognosis and survival in stage I-II colon cancer patients: the Enroute plus sign in circle study. *BMC Surg* 2011;11:11.
7. Cutait R, Alves VA, Lopes LC, et al. Restaging of colorectal cancer based on the identification of lymph node micrometastases through immunoperoxidase staining of CEA and cytokeratins. *Dis Colon Rectum* 1991;34:917.
8. Liefers GJ, Cleton-Jansen AM, van de Velde CJ, et al. Micrometastases and survival in stage II colorectal cancer. *N Engl J Med* 1998;339:223.
9. van der Pas MH, Meijer S, Hoekstra OS, et al. Sentinel-lymphnode procedure in colon and rectal cancer: a systematic review and meta-analysis. *Lancet Oncol* 2011;12:540.
10. Ankersmit M, van der Pas MH, van Dam DA, et al. Near infrared fluorescence lymphatic laparoscopy of the colon and mesocolon. *Colorectal Dis* 2011;13(Suppl 7):70.
11. Cahill RA, Anderson M, Wang LM, et al. Near-infrared (NIR) laparoscopy for intraoperative lymphatic road-mapping and sentinel node identification during definitive surgical resection of early stage colorectal neoplasia. *Surg Endosc* 2012;26:197.
12. Hirche C, Mohr Z, Kneif S, et al. Ultrastaging of colon cancer by sentinel node biopsy using fluorescence navigation with indocyanine green. *Int J Colorectal Dis* 2012;27:319.
13. Schaafsma BE, Mieog JS, Hutteman M, et al. The clinical use of indocyanine green as a near-infrared fluorescent contrast agent for image-guided oncologic surgery. *J Surg Oncol* 2011;104:323.
14. Crane LM, Themelis G, Arts HJ, et al. Intraoperative near-infrared fluorescence imaging for sentinel lymph node detection in vulvar cancer: first clinical results. *Gynecol Oncol* 2011;120:291.
15. van der Vorst JR, Hutteman M, Gaarenstroom KN, et al. Optimization of near-infrared fluorescent sentinel lymph node mapping in cervical cancer patients. *Int J Gynecol Cancer* 2011;21:1472.
16. Mieog JS, Vahrmeijer AL, Hutteman M, et al. Novel intraoperative near-infrared fluorescence camera system for optical image-guided cancer surgery. *Mol Imaging* 2010;9:223.
17. Fujiwara M, Mizukami T, Suzuki A, et al. Sentinel lymph node detection in skin cancer patients using real-time fluorescence navigation with indocyanine green: preliminary experience. *J Plast Reconstr Aesthet Surg* 2009;62:e373.
18. Kusano M, Tajima Y, Yamazaki K, et al. Sentinel node mapping guided by indocyanine green fluorescence imaging: a new method for sentinel node navigation surgery in gastrointestinal cancer. *Dig Surg* 2008; 25:103.
19. Ohnishi S, Lomnes SJ, Laurence RG, et al. Organic alternatives to quantum dots for intraoperative near-infrared fluorescent sentinel lymph node mapping. *Mol Imaging* 2005;4:172.
20. Hutteman M, Choi HS, Mieog JS, et al. Clinical translation of ex vivo sentinel lymph node mapping for colorectal cancer using invisible near-infrared fluorescence light. *Ann Surg Oncol* 2011;18:1006.
21. Mieog JS, Troyan SL, Hutteman M, et al. Towards optimization of imaging system and lymphatic tracer for near-infrared fluorescent sentinel lymph node mapping in breast cancer. *Ann Surg Oncol* 2011;18:2483.

22. Troyan SL, Kianzad V, Gibbs-Strauss SL, et al. The FLARE intraoperative near-infrared fluorescence imaging system: a first-in-human clinical trial in breast cancer sentinel lymph node mapping. *Ann Surg Oncol* 2009;16:2943.
23. Murawa D, Hirche C, Dresel S, et al. Sentinel lymph node biopsy in breast cancer guided by indocyanine green fluorescence. *Br J Surg* 2009;96:1289.
24. Frangioni JV. In vivo near-infrared fluorescence imaging. *Curr Opin Chem Biol* 2003;7:626.
25. Fujisawa Y, Nakamura Y, Kawachi Y, et al. Indocyanine green fluorescence-navigated sentinel node biopsy showed higher sensitivity than the radioisotope or blue dye method, which may help to reduce false-negative cases in skin cancer. *J Surg Oncol* 2012;16:41.
26. Dawson K, Wiebusch A, Thirlby RC. Preoperative tattooing and improved lymph node retrieval rates from colectomy specimens in patients with colorectal cancers. *Arch Surg* 2010;145:826.
27. Viehl CT, Guller U, Hamel CT, et al. Carbon dye staining of sentinel lymph nodes facilitates microstaging of colon cancer patients. *World J Surg* 2006;30:453.
28. Spatz H, Probst A, Oruzio D, et al. Sentinel lymph node mapping as a side-effect of colonoscopic tattooing. *Surg Endosc* 2010;24:589.
29. Cahill RA, Lindsey I, Cunningham C. Sentinel node mapping by colonic tattooing. *Surg Endosc* 2010;24:2365.
30. Cahill RA, Leroy J, Marescaux J. Could lymphatic mapping and sentinel node biopsy provide oncological providence for local resectional techniques for colon cancer? A review of the literature. *BMC Surg* 2008;8:17.
31. Heuveling DA, Visser GW, de GM, et al. Nanocolloidal albumin-IRDye 800CW: a near-infrared fluorescent tracer with optimal retention in the sentinel lymph node. *Eur J Nucl Med Mol Imaging* 2012;39:1161.
32. van der Poel HG, Buckle T, Brouwer OR, et al. Intraoperative laparoscopic fluorescence guidance to the sentinel lymph node in prostate cancer patients: clinical proof of concept of an integrated functional imaging approach using a multimodal tracer. *Eur Urol* 2011;60:826.
33. Brouwer OR, Klop WM, Buckle T, et al. Feasibility of sentinel node biopsy in head and neck melanoma using a hybrid radioactive and fluorescent tracer. *Ann Surg Oncol* 2012;19:1988.
34. Brigic A, Fraser C, Sibbons P, et al. Individualization of surgical management for early-stage colonic cancer. *Colorectal Dis* 2011;13(Suppl 7):59.
35. Cahill RA, Asakuma M, Trunzo J, et al. Intraperitoneal virtual biopsy by fibered optical coherence tomography (OCT) at natural orifice transluminal endoscopic surgery (NOTES). *J Gastrointest Surg* 2010;14:732.

PART II

Clinical translation of optical tumor imaging



Chapter 6

Optical mammography using diffuse optical spectroscopy for monitoring tumour response to neoadjuvant chemotherapy in women with locally advanced breast cancer

Schaafsma BE, van de Giessen M, Charehbili A, Smit VTHBM, Kroep JR, Lelieveldt BPF, Liefers GJ, Chan A, Löwik CWGM, Dijkstra J, van de velde CJH, Wasser MNJM, Vahrmeijer AL

Clinical Cancer Research 2014;21;577–584

ABSTRACT

Purpose

Diffuse optical spectroscopy (DOS) has the potential to enable monitoring of tumour response during chemotherapy, particularly in the early stages of treatment. This study aims to assess feasibility of DOS for monitoring treatment response in HER2-negative breast cancer patients receiving neoadjuvant chemotherapy (NAC) and compare DOS with tumour response assessment by MRI.

Experimental Design

Patients received NAC in six cycles of 3 weeks. In addition to standard treatment monitoring by dynamic contrast enhanced MRI (DCE-MRI), DOS scans were acquired after the first, third, and last cycle of chemotherapy. The primary goal was to assess feasibility of DOS for early assessment of tumour response. The predictive value of DOS and DCE-MRI compared with pathologic response was assessed.

Results

Of the 22 patients, 18 patients had a partial or complete tumour response at pathologic examination, whereas 4 patients were nonresponders. As early as after the first chemotherapy cycle, a significant difference between responders and nonresponders was found using DOS (HbO_2 86% \pm 25 vs. 136% \pm 25, $P = 0.023$). The differences between responders and nonresponders continued during treatment (halfway treatment, HbO_2 68% \pm 22 vs. 110% \pm 10, $P = 0.010$). Using DCE-MRI, a difference between responders and nonresponders was found halfway treatment ($P = 0.005$) using tumour volume measurement calculations.

Conclusions

DOS allows for tumour response assessment and is able to differentiate between responders and nonresponders after the first chemotherapy cycle and halfway treatment. In this study, DOS was equally effective in predicting tumour response halfway treatment compared with DCE-MRI. Therefore, DOS may be used as a novel imaging modality for (early) treatment monitoring of NAC.

INTRODUCTION

Neoadjuvant chemotherapy (NAC) has been established as the standard-of-care treatment for locally advanced inoperable breast cancer, and is increasingly being used for patients with operable cancer.^{1,2} A pathologic complete response (pCR) has been consistently shown to be associated with increased long term survival.² A significant number of patients, however, is unresponsive to NAC or even experience tumour growth under NAC.^{3,4} A key advantage of NAC is the opportunity to assess response during treatment as a predictor of final pathologic response, with the potential to modify therapy. Therefore, the early knowledge of response to NAC is essential for providing the optimal treatment strategy.

Currently, response of the tumour to NAC is most often monitored by a combination of clinical examination and conventional imaging techniques, such as mammography, ultrasound, or dynamic contrast enhanced MRI (DCE-MRI). However, clinical examination and these imaging techniques are often unable to objectively assess treatment response during the course of treatment.⁵ Moreover, the correlation between MRI and pCR assessment is limited.⁶⁻⁸ Therefore, novel, noninvasive imaging techniques are needed to improve early monitoring response of the tumour to NAC. In addition to DCE MRI and PET modalities, optical imaging has received new interest as a noninvasive and nonionizing technique to assess tumour response.⁹⁻¹⁴

Diffuse optical spectroscopy (DOS) uses near-infrared light to provide quantitative spectral information about tissue absorption and scattering properties.^{15,16} These optical properties of tissue can be used to assess tissue microstructure and functional parameters, such as oxygenated hemoglobin, deoxygenated hemoglobin, relative oxygen desaturation, and water and lipid composition. Hypoxia, blood flow, oxygen saturation, and hemoglobin concentration are correlated to tumour response.¹⁷ As DOS is noninvasive and does not require contrast agents, it is a promising modality for frequent measurements of tumour response.

Multiple studies have assessed DOS for monitoring NAC treatment in patients with breast cancer.⁹⁻¹⁴ These studies have suggested that DOS may provide clinically useful information on tumour response on NAC treatment. In previous studies, patients using different chemotherapeutic regimes were included. This study aims to assess the feasibility and predictive power of DOS for monitoring treatment response in patients with breast cancer receiving NAC directly after the start of NAC until surgery. Moreover, this study compares the tumour response assessment by DOS to tumour response assessment by MRI.

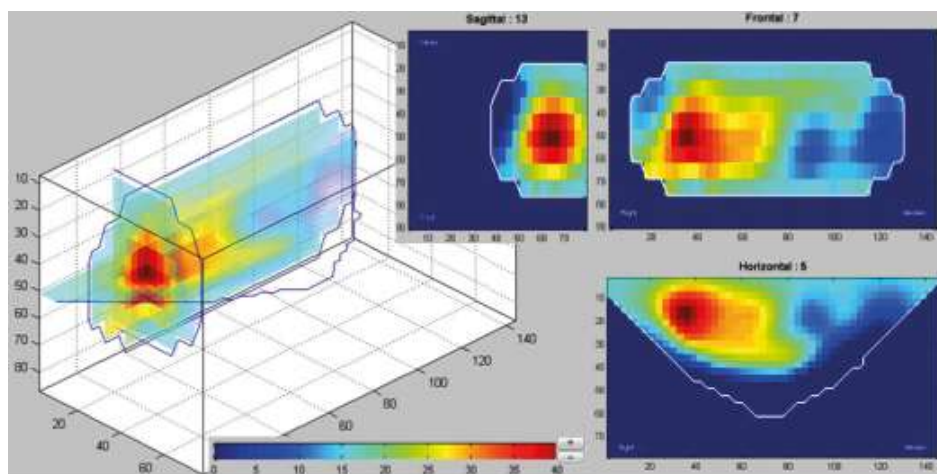


Fig. 1. Acquired DOS data of HbO₂ (μmol/L) was reconstructed to allow 3D analysis (BreastViewer 3.1).

MATERIALS AND METHODS

This prospective, single-arm, single-center study was approved by the Medical Ethics Committee of the Leiden University Medical Center (Leiden, the Netherlands) and was performed in accordance with the ethical standards of the Helsinki Declaration of 1975. Inclusion criteria were patients with breast cancer with- HER2 negative tumours larger than 2 cm or HER2-negative tumours with lymph node metastases, without distant metastases and eligible for neoadjuvant treatment. Patients with known allergies to materials used in the DOS apparatus, prior breast surgery or chemotherapy or radiation therapy were excluded. Patients were included in the period from March 2011 to October 2012. All included patients gave informed consent and the acquired data were anonymized.

Clinical trial

Patients received TAC (docetaxel, doxorubicin, and cyclophosphamide) with or without zoledronic acid in six cycles of 3 weeks. Patients were mainly enrolled in the context of the NEOZOTAC trial (NCT01099436). Standard monitoring of treatment response of the tumour to NAC was based on clinical examination before each cycle and three dynamic contrast enhanced MRI (DCE-MRI) scans (before NAC, before fourth cycle, before surgery) performed on a 1.5 Tesla system (Philips Medical Systems). In addition, patients were scheduled for four optical mammographies using DOS (before NAC, before second cycle, before fourth cycle, before surgery). DOS was performed using a commercially available breast imaging system (Softscan; Softscan Healthcare Group) as described previously.¹⁸ Briefly, Softscan is a bed-based imaging system on which the patient has to lie down with the breast inserted into an aquarium filled with

optical compensation media (OCM). OCM is an oil-in-water emulsion that mimics average optical properties of the human breast. It is used to minimize light reflections at the breast surface to improve image quality. The system consists of four individual pulsed diode lasers operating at 690, 730, 780, and 830 nm. Light is collected by a mobile detector in a 1 cm-X constellation composed of five optical fibers and detected by a photomultiplier. The breast is scanned in approximately 10 to 20 minutes. The count by the detector was time correlated with the synchronization signal provided by the laser system driver. Using the measured absorption and scattering, an accurate estimate of the oxyhemoglobin (HbO_2), deoxyhemoglobin (Hb), total hemoglobin (HbT), and scattering amplitude (SA) and power (SP) can be obtained. Water (H_2O) and %lipids have low, but non-negligible absorption coefficients at the higher NIR wavelengths and were estimated as well. Patients were positioned into the Softscan aperture under guidance of a radiology technician. Breasts were scanned in the craniocaudal angle and the scanning area encompassed the whole breast. To ensure consistency, stabilizing plates were used to secure the breast in place. The acquired data were reconstructed using the software associated with the Softscan device, and three-dimensional (3D) tomographic images were created from the optical parameters with a typical voxel size of $3 \times 3 \times 7 \text{ mm}^3$ (Fig. 1).

MRI- and pathologic assessment of tumour response to neoadjuvant chemotherapy

DCE-MRI response assessment. Tumour response to NAC on DCE-MRI was assessed in two ways: (i) according to the response evaluation criteria in solid tumours (RECIST 1.1) guidelines and (ii) by semiautomated measurement of tumour volume using a dedicated software program. All measurements were performed by a single observer (M.N.J.M. Wasser).

Following RECIST 1.1, tumour response was measured by changes in the longest diameter of the enhancing tumour target lesions. Complete reduction of the target lesions was termed as a complete response (CR). Partial response (PR) was deemed to have occurred if tumour size was reduced by at least 30%. Progressive disease (PD) was defined as an increase in tumour size of at least 20%. The remaining cases were considered to have stable disease (SD).

Measurement of tumour volumes on the subtracted 3D T1- weighted DCE-MR images was done using dedicated software (Vitrea Enterprise Suite version 6.6.3 software, Vital Images Inc.). Calculation of tumour volume consisted of semiautomated summing of all voxels with enhancement above background parenchymal enhancement.

Pathology. Following definitive surgery, the excised specimens were cut in multiple serial sections of approximately 5 mm, fixed in 10% formalin, paraffin embedded as tissue blocks, stained by hematoxylin and eosin, and evaluated by an experienced

Table 1. Patient and Tumour Characteristics

Characteristic	All patients (N=22) N	Responders (N=18) N	Non-responders (N=4) N
Age in years (median; range)	50 (38-66)	50 (38-59)	50 (46-66)
Menopausal status			
-Premenopausal	16	13	3
-Postmenopausal	6	5	1
Tumour histology			
-Invasive ductal carcinoma	16	12	4
-Invasive lobular carcinoma	6	6	0
Estrogen receptor status			
-Positive	20	17	3
-Negative	22	1	1
Progesterone receptor status			
-Positive	15	12	3
-Negative	7	6	1
HER receptor status			
-Positive	0	0	0
-Negative	22	18	4
Tumour size in mm (median; range)	30 (16-81)	33 (16-81)	29 (16-36)

* staging according to AJCC guidelines

pathologist to determine the degree of pathologic tumour response of the primary breast lesion. Pathologic response was scored according to the Miller and Payne criteria.

Diffuse optical spectroscopy assessment of neoadjuvant chemotherapy

Tumour regions in each of the four DOS scans were manually annotated. The tumour in the baseline scan was annotated as an ellipsoid with axes of the sizes reported in the first radiologic assessment. The annotated region was centered on the maximum scatter amplitude in breast section containing the tumour based on conventional radiology. In DOS scans 2 to 4, an annotated region of the same size and shape as in the first scan was centered at the maximum scatter amplitude in these respective scans. Within each annotated region, the mean Hb and HbO₂ contents were measured in µmol/L. Hb and HbO₂ contents in follow-up scans were normalized by the baseline scan for inter-subject comparison. Subjects where the baseline scan was unreliable were completely excluded. Subjects where a follow-up scan was unreliable were removed from the respective groups. Criteria for unreliable scans were tumour on the edge of the scan or outside the scan and severe reconstruction artifacts in the breast section containing the tumour. Severe reconstruction artifacts were identified as physically improbable measurements, particularly zero SA and negative scatter power.

Patient and tumour characteristics

A total of 25 patients were initially included in the study. Two patients were excluded because of a failed baseline DOS scan and one patient due to a failed scan after one cycle. Patient and tumour characteristics of the 22 analyzed patients are summarized in Table 1. The median age was 50 years (range, 38–66), and median tumour size before NAC was 30mm(range, 16–81). Of the patients, 6 patients had lobular carcinoma, 16 had ductal carcinoma, 20 had an ER-positive tumour, and 15 had a PR-positive tumour. All patients received a DOS scan before NAC and before the second cycle. In 2 patients, the DOS scan halfway therapy and in 4 patients the DOS scan before surgery was not performed because of patient complications (not related to Softscan) or logistic reasons.

Data and statistical analysis

The primary goal of this study was to assess feasibility of DOS for assessment of tumour response to NAC based on pathologic response before the second NAC cycle. Failure of a missed first or second DOS scan resulted in exclusion from further DOS scans. All subjects were divided in two groups based on the Miller and Payne criteria: nonresponders (MP 1; i.e., 0% decrease of tumour cellularity after NAC) and (partial) responders (MP 2-5). For DOS time points, the changes in Hb and HbO₂ with respect to baseline were compared between the two groups and tested for significant differences using the Mann–Whitney U test. To test the predictive power of the DOS scans for identification of nonresponders, a linear logistic classifier was trained. For the DOS scans, HbO₂ was used as the feature. The classification performance was tested by training on 50% of the data, using the other 50% for testing. The classifier was evaluated by estimating an ROC. Because of the small number of patients, the training and testing were repeated 100 times with different permutations of training and test datasets. The average ROC was computed for final predictive power evaluation.

To compare DOS with DCE-MRI, the sensitivity and specificity of both RECIST and MRI volume measurements to predict tumour response (pathologic) to chemotherapy were assessed. The radiologic assessment by RECIST criteria was converted into a numerical ordering as: PD: 1, SD: 2, PR: 3 and CR: 4. Volume measurements after three and six cycles were normalized to the baseline tumour volume. Subjects were divided in two groups based on the same Miller and Payne criteria: nonresponders (MP 1) and (partial) responders (MP 2-5). The RECIST criteria and normalized volumes after three and six cycles were compared between the two groups and tested for significant differences using the Man Whitney U test. Moreover, the predictive power of MRI was assessed. Both assessment by MRI using

the RECIST 1.1 criteria and MRI volume were used to predict tumour response to NAC (MP criteria) by training a logistic classifier as for DOS.

Predictive power is estimated from classification results. The classification result is a trade-off between the desired fraction of true positives (nonresponders classified as nonresponders) and the accepted fraction of false positives (responders classified as nonresponders). The area under the curve (AUC) is a measure for the predictive power and is 1 for a perfect classifier (100% true positives for 0% false negatives), 0.5 for a random classification (similar to a coin-flip), and 0 for a completely wrong classification (0% true positives for 100% false negatives).

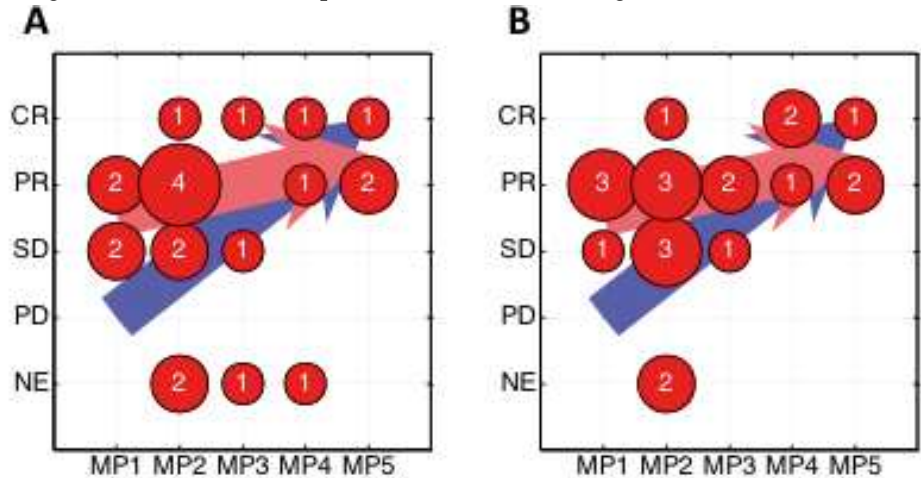


Fig. 2. Agreement between Miller and Payne (MP) criteria and radiology assessment by DCE-MRI using RECIST criteria after three cycles (A) and after six cycles (B) of NAC. The values indicate the patient count. The blue arrow denotes the expected relation, whereas the red arrow shows the linear regression Between MP and DCE-MRI. MRI was assessed according to the RESIST criteria. NE, not evaluated.

RESULTS

MRI and pathologic assessment of tumour response

A summary of DCE-MRI response (RECIST criteria) and pathologic response (Miller and Payne criteria) measurements is given in Fig. 2. In 4 patients after three cycles and in 2 patients after six cycles, RECIST criteria could not be applied because of scattered presentation of the contrast-enhanced lesions and as in 1 patient no, MRI was obtained. Tumour volume could not be accurately measured in 1 patient after six cycles because of too scattered presentation.

MRI response measurements after three cycles (halfway treatment) indicated zero patients with PD, 5 patients with SD, 9 patients with a PR, and 4 patients with a CR.

After six cycles and before surgery, MRI response measurements indicated 0 patients with PD, 5 patients with SD, 11 patients with a PR, and 4 patients with a CR.

The distribution of the pathologic response classification, following Miller and Payne, was as follows: grade 1, 4 patients; grade 2, 9 patients; grade 3, 3 patients; grade 4, 3 patients; grade 5, 3 patients.

Comparison between responders and nonresponders

Diffuse optical spectroscopy. In all 22 patients, the tumour could be located on the optical mammography. The mean HbO₂ content (SDs between parentheses) for tumours at baseline were 25.9 (7.8) $\mu\text{mol/L}$ for responders and 16.7 (3.8) $\mu\text{mol/L}$ for nonresponders. Corresponding Hb content was 10.5 (3.8) $\mu\text{mol/L}$ and 8.2 (0.8) $\mu\text{mol/L}$. These differences were nonsignificant: $P = 0.064$ (HbO₂), $P = 0.335$ (Hb). In follow-up scans, interpatient variability remained and Hb and HbO₂ content ($\mu\text{mol/L}$) was not significantly different between responders and nonresponders: $P > 0.500$ for all follow-up scans.

However, the average Hb and HbO₂ contents relative to baseline in Table 2 show clear significant differences between responders and nonresponders that are distributed on the basis of pathologic criteria. The relative HbO₂ content (compared with baseline) is significantly lower in all three treatment stages: $P = 0.023$ after one cycle, $P = 0.010$ after three cycles, and $P = 0.009$ after therapy completion. Representative examples of DOS in responders ($n = 18$; decrease of HbO₂ content) and nonresponders ($n = 4$; stable or increasing HbO₂ content) are shown in Fig. 3. The average Hb content for responders is lower for all cycles, but this is not statistically significant.

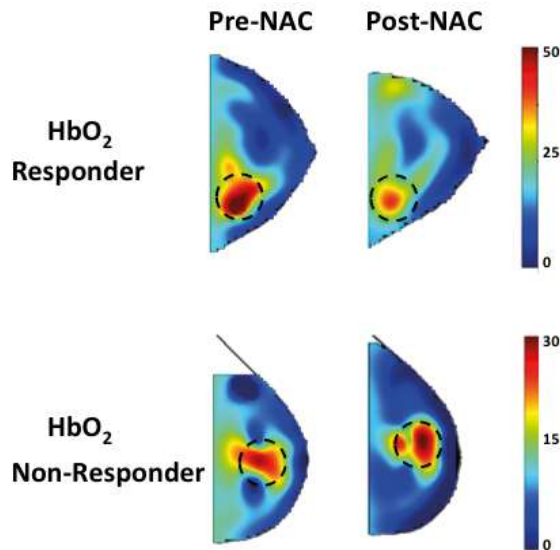


Fig. 3. Transverse DOS images (after interpolation) before and after NAC of a typical responder, which shows a significant decrease of HbO₂ ($\mu\text{mol/L}$) in the area of the tumour after NAC (top row), and nonresponder, which shows increase of HbO₂ in the area of the tumour after NAC (bottom row). The circle indicates where the tumour is located.

Table 2. Differentiation between responders and non-responders using DOS

DOS Measurements				
Hb	Baseline	1 Cycle	3 Cycles	6 Cycles
Responder Hb (%)	100 (0)	91 (42)	76 (25)	83 (40)
Nonresponder Hb (%)	100 (0)	118 (11)	101 (3)	119 (39)
U-test p-value	1	0.109	0.076	0.233
HbO2	Baseline	1 Cycle	3 Cycles	6 Cycles
Responder HbO ₂ (%)	100 (0)	86 (25)	68 (22)	65 (20)
Nonresponder HbO ₂ (%)	100 (0)	136 (25)	110 (10)	109 (18)
U-test p-value	1	0.023	0.010	0.009

MRI volume measurements			
	Baseline	3 Cycles	6 Cycles
Responder	100 (0)	32 (23)	12 (24)
Nonresponder	100 (0)	78 (11)	65 (64)
U-test p-value	1	0.005	0.011

Average Hb and HbO₂ content relative to baseline for responders and non-responders selected based on pathology criteria. Standard deviations are between parentheses. The Mann-Whitney U-test p-values estimate significance of the differences between the two groups. Bold text highlights p-values indicating statistically significant differences (p<0.05).

Dynamic contrast enhanced MRI. The Mann–Whitney U test shows no significant difference in DCE- MRI assessment using RECIST for pathologic responders (MP 2-5, n = 18) and nonresponders (MP 1, n = 4) both after three cycles (P = 0.10) and after six cycles (P = 0.77). This is further illustrated in Fig. 2. After both three and six cycles, a weak trend is visible in which a better response seems to correspond to a higher Miller and Payne ranking. This is, however, far from statistically significant. Correlation coefficients between Miller and Payne and RECIST assessment were 0.43 after both three and six cycles of NAC.

MRI volume measurements show statistically significant differences between responders and nonresponders after both three (P = 0.005) and six cycles (P = 0.011; Table 2). In both responders and nonresponders, the tumour has decreased halfway therapy and decreased even further in the scan before surgery. The decrease in tumour volume is much stronger in the group with responders. Correlations between normalized MRI volumes and normalized Hb/HbO₂ content after three cycles were 0.46 and 0.69 for Hb and HbO₂, respectively, and 0.64 (Hb) and 0.70 (HbO₂) after six cycles.

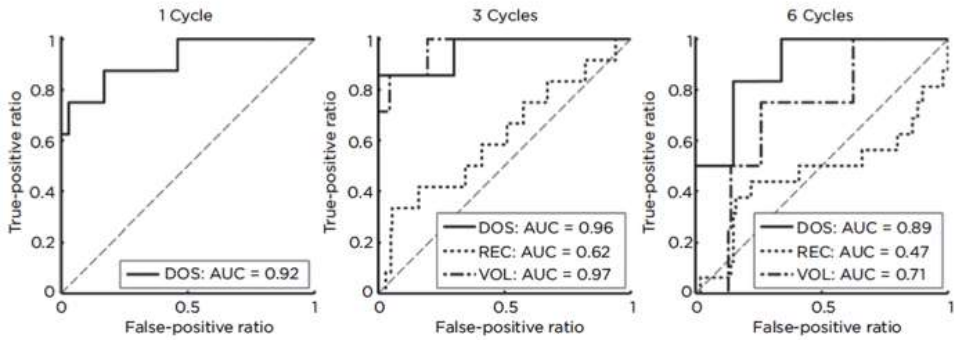


Fig. 4. Predictive value of DOS and MRI-ROC curves for DOS and conventional radiology by MRI using RECIST (REC) and volume measurements (VOL.) after one, three, and six cycles of NAC. The dashed diagonal shows a ROC for a completely random classification result with an AUC of 0.5.

Predictive power of diffuse optical spectroscopy and MRI

The ROC curves in Fig. 4 show the prediction sensitivity and specificity for different trade-offs for DOS, RECIST, and DCE-MRI volumes normalized to baseline. For DOS assessment after only one cycle, accepting incorrect classification of 5% of the responders as nonresponders would correctly identify 75% of the nonresponders and allow them to change therapy. Similarly, accepting 10% incorrectly identified responders would correctly identify 87% of the nonresponders as responders.

The ROC curves show that DOS and normalized volume measurements have a comparable predictive power, both far better than RECIST. For example, predicting if a patient is a nonresponder after three cycles with a 20% false-positive rate is correct in 86% of the DOS scans and volume measurements, while this is only correct in 58% of the RECIST assessments. Considering the AUC, the predictive power for DOS is similar for all time points, with AUC values of 0.92, 0.96, and 0.89 after, respectively, one, three, and six cycles. The MRI volume AUC is 0.97 after three cycles and 0.71 after six cycles. The RECIST AUC is 0.62 after three cycles and only 0.47 after six cycles. These RECIST figures are much lower than that for DOS and MRI volume measurements, especially when taking into account that an AUC of 0.5 corresponds to a random prediction. The MRI volume measurements at six cycles have a decreased predictive power due to tumours that were nonresponders based on the MP criteria, but showed no contrast enhancement after six cycles. The large SD of 64 in Table 2 is indicative for the wide spread of nonresponding tumour volumes after six cycles.

DISCUSSION

The present study demonstrates the clinical use of DOS for treatment monitoring of NAC in patients with breast cancer. Treatment monitoring using DOS showed a significant difference in the physiologic tumour parameters between responders and nonresponders as early as after the first gift of NAC. Moreover, the predictive value of DOS to determine tumour response corresponded to MRI volume measurements after three cycles but appeared to outperform DCE-MRI evaluation based on RECIST.

DOS showed a decrease in Hb and HbO₂ content in the patients with a response of the tumour to NAC. We found this decrease to be only statistically significant for HbO₂, but not for Hb. Similar results were obtained in previous studies.^{9–13, 20} In comparative studies between Hb and HbO₂ levels in tumour tissue and healthy tissue, tumour tissue shows nearly a 2-fold increased level of Hb and HbO₂ as a result of increased vascular supply.¹⁷ The decrease of Hb and HbO₂ levels observed in the study suggests a decrease of tumour tissue and an increase of nontumorous tissue in the region of interest (ROI) where the tumour was located. The reason we did not find a statistically significant decrease of Hb can be partly attributed to the small number of nonresponders (N = 4), compared with the large number of responders. Under these circumstances, the Mann–Whitney U test has a strongly decreased sensitivity and only large group differences as in the relative HbO₂ changes were tested as statistically significantly different.

The absolute quantities of Hb and HbO₂ at baseline were varying greatly between tumours and did not show significant differences between potential responders and nonresponders. This large inter patient variability was also present in the follow-up scans, and responders and nonresponders could not be separated on the basis of absolute Hb and HbO₂ content (μmol/L). Normalization with respect to the baseline scan is thus essential. Apart from Hb and HbO₂, the two most important absorbers in NIR are water and lipids. The low absorption coefficients of the latter two, compared with Hb and HbO₂, prevented reliable estimates, with frequent erroneous estimates (0% or 100% water/lipids content).

Correlating the normalized DOS parameters Hb, HbO₂ with normalized MRI volume measurements showed a strong positive relationship between changes in MRI volume and changes in (de)oxyhemoglobin content. Although it is likely that tumour volume and oxygenation have a positive relationship, a confounder may be in the hemoglobin measurements where a constant volume is used to measure these parameters, while the tumour volume has decreased and additional normal tissue can be in the measurement volume. One should therefore be careful with interpreting the absolute hemoglobin measurements in relation to tumour viability.

In the current study, a homogenous HER2-negative group of patients with locally advanced breast cancer was used receiving the same NAC regime. It is important

to validate DOS in a homogenous patient group as tumour variables such as HER2 status and tumour size have a significant effect on the optical properties of tumours. Positive HER2 tumours have a significant higher Hb level by DOS assessment.²¹ This is most likely related to angiogenesis as HER2 overexpression is associated with increased angiogenesis. As the difference between Hb levels between HER2-positive tumours and healthy tissue is larger compared with HER2-negative tumours, it can be expected that DOS assessment of NAC in HER2-positive tumours will result in even a more distinct difference between responders and nonresponders.

Moreover, in addition to NAC, neoadjuvant hormonal therapy is also increasing rapidly and has shown similar patient outcomes compared with NAC.²² Many different anticancer agents are available (chemotherapy, hormonal therapy, monoclonal agents), all have different antitumour and antiangiogenic effects. Therefore, when assessing early treatment response, it is crucial to use a homogenous treatment regime. As the therapeutic effect of hormonal therapy acts on a different mechanism compared with chemotherapy, validation of using DOS for treatment monitoring in neoadjuvant hormonal therapy is essential to provide wide clinical use of DOS in the treatment monitoring of patients with breast cancer.²³

With the increasing interest in neoadjuvant treatment, improved imaging modalities that can provide early prediction of tumour response will be required to select patient who may benefit from a different treatment. In case of locally advanced breast cancer, early detection of nonresponders could prevent unnecessary toxic NAC treatment and allow selecting patient who would benefit from a different neoadjuvant treatment regime or early surgery. In the current study, after one cycle of NAC, DOS would correctly identify most nonresponders, allowing them to change treatment strategy early. Prediction accuracies were evaluated as AUCs of 0.92, 0.96, and 0.87 after one, three, and six cycles, respectively. The lower AUC after six cycles is due to a smaller number of available scans for classifier training. Previous studies have shown similar results showing specificity of 80% to 83%.^{9,11} These data suggest that DOS is able to identify a large set of patients early during treatment that would benefit from a different treatment regime. However, it should be emphasized that prospective studies are necessary to validate these results.

In the current study, the predictive value of DOS to determine tumour response corresponded to MRI volume measurements after three cycles but appeared to outperform DCE-MRI evaluation based on RECIST. To date, DCE-MRI is the most accurate response assessment.²⁴ However, this modality is not in all breast tumours equally reliable. Several breast tumour subtypes, such as HER2-negative and ER-positive breast tumours, are associated with reduced accuracy.²⁵ This might explain the poor adequacy of MRI in our study, as our study population consisted almost completely of HER2-negative and ER-positive patients. The biologic explanation for this may be that HER2-negative breast cancer is associated with decreased angiogenesis, resulting in

impaired tumour tissue perfusion of MRI contrast.²⁶ Also, hormone receptor-positive tumours have a different growth pattern than hormone receptor-negative tumours, with less often (unifocal) mass-like lesions, making it more difficult to accurately determine the residual tumour diameter.^{8,27}

Limitation of the used DOS device in our study is that determination of the correct ROI for the DOS was difficult because DOS provided limited anatomical context. Therefore, the ROI at baseline was partly based upon data of conventional mammography and MRI acquired before therapy. Localization of the ROI was not trivial during data analysis and incorrect ROI placement can lead to an underestimation of tissue changes and consequently decrease the sensitivity. A 5-mm displacement of the ROI introduces variations in Hb/HbO₂ estimates of about 2% for tumours of about 30 cm³, whereas for smaller tumours of approximately 5 cm³, estimates could differ by up to 8%. The possibility of merging MRI and DOS could therefore improve DOS assessment and provide more functional parameters to the MRI and further increase the sensitivity.

DOS is a relatively novel imaging modality in the field of breast cancer and is rapidly evolving by increasing spatial resolution and by increasing analytic techniques to provide more accurate assessment of functional parameters.^{28,29} A recent study by Roblyer and colleagues indicated that DOS as early as the first day after NAC may possibly discriminate nonresponding from responding patients.³⁰ Remarkably, this study found an increase in HbO₂ for responders, compared with nonresponders, while monitoring in the first week. Roblyer and colleagues hypothesized that this increase can be attributed to an acute inflammatory reaction in the responding tumours. Measurements with the same device as Roblyer and colleagues at mid-therapy and before surgery showed lower HbO₂ values for responders, comparable with our findings.³⁰ We therefore hypothesize that after the acute inflammatory reaction stops, the responding tumours have a lower metabolism and that our measurement after 3 weeks (one cycle) is measuring the same decrease in metabolism in the tumour as response to NAC as the measurements after three and six cycles. A future study with frequent measurements during the first 3 weeks after NAC therapy starts could provide further insight.

Moreover, several optical contrast agents are available, which may improve contrast and sensitivity.^{31,32} Furthermore, DOS can be combined with other imaging modalities, such as ultrasound, for improved tumour localization accuracy.¹¹ These developments will allow further improvement of DOS sensitivity and accuracy.

In conclusion, DOS allows early response monitoring of tumour tissue to chemotherapy and is able to differentiate between responders and nonresponders in early stages of therapy. Therefore, DOS could be used as a novel imaging modality for treatment monitoring of NAC to assist patient tailored medicine.

ACKNOWLEDGMENTS

The authors thank the Softscan Healthcare Group for providing OCM and technical support and for providing the Softscan breast imaging system, and Gemma Ranke and Elly Krol-Warmerdam (Breast Cancer Unit) for their contribution to this study. This work was supported in part by the Dutch Cancer Society grants UL2010- 4732. This research was performed within the framework of CTMM, the Center for Translational Molecular Medicine, project MUSIS (grant 03O-202). The costs of publication of this article were defrayed in part by the payment of page charges. This article must therefore be hereby marked advertisement in accordance with 18 U.S.C. Section 1734 solely to indicate this fact.

REFERENCES

1. Mieog JS, van derHage JA, van de Velde CJ. Neoadjuvant chemotherapy for operable breast cancer. *Br J Surg* 2007;94:1189–200.
2. Kaufmann M, von Minckwitz G, Mamounas EP, et al. Recommendations from an international consensus conference on Optical Imaging for Treatment Monitoring in Breast Cancer the current status and future of neoadjuvant systemic therapy in primary breast cancer. *Ann Surg Oncol* 2012;19:1508–16.
3. von Minckwitz G, Blohmer JU, Raab G, et al. In vivo chemosensitivity-adapted preoperative chemotherapy in patients with early-stage breast cancer: the GEPARTRIO pilot study. *Ann Oncol* 2005;16:56–63.
4. Caudle AS, Gonzalez-Angulo AM, Hunt KK, et al. Predictors of tumor progression during neoadjuvant chemotherapy in breast cancer. *J Clin Oncol* 2010;28:1821–8.
5. Yeh E, Slanetz P, Kopans DB, et al. Prospective comparison of mammography, sonography, and MRI in patients undergoing neoadjuvant chemotherapy for palpable breast cancer. *AJR Am J Roentgenol* 2005;184:868–77.
6. Croshaw R, Shapiro-Wright H, Svensson E, et al. Accuracy of clinical examination, digital mammogram, ultrasound, and MRI in determining postneoadjuvant pathologic tumor response in operable breast cancer patients. *Ann Surg Oncol* 2011;18:3160–3.
7. Marinovich ML, Sardanelli F, Ciatto S, et al. Early prediction of pathologic response to neoadjuvant therapy in breast cancer: systematic review of the accuracy of MRI. *Breast* 2012; 21:669–77.
8. Loo CE, Straver ME, Rodenhuis S, et al. Magnetic resonance imaging response monitoring of breast cancer during neoadjuvant chemotherapy: relevance of breast cancer subtype. *J Clin Oncol* 2011;29:660–6.
9. Falou O, Soliman H, Sadeghi-Naini A, et al. Diffuse optical spectroscopy evaluation of treatment response in women with locally advanced breast cancer receiving neoadjuvant chemotherapy. *Transl Oncol* 2012;5:238–46.
10. Ueda S, Roblyer D, Cerussi A, et al. Baseline tumor oxygen saturation correlates with a pathologic complete response in breast cancer patients undergoing neoadjuvant chemotherapy. *Cancer Res* 2012;72:4318–28.
11. Zhu Q, DeFusco PA, Ricci A Jr, et al. Breast cancer: assessing response to neoadjuvant chemotherapy by using US-guided near-infrared tomography. *Radiology* 2013;266:433–42.
12. O'Sullivan TD, Leproux A, Chen JH, et al. Optical imaging correlates with magnetic resonance imaging breast density and reveals composition changes during neoadjuvant chemotherapy. *Breast Cancer Res* 2013;15:R14.
13. Soliman H, Gunasekara A, Rycroft M, et al. Functional imaging using diffuse optical spectroscopy of neoadjuvant chemotherapy response in women with locally advanced breast cancer. *Clin Cancer Res* 2010;16:2605–14.
14. Busch DR, Choe R, Rosen MA, et al. Optical malignancy parameters for monitoring progression of breast cancer neoadjuvant chemotherapy. *Biomed Opt Express* 2013;4:105–21.
15. Tromberg BJ, Shah N, Lanning R, et al. Noninvasive in vivo characterization of breast tumors using photon migration spectroscopy. *Neoplasia* 2000;2:26–40.
16. Ntziachristos V, Chance B. Probing physiology and molecular function using optical imaging: applications to breast cancer. *Breast Cancer Res* 2001;3:41–6.
17. Tromberg BJ, Cerussi A, Shah N, et al. Imaging in breast cancer: diffuse optics in breast cancer: detecting tumors in pre-menopausal women and monitoring neoadjuvant chemotherapy. *Breast Cancer Res* 2005;7:279–85.
18. Intes X. Time-domain optical mammography SoftScan: initial results. *Acad Radiol* 2005;12:934–47.
19. Ogston KN, Miller ID, Payne S, et al. A new histological grading system to assess response of breast cancers to primary chemotherapy: prognostic significance and survival. *Breast* 2003; 12:320–7.
20. Jiang S, Pogue BW, Carpenter CM, et al. Evaluation of breast tumor response to neoadjuvant chemotherapy with tomographic diffuse optical spectroscopy: case studies of tumor region-of-interest changes. *Radiology* 2009;252:551–60.

21. Choi JS, Kim MJ, Youk JH, et al. US-guided optical tomography: correlation with clinicopathologic variables in breast cancer. *Ultrasound Med Biol* 2013;39:233–40.
22. Charehbili A, Fontein DB, Kroep JR, et al. Neoadjuvant hormonal therapy for endocrine sensitive breast cancer: a systematic review. *Cancer Treat Rev* 2014;40:86–92.
23. Enfield L, Cantanhede G, Douek M, et al. Monitoring the response to neoadjuvant hormone therapy for locally advanced breast cancer using three dimensional time-resolved optical mammography. *J Biomed Opt* 2013;18:56012.
24. Marinovich ML, Macaskill P, Irwig L, et al. Meta-analysis of agreement between MRI and pathologic breast tumour size after neoadjuvant chemotherapy. *Br J Cancer* 2013;109:1528–36.
25. Charehbili A, Wasser MN, Smit VT, et al. Accuracy of MRI for treatment response assessment after taxane- and anthracycline-based neoadjuvant chemotherapy in HER2-negative breast cancer. *Eur J Surg Oncol* 2014;40:1216–21.
26. Blackwell KL, Dewhirst MW, Liotcheva V, et al. HER-2 gene amplification correlates with higher levels of angiogenesis and lower levels of hypoxia in primary breast tumors. *Clin Cancer Res* 2004;10:4083–8.
27. Kuzucan A, Chen JH, Bahri S, et al. Diagnostic performance of magnetic resonance imaging for assessing tumor response in patients with HER2-negative breast cancer receiving neoadjuvant chemotherapy is associated with molecular biomarker profile. *Clin Breast Cancer* 2012;12:110–8.
28. Karkala D, Yalavarthy PK. Data-resolution based optimization of the data collection Strategy for near infrared diffuse optical tomography. *Med Phys* 2012;39:4715–25.
29. Lin AJ, Ponticorvo A, Konecky SD, et al. Visible spatial frequency domain imaging with a digital light microprojector. *J Biomed Opt* 2013;18:096007.
30. Roblyer D, Ueda S, Cerussi A, et al. Optical imaging of breast cancer oxyhemoglobin flare correlates with neoadjuvant chemotherapy response one day after starting treatment. *PNAS U S A* 2011;108:14626–31.
31. Poellinger A, Burock S, Grosenick D, et al. Breast cancer: early- and late-fluorescence near-infrared imaging with indocyanine green—a preliminary study. *Radiology* 2011;258:409–16.
32. van de Ven S, Wiethoff A, Nielsen T, et al. A novel fluorescent imaging agent for diffuse optical tomography of the breast: first clinical experience in patients. *Mol Imaging Biol* 2010;12:343–8.

Chapter 7

Near-infrared fluorescence-guided resection of colorectal liver metastases

Schaafsma BE¹, Van der Vorst JR¹, Hutteman M, Verbeek FPR, Liefers GJ, Hartgrink HH, Smit VTHBM, Löwik CWGM, van de Velde CJH, Frangioni JV, Vahrmeijer AL

¹ Shared first authorship

Cancer 2013;119:3411-3418

ABSTRACT

Background

The fundamental principle of oncologic surgery is the complete resection of malignant cells. However, small tumours are often difficult to find during surgery using conventional techniques. The objectives of this study were to determine if optical imaging, using a contrast agent already approved for other indications, could improve hepatic metastasectomy with curative intent, to optimize dose and timing, and to determine the mechanism of contrast agent accumulation.

Methods

The high tissue penetration of near-infrared (NIR) light was exploited by use of the FLARE (Fluorescence-Assisted Resection and Exploration) image-guided surgery system and the NIR fluorophore indocyanine green in a clinical trial of 40 patients undergoing hepatic resection for colorectal cancer metastases.

Results

A total of 71 superficially located (<6.2 mm beneath the liver capsule) colorectal liver metastases were identified and resected using NIR fluorescence imaging. Median tumour-to-liver ratio was 7.0 (range, 1.9–18.7) and no significant differences between time points or doses were found. Indocyanine green fluorescence was seen as a rim around the tumour, which is shown to be entrapment around cytokeratin 7 positive hepatocytes compressed by the tumour. Importantly, in 5 of 40 patients (12.5%, 95% confidence interval 55.0–26.6), additional small and superficially located lesions were detected using NIR fluorescence, and were otherwise undetectable by preoperative computed tomography, intraoperative ultrasound, visual inspection, and palpation.

Conclusions

NIR fluorescence imaging, even when used with a nontargeted, clinically available NIR fluorophore, is complementary to conventional imaging and able to identify missed lesions by other modalities.

INTRODUCTION

Prognosis and survival of patients with colorectal cancer depends primarily on the occurrence of distant metastases, which occur most frequently in the liver.¹ A resection with curative intent can offer patients with colorectal liver metastases a 5-year survival rate of 36% to 60%.²⁻⁵ Despite improvements in preoperative imaging modalities, surgical techniques, and chemotherapy regimens, intrahepatic recurrence rates vary from 11% to 37.5% after hepatic metastasectomy, and 65% to 85% of these recurrences appear within 2 years after resection.^{2,6-9} A possible explanation for this high intrahepatic recurrence rate is that some hepatic metastases are already present at the time of liver resection, but were undetected by the technology typically available in the community setting, namely, preoperative imaging, intraoperative ultrasound (IOUS), and inspection/palpation by the surgeon. For example, it is known that small and superficially located liver metastases are difficult to identify using available imaging modalities such as preoperative computed tomography (CT), magnetic resonance imaging (MRI), and IOUS.¹⁰⁻¹²

Near-infrared (NIR) fluorescence imaging using indocyanine green (ICG) is a promising technique to intraoperatively visualize the contrast between liver metastases and normal liver tissue in real time.¹³⁻¹⁵ This type of optical imaging is relatively inexpensive and is quickly becoming widely available. Unlike visible light, which is used to excite fluorophores such as fluorescein, NIR light can penetrate several millimeters into tissue and through blood. ICG is excreted exclusively into the bile after intravenous injection; it has been hypothesized that colorectal liver metastases can be visualized due to passive accumulation of ICG caused by hampered biliary excretion, which results in a fluorescent rim around the metastases. However, the mechanism of ICG accumulation has not yet been explored.

Recently, Ishizawa et al¹³ described the intraoperative detection of colorectal liver metastasis using NIR fluorescence imaging after intravenous injection of 0.5 mg/kg ICG, 1 to 14 days prior to surgery, as part of an ICG retention liver function test. The dose and interval between ICG injection and surgery are key determinants of the remaining background fluorescence signal in the liver and the fluorescent rim surrounding the tumour. In a preclinical study in rats performed by our group, the influence of injection time prior to surgery and dose of ICG pertaining to the contrast between the fluorescent rim around the hepatic metastases and normal liver tissue (tumour-to-liver ratio) was examined.¹⁶ In this preclinical study, the highest tumour-to-liver ratio (TLR) was reached when ICG was injected 72 hours prior to surgery. Furthermore, this study demonstrated that even small liver metastases (≈ 1 mm in size) could be identified using NIR fluorescence. In this study, these preclinical results were translated to a clinical trial in patients with colorectal liver metastases in order to optimize intraoperative identification of liver metastases by using ICG. Furthermore, the mechanism of ICG accumulation in the transition area between tumour and

normal liver tissue was investigated, and the value added by NIR fluorescence imaging was determined.

MATERIALS AND METHODS

Preparation and Administration of ICG

ICG (25 mg vials) was purchased from Pulsion Medical Systems (Munich, Germany) and resuspended in 10 mL of sterile water for injection to yield a stock solution of 2.5 mg/mL (3.2 mM). Of this stock solution, 4 or 8 mL, corresponding to doses of 10 or 20 mg, were administered intravenously.

Clinical Trial

The study was approved by the Local Medical Ethics Committee of the Leiden University Medical Center, Leiden, The Netherlands, and was performed in accordance with the ethical standards of the Helsinki Declaration of 1975. All patients were evaluated for hepatic treatment by a multidisciplinary specialized liver unit (surgeon, oncologist, interventional radiologist, and an experienced abdominal radiologist). From 2010 to 2012, a total of 40 patients with suspected colorectal liver metastases, based on a preoperative 4-phase CT scan (Aquilion 64; Toshiba, Tokyo, Japan) of the thorax and abdomen with a slice thickness of 5 mm, who were planned to undergo curative-intended liver resection, were included. All patients provided informed consent. Exclusion criteria were pregnancy, lactation, or an allergy to iodine, shellfish, or ICG.

Patients received 10 or 20 mg of ICG diluted in a total volume of 4 and 8 mL, respectively, as an intravenous bolus at 24 or 48 hours prior to surgery on an inpatient basis. This resulted in 4 groups of 4 patients per group (N=16 patients). Subsequently, 24 patients were included at the optimal combination of ICG dose and injection time. After mobilization of the liver, first visual inspection, palpation, and IOUS were performed to determine the number and location of the liver metastases. To evaluate the additional benefit of NIR fluorescence imaging, all liver segments were imaged using the Mini-FLARE imaging system, which has been described.¹⁷ Directly following liver resection, resection specimens were delivered to the Department of Pathology, where the specimens were sliced into 5- to 7-mm-thick slices and examined by an experienced pathologist for NIR fluorescence, using the Mini-FLARE imaging system.

Table 1. Study Subject Characteristics (N=40)

Characteristic	Median [Range] or (%)
Age	63 [45 - 77]
BMI	25 [19 - 38]
Sex	Male: 21 (52.5%) Female: 19 (47.5%)
Primary tumour location	
Colon	21 (52.5%)
Sigmoid	5 (12.5%)
Rectum	13 (32.5%)
Anus	1 (2.5%)
Neo-adjuvant chemotherapy	22 (55.0%)
Type of resection	
Hemihepatectomy	6 (15.0%)
Metastasectomy / segmentectomy	19 (47.5%)
Metastasectomy / segmentectomy + RFA	7 (17.5%)
RFA only	1 (2.5%)
No resection	7 (17.5%)

Abbreviations: BMI: body mass index; RFA: radiofrequency ablation.

Fluorescence Microscopy

On the basis of macroscopic evaluation and ex vivo fluorescence imaging, tissue was acquired from the transition zone between the tumour and the normal liver from multiple patients. Excised tissue was snap-frozen and sectioned at 5 μ m for fluorescence and regular microscopy. Sections were measured for fluorescence using the Nuance multispectral imager (CRi, Woburn, Mass) mounted on a Leica DM IRE2 inverted microscope (Leica, Wetzlar, Germany). Subsequently, these slides were stained with hematoxylin and eosin. Consecutive slides were stained for the presence of CD31 (M0823; Dako, Glostrup, Denmark), CK7 (M7018; Dako), and CD68 (M0814; Dako) to correlate fluorescence to blood vessels, bile ducts, and macrophages, respectively. White light images were subsequently merged with fluorescence images.

Statistical Analysis

For statistical analysis, the SPSS version 17.0 statistical software package (SPSS, Chicago, Ill) was used. TLR signal, rim fluorescence, and background fluorescence were reported as median and range. Tumour size was reported as mean with standard deviation. To test differences between groups, the Kruskal-Wallis 1-way analysis of variance test was used to test for differences between time and dose groups. Statistical tests were 2-tailed, and $P < .05$ was considered significant. The 95% binomial confidence intervals (CIs) of the percentage of patients in whom additional metastases were identified were calculated using the adjusted Wald method by GraphPad QuickCalcs (Graph- Pad Software, La Jolla, Calif).

Table 2. Methods of detection

Modality	Number of hepatic metastases identified*(%)	Number of patients	Size of metastases (mm)
Preoperative CT-scan	73 (75)	39	29.9 ± 19.1
IOUS, palpation and inspection	92 (95)	40	26.3 ± 19.5
NIR fluorescence	71 (73)	37	29.0 ± 29.8
Preoperative CT-scan, IOUS, inspection palpation and/or NIR fluorescence	97 (100)	40	24.5 ± 19.7

*Liver metastases were confirmed by histology or in the case of nonresected lesions by clinical appearance, IOUS, and CT.

RESULTS

Study Subjects

Patient and tumour characteristics of the 40 patients are listed in Table 1. None of the patients suffered from hepatitis or liver cirrhosis, and 22 patients received neoadjuvant chemotherapy. In 7 patients, no liver resection was performed due to invasion of tumour into the portal vein (N=3), the presence of additional unresectable liver metastases (N=2), or the appearance of lymph node metastases (N=2). Nevertheless, these patients were included for TLR, rim fluorescence, and background fluorescence analysis.

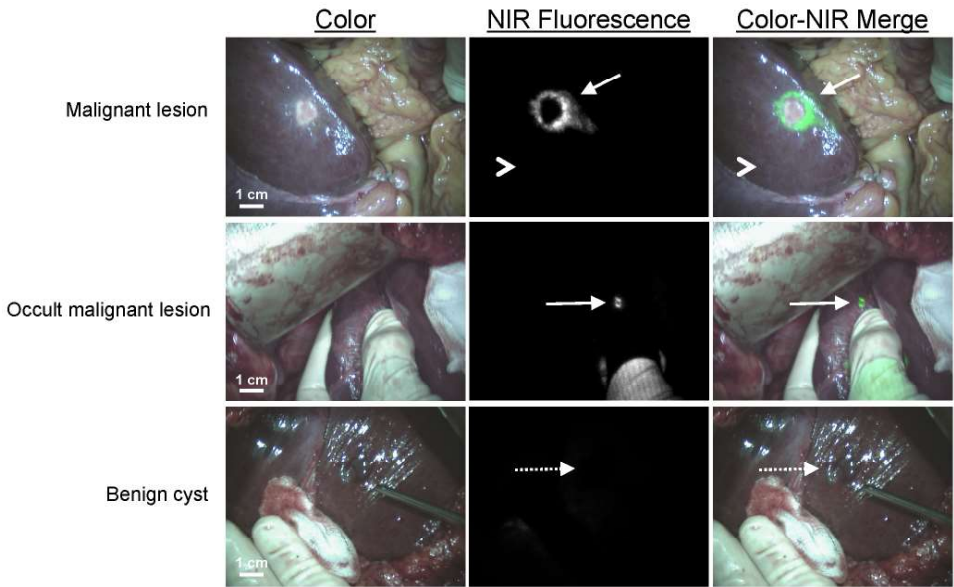


Fig. 1. Near-infrared (NIR) fluorescence imaging of colorectal liver metastases is shown. A colorectal liver metastasis (arrow) is clearly identified by a rim around the tumour in vivo (top row), 24 hours after injection of 10 mg indocyanine green. Normal liver tissue (arrowhead) shows minimal background uptake of indocyanine green. In 5 patients, small, superficial, otherwise occult metastases (middle row, arrow) were identified by NIR fluorescence imaging. Benign lesions (bottom row, dashed arrow) could be differentiated from malignant lesions by a lack of a fluorescent rim around the lesion.

Optimization of ICG Dose and Injection Timing (N=16 Patients)

To determine the effect of ICG dosage and postinjection imaging time, patients were allocated to 2 dose groups and imaged at 2 time points after ICG administration, resulting in 4 groups containing 4 patients per group. Fluorescence intensity of the rim around the liver metastases was significantly higher than the fluorescent signal in the liver ($P<.001$). Median TLR in all 16 patients was 7.3 (range, 1.9-18.7). Median TLRs were 5.0 (range, 2.2-15.4), 6.7 (range, 2.7-9.2), 10.5 (range, 1.9-18.7), 8.0 (range, 7.0-9.3) for the patient groups of 10 mg at 24 hours, 20 mg at 24 hours, 10 mg at 48 hours, and 20 mg at 48 hours, respectively. Median rim fluorescence (normalized pixel value) was 530.1 (range, 257.89-823.0), 938.4 (range, 902.3-1239.1), 648.6 (range, 137.1-1929.36), and 608.5 (range, 507.6-688.1) for the patient groups of 10 mg at 24 hours, 20 mg at 24 hours, 10 mg at 48 hours, and 20 mg at 48 hours, respectively. Median background fluorescence (normalized pixel value) was 98.3 (range, 53.6-127.6), 209.1 (range, 96.1-356.5), 64.6 (range, 53.4-112.4), and 77.4 (range, 67.5-96.2) for the patient groups of 10 mg at 24 hours, 20 mg at 24 hours, 10 mg at 48 hours, and 20 mg at 48 hours, respectively. Using the independent samples Kruskal Wallis test, no significant differences in signal-to-background ratios ($P=.70$), rim fluorescence ($P=.67$), and background fluorescence were observed ($P=.08$). Because no differences in TLRs were observed between the various groups, the optimal dose was determined by clinical and logistical preferences (the minimal dose of 10 mg of ICG administered 24 hours prior to surgery).

Intraoperative Detection of Colorectal Liver Metastases (N=40 Patients)

Subsequently, 24 more patients were included to assess the added value of NIR fluorescence imaging during resection of colorectal liver metastases. Results of liver metastases detection are summarized in Table 2. Using a combination of preoperative CT scanning, IOUS, visual inspection, and/or palpation, a total of 100 lesions were identified as suspected colorectal liver metastases. After resection, 3 of these lesions were histologically proven to be benign, for a net detection of 97 metastatic lesions by conventional imaging. NIR fluorescence imaging (Fig. 1 and Supplementary Video) detected a total of 71 lesions proven histologically to be metastases, all of which were ≤ 6.2 mm from the surface of the liver capsule. However, only 66 of the 71 lesions identified using NIR fluorescence overlapped with conventional imaging (Table 2 and Fig. 2). Most important, in 5 patients (12.5%, 95%CI = 5.0-26.6), superficially located, otherwise occult liver metastases were detected using NIR fluorescence only, but not by conventional imaging (ie, preoperative CT, IOUS, intraoperative visualization, and intraoperative palpation) (Fig. 1). Sensitivity of the preoperative CT scanning, intraoperative visual inspection/palpation in combination with IOUS, and

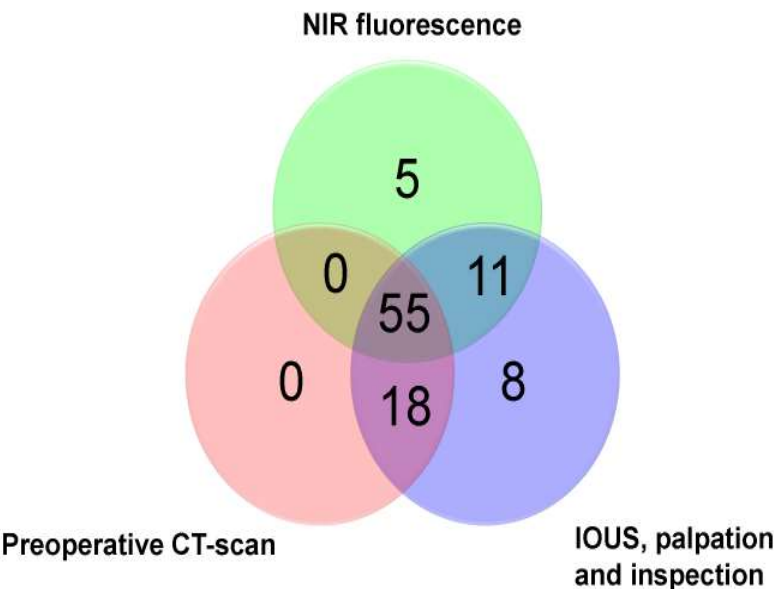


Fig. 2. Methods of detection of colorectal liver metastases are shown. Venn diagram shows how the 97 hepatic metastases were detected as a function of each modality alone or in combination. Abbreviations: CT, computed tomography; IOUS, intraoperative ultrasound; NIR, near infrared.

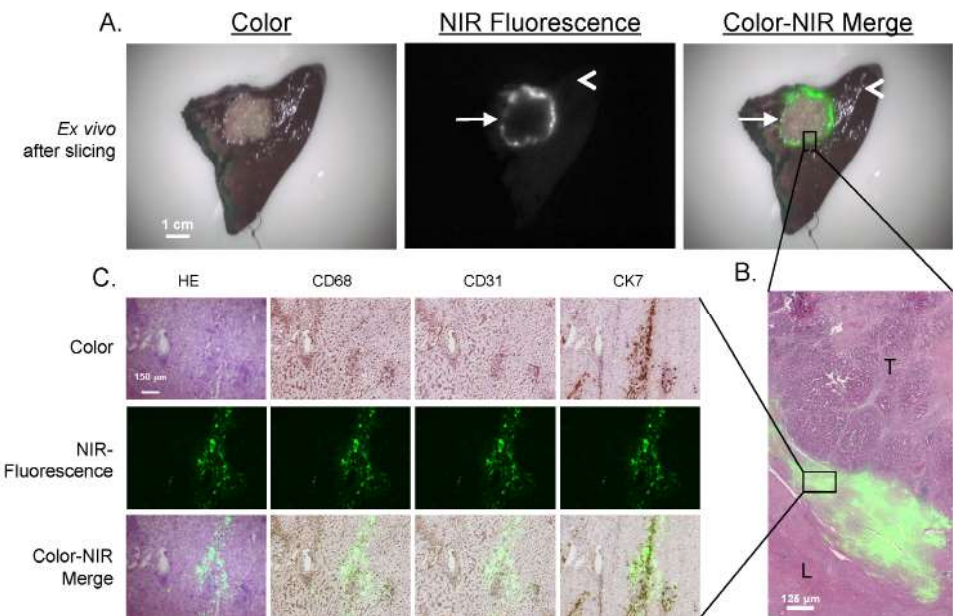


Fig.3. Pathologic examination of the tumour border is shown. (A) After resection and slicing of the same specimen, the rim around the tumour (arrow) can be visualized ex vivo. (B) Shown are hematoxylin and eosin (HE) staining with a pseudocolored green near-infrared (NIR) fluorescence overlay of a 20 µm tissue section of a colorectal liver metastasis using a 53 objective. The fluorescent rim in stromal tissue appears in the transition zone between tumour (T) and normal liver tissue (L). (C) Shown is liver tissue located in the fluorescent rim of a colorectal liver metastasis. Consecutive frozen sections (5 µm) are stained with HE and for CD68, CD31, and CK7. Microscopic color images (left column), NIR fluorescence images (middle column), and a pseudocolored green merge (right column) were obtained (1003 zoom). The NIR fluorescence signal is mainly located intracellularly and shows a high correlation with CK7 staining.

NIR fluorescence imaging were 75%, 95%, and 73%, respectively. In 3 patients, an additional wedge resection was performed to resect these metastases, and in 2 patients, the preoperatively planned metastasectomy was extended to resect the additional metastases. In these 5 patients, the total number of metastases (including the occult metastases detected only by NIR fluorescence) were 4, 3, 3, 2, and 2. After resection, these lesions were found to be 2, 3, 4, 6, and 9 mm in diameter, and histopathological examination confirmed these lesions to be colorectal liver metastases. One of these 5 occult lesions, which was 9 mm in diameter, was labeled as a complicated cyst based on IOUS and CT, whereas the clear NIR fluorescent ring around the lesion suggested that it was a liver metastasis. Twenty-six liver metastases (27%) identified by conventional imaging could not be detected using NIR fluorescence, and all were deeper than 8 mm from the liver surface. All fluorescent liver metastases presented a fluorescent rim around the tumour. The overall (N=40) median TLR was 7.0 (range, 1.9-18.7). The use of neoadjuvant chemotherapy did not significantly influence the TLR (7.5 ± 5.1 versus 7.1 ± 2.9 , $P=0.77$). In addition to liver metastases, a total of 8 hemangiomas, 13 cysts, and 4 bile duct hamartomas were identified in 13 patients. These hemangiomas, cysts, and bile duct hamartomas did not show an NIR fluorescent signal or rim (Fig. 1). Thus, NIR fluorescence imaging might help differentiate malignant liver lesions from some benign lesions. As might be expected based on the mechanism of ICG contrast (described below), extrahepatic tumour-positive lymph nodes were not fluorescent (data not shown).

Ex Vivo Detection of Colorectal Liver Metastases

Liver resection specimens were sliced into 5- to 7-mm slices, and subsequently the slices were imaged with the Mini-FLARE imaging system. In all patients for whom a liver resection was performed (N=33), ex vivo NIR fluorescence imaging was performed. All known metastases were identified ex vivo by a clear fluorescent ring around the lesion.

Immunohistochemistry and Fluorescence Microscopy

Fluorescence signal was located in liver tissue directly surrounding the tumour and was located both intracellularly and extracellularly (Fig. 3B). In liver tissue, in the area near the tumour, compressed hepatocytes and increased ductular transformation, periportal fibrosis, and presence of Kupffer cells were observed. Immunohistochemical analysis showed a close relation between fluorescence and CK7 staining (Fig. 3C). CK7 is expressed by immature hepatocytes in the areas of ductular transformation. No relation was found between fluorescence and the presence of Kupffer cells (CD68) and blood vessels (CD31).

DISCUSSION

The main objective of this study was to evaluate the potential of intraoperative NIR fluorescence imaging to improve oncologic resection of colorectal metastases to liver. As confirmed by pathological analysis, all superficially located (<6.2 mm beneath the liver surface) metastases were identified by NIR fluorescence. In addition, in 5 patients, occult metastases were detected using NIR fluorescence only and were missed by conventional detection methods (Fig. 2). Moreover, this study provides increased understanding of the mechanism responsible for the rim fluorescence and increases the understanding of the effect of different administration time points and doses of ICG on tumour detection. This is crucial for the implementation of this technique and interpretation of results in future studies.

An important recent study using visible wavelength optical imaging showed real-time identification of ovarian cancer metastases.¹⁸ Because of the relatively low tissue penetration of visible light, this technology is limited to tumours already on the surface of anatomical structures. Even when NIR fluorescence imaging is used, however, penetration depth is still a major issue. The penetration depth of NIR light is highly dependent on the optical properties, ie, absorption and scatter, of the tissue being imaged. Liver is highly absorbing compared with other tissues, such as breast and subcutaneous tissue of axilla, resulting in higher attenuation (ie, lower signal).¹⁹ In the current study, 26 metastases that were located 8 mm or more beneath the liver capsule could not be identified using NIR fluorescence. Preoperative CT scanning and IOUS are more appropriate for deeper lesions and did successfully identify these 26 lesions. However, superficially located, small occult metastases are known to be difficult to detect using IOUS, inspection, and palpation.^{10,11} Although IOUS is still required to identify deep (≥ 6 mm) metastases in the liver, our results suggest that NIR fluorescence imaging is complementary and helps to find small, superficially located liver metastases.

The use of NIR fluorescence imaging to detect liver metastases is dependent on the clearance of ICG by the liver. To optimize the use of this technique, it is necessary to examine the influence of ICG dose and timing of ICG administration prior to surgery. In this study, differences in dose and timing did not significantly influence the TLR. A previous study in rats by our group showed an optimal TLR in the group where ICG was administered at 72 hours prior to surgery.¹⁶ In the current clinical study, liver signal at 24 to 48 hours after injection of 10 mg ICG was comparable to the preinjection baseline level, which we measured in a previous study in patients undergoing a pancreatoduodenectomy, eliminating the need to test other time points.²⁰ Therefore, NIR fluorescence imaging at 72 hours after ICG administration was not performed. Other clinical work performed by Ishizawa et al suggested an interval between administration of ICG and liver surgery of at least 2 days to lower

background fluorescence and to obtain adequate TLRs.¹³ However, in the latter study, a substantially higher dose of ICG (0.5 mg/kg; ≈ 35 mg per subject) was administered. In the current study, a relatively low dose of ICG (0.13–0.26 mg/kg) was used, and it was therefore possible to reach acceptable TLRs and sufficiently low background liver fluorescence at 24 hours after administration of 10 mg ICG, which is safe and desirable from a logistical point of view.

Because no clinical data on lesion detection rates and standard deviation of the measurements were available prior to the study, a formal sample size calculation was not possible. However, we have provided 95% CIs for the 12.5% of patients in which additional lesions were detected only by NIR fluorescence (95%CI = 5.0–26.6). Well-powered future studies can now be designed on the basis of these data.

The detection rate of additional occult liver metastases during surgery is strongly dependent on the preoperative and intraoperative imaging modalities used. In this study, preoperative CT and IOUS were acquired to assess the extent of the disease. However, multiple novel imaging instruments are available for improved preoperative and intraoperative assessment of occult liver metastases. MRI benefits from increased soft tissue contrast and the availability of hepatocyte-specific contrast agents, which yields a higher sensitivity compared with CT for the detection of subcentimeter liver metastases and in case of neoadjuvant chemotherapy.^{21,22} Moreover, [18F] fluorodeoxyglucose positron emission tomography (FDG-PET) or PET-CT has been shown to be of additional value to detect extrahepatic disease.²¹ However, the sensitivity of detection of occult liver metastases using PET is not higher than that of CT.²¹ Despite the possible higher detection rate using MRI, it can be expected that lesions missed during preoperative imaging could be detected during IOUS or palpation, which will therefore not significantly alter the finding of the current study. Next to preoperative imaging modalities, novel modalities for intraoperative assessment of occult liver metastases, such as contrast-enhanced IOUS, have been introduced to improve sensitivity.^{23,24} However, NIR fluorescence has been shown to add value when used in combination with contrast-enhanced IOUS as well.²³

An important aspect of our study is that it can be readily translated to the community setting. First, it uses a contrast agent already approved by the US Food and Drug Administration for other indications. Second, multiple optical imaging systems are now available commercially and are comparable in size, cost, and upkeep to an IOUS instrument. Finally, unlike PET, MRI, and other emerging imaging technologies that require significant infrastructure investment and high operational costs, cart-based optical imaging is potentially viable in any clinical setting.

Although the false-positive rate in the current study was zero, previous studies have reported that nonmalignant lesions (large regenerative nodules and atypical hyperplastic nodules) display ICG uptake.^{13,14} The pattern of uptake appears to be important. In large regenerative nodules and atypical hyperplastic nodules, NIR

fluorescence is seen throughout the tumour (versus only in the rim). In the benign lesions (hemangiomas, cysts, and bile duct hamartomas) of our study, no fluorescence rim was seen. Clearly, larger clinical trials will be needed to determine the true false-positive rate and pattern of uptake of ICG as a function of benign lesion histology.

Using fluorescence microscopy, we observed intracellular accumulation of ICG in and around CK7-positive cells directly surrounding the tumour, and being compressed by it. The architecture of the liver parenchyma is often changed by the presence of hepatic metastases leading to compression of hepatic parenchyma, inflammatory infiltrate, ductular transformation, and increased presence of immature hepatocytes.²⁵⁻²⁷ It is known that immature hepatocytes often have impaired expression of their organic anion transporters, which are essential for the transport of many organic anions, including ICG.²⁸⁻³² For example, in the absence of multidrug resistance P-glycoprotein 2, the biliary excretion of ICG can be reduced by 90%.³³ Therefore, the pattern of rim fluorescence could be explained by the presence of immature hepatocytes in the liver tissue surrounding the tumour that have taken up ICG, but exhibit impaired biliary clearance.

As in other areas of surgery, the use of laparoscopy is expanding to liver surgery. Minor liver resections such as left lateral hepatectomies are being performed laparoscopically as standard-of-care in several centers.³⁴ NIR fluorescence may also be of great value in laparoscopic surgery, because palpation of the liver is not possible and the surgeon can only rely on visual inspection, IOUS, and preoperative imaging. To implement NIR fluorescence in laparoscopic liver surgery, laparoscopic NIR fluorescence camera systems are currently being developed and tested.³⁵⁻³⁷

In conclusion, this study demonstrates identification of otherwise undetectable cancer metastases in 12.5% of patients and suggests that intraoperative NIR fluorescence imaging is complementary to conventional techniques for the detection of liver metastases from colorectal cancer, and has great potential for laparoscopic procedures

ACKNOWLEDGMENTS

This study was performed within the framework of CTMM, the Center for Translational Molecular Medicine (DeCoDe project, grant 03O-101 and MUSIS project, grant 03O-202). This work was supported in part by the Gastrostart grant (Dutch Association for Gastroenterology), the Dutch Cancer Society grant UL2010-4732 and National Institutes of Health grant R01-CA-115296. Dr. van der Vorst is an MD medical research trainee funded by the Netherlands Organisation for Health Research and Development (grant 92003593).

REFERENCES

1. Manfredi S, Lepage C, Hatem C, et al. Epidemiology and management of liver metastases from colorectal cancer. *Ann Surg.* 2006;244:254-259.
2. Abdalla EK, Vauthey JN, Ellis LM, et al. Recurrence and outcomes following hepatic resection, radiofrequency ablation, and combined resection/ablation for colorectal liver metastases. *Ann Surg.* 2004;239:818-825.
3. Choti MA, Sitzmann JV, Tiburi MF, et al. Trends in long-term survival following liver resection for hepatic colorectal metastases. *Ann Surg.* 2002;235:759-766.
4. Pawlik TM, Izzo F, Cohen DS, et al. Combined resection and radiofrequency ablation for advanced hepatic malignancies: results in 172 patients. *Ann Surg Oncol.* 2003;10:1059-1069.
5. Rees M, Tekkis PP, Welsh FK, et al. Evaluation of long-term survival after hepatic resection for metastatic colorectal cancer: a multifactorial model of 929 patients. *Ann Surg.* 2008;247: 125-135.
6. Wei AC, Greig PD, Grant D, et al. Survival after hepatic resection for colorectal metastases: a 10-year experience. *Ann Surg Oncol.* 2006;13:668-676.
7. Pawlik TM, Scoggins CR, Zorzi D, et al. Effect of surgical margin status on survival and site of recurrence after hepatic resection for colorectal metastases. *Ann Surg.* 2005;241:715-722.
8. Karanjia ND, Lordan JT, Fawcett WJ, et al. Survival and recurrence after neo-adjuvant chemotherapy and liver resection for colorectal metastases: a ten year study. *Eur J Surg Oncol.* 2009;35:838-843.
9. Fong Y, Cohen AM, Fortner JG, et al. Liver resection for colorectal metastases. *J Clin Oncol.* 1997;15:938-946.
10. Leen E, Ceccotti P, Moug SJ, et al. Potential value of contrastenhanced intraoperative ultrasonography during partial hepatectomy for metastases: an essential investigation before resection? *Ann Surg.* 2006;243:236-240.
11. Sahani DV, Kalva SP, Tanabe KK, et al. Intraoperative US in patients undergoing surgery for liver neoplasms: comparison with MR imaging. *Radiology.* 2004;232:810-814.
12. Nomura K, Kadoya M, Ueda K, et al. Detection of hepatic metastases from colorectal carcinoma: comparison of histopathologic features of anatomically resected liver with results of preoperative imaging. *J Clin Gastroenterol.* 2007;41:789-795.
13. Ishizawa T, Fukushima N, Shibahara J, et al. Real-time identification of liver cancers by using indocyanine green fluorescent imaging. *Cancer.* 2009;115:2491-2504.
14. Gotoh K, Yamada T, Ishikawa O, et al. A novel image-guided surgery of hepatocellular carcinoma by indocyanine green fluorescence imaging navigation. *J Surg Oncol.* 2009;100:75-79.
15. Verbeek FP, van der Vorst JR, Schaafsma BE, et al. Image-guided hepatopancreatobiliary surgery using near-infrared fluorescent light. *J Hepatobiliary Pancreat Sci.* 2012;19:626-637.
16. van der Vorst JR, Hutteman M, Mieog JS, et al. Near-infrared fluorescence imaging of liver metastases in rats using indocyanine green. *J Surg Res.* 2012;174:266-271.
17. Mieog JS, Troyan SL, Hutteman M, et al. Toward optimization of imaging system and lymphatic tracer for near-infrared fluorescent sentinel lymph node mapping in breast cancer. *Ann Surg Oncol.* 2011;18:2483-2491.
18. van Dam GM, Themelis G, Crane LM, et al. Intraoperative tumorspecific fluorescence imaging in ovarian cancer by folate receptoralpha targeting: first in-human results. *Nat Med.* 2011;17:1315-1319.
19. Stolik S, Delgado JA, Perez A, et al. Measurement of the penetration depths of red and near infrared light in human "ex vivo" tissues. *J Photochem Photobiol B.* 2000;57:90-93.
20. Hutteman M, van der Vorst JR, Mieog JS, et al. Near-infrared fluorescence imaging in patients undergoing pancreaticoduodenectomy. *Eur Surg Res.* 2011;47:90-97.
21. Frankel TL, Gian RK, Jarnagin WR. Preoperative imaging for hepatic resection of colorectal cancer metastasis. *J Gastrointest Oncol.* 2012;3:11-18.
22. van Kessel CS, Buckens CF, van den Bosch MA, et al. Preoperative imaging of colorectal liver metastases after neoadjuvant chemotherapy: a meta-analysis. *Ann Surg Oncol.* 2012;19:2805-2813.

23. Uchiyama K, Ueno M, Ozawa S, et al. Combined use of contrast-enhanced intraoperative ultrasonography and a fluorescence navigation system for identifying hepatic metastases. *World J Surg.* 2010;34:2953-2959.
24. Takahashi M, Hasegawa K, Arita J, et al. Contrast-enhanced intraoperative ultrasonography using perfluorobutane microbubbles for the enumeration of colorectal liver metastases. *Br J Surg.* 2012;99:1271-1277.
25. Irie T, Tsushima Y, Terahata S, et al. Rim enhancement in colorectal metastases at CT during infusion hepatic arteriography. Does it represent liver parenchyma or live tumor cell zone? *Acta Radiol.* 1997;38:416-421.
26. Marchal GJ, Pylyser K, Tshibwabwa-Tumba EA, et al. Anechoic halo in solid liver tumors: sonographic, microangiographic, and histologic correlation. *Radiology.* 1985;156:479-483.
27. Vermeulen PB, Colpaert C, Salgado R, et al. Liver metastases from colorectal adenocarcinomas grow in three patterns with different angiogenesis and desmoplasia. *J Pathol.* 2001;195:336-342.
28. Oshima H, Kon J, Ooe H, et al. Functional expression of organic anion transporters in hepatic organoids reconstructed by rat small hepatocytes. *J Cell Biochem.* 2008;104:68-81.
29. de Graaf W, Hëausler S, Heger M, et al. Transporters involved in the hepatic uptake of (99m) Tc-mebrofenin and indocyanine green. *J Hepatol.* 2011;54:738-745.
30. Cui Y, Konig J, Leier I, et al. Hepatic uptake of bilirubin and its conjugates by the human organic anion transporter SLC21A6. *J Biol Chem.* 2001;276:9626-9630.
31. Yang YM, Tian XD, Zhuang Y, et al. Risk factors of pancreatic leakage after pancreaticoduodenectomy. *World J Gastroenterol.* 2005;11:2456-2461.
32. Ros JE, Roskams TA, Geuken M, et al. ATP binding cassette transporter gene expression in rat liver progenitor cells. *Gut.* 2003;52: 1060-1067.
33. Huang L, Vore M. Multidrug resistance p-glycoprotein 2 is essential for the biliary excretion of indocyanine green. *Drug Metab Dispos.* 2001;29:634-637.
34. Chang S, Laurent A, Tayar C, et al. Laparoscopy as a routine approach for left lateral sectionectomy. *Br J Surg.* 2007;94:58-63.
35. Matsui A, Tanaka E, Choi HS, et al. Real-time intra-operative near-infrared fluorescence identification of the extrahepatic bile ducts using clinically available contrast agents. *Surgery.* 2010;148:87-95.
36. van der Poel HG, Buckle T, Brouwer OR, et al. Intraoperative laparoscopic fluorescence guidance to the sentinel lymph node in prostate cancer patients: clinical proof of concept of an integrated functional imaging approach using a multimodal tracer. *Eur Urol.* 2011;60:826-833.
37. Ishizawa T, Bandai Y, Kokudo N. Fluorescent cholangiography using indocyanine green for laparoscopic cholecystectomy: an initial experience. *Arch Surg.* 2009;144:381-382.

Chapter 8

Summary and Future perspectives

SUMMARY

Intraoperative imaging using near-infrared (NIR) fluorescence is a fast developing imaging modality as it provides real-time visual information during surgery (**Chapter 1**). The ability to detect lymph nodes and tumours that need to be resected can assist the surgeon to improve surgery by reducing time of the procedure, reducing iatrogenic damage, and improve the number of radical resections. This thesis focuses on the introduction of NIR fluorescence imaging into the clinic. **Part 1** of this thesis describes the optimization of NIR fluorescence imaging for sentinel lymph node (SLN) biopsy using the clinically available NIR tracer Indocyanine green (ICG) in various cancer types. Moreover, these studies show both the limitations as the clinical benefit of NIR fluorescence for SLN biopsy. **Part 2** describes the use of NIR light for tumour detection. Tissue absorption and scattering in the NIR light spectrum was used for neoadjuvant treatment response monitoring in breast cancer patients. Moreover, NIR fluorescence imaging using NIR contrast agents was used for the intraoperative detection of otherwise difficult to localize liver metastases of colorectal cancer.

PART 1. Sentinel lymph node mapping

Sentinel lymph node mapping has been introduced for various types of cancer for either avoiding complete lymphadenectomy or improving nodal staging by selecting lymph nodes for ultrastaging. Up to now, radioactive colloids and blue dyes are most often used as standard of care for SLN biopsy in clinical practise. However, the use of radioactive colloids requires the involvement of a nuclear physician and localisation of the SLN can be difficult using a handheld gamma probe due the lack of visual information and interference of the injection site. Blue dyes cannot be seen easily through the skin and fatty tissue. Moreover, blue dye migrates quickly to 2nd-tier lymph nodes, which complicates differentiation between the SLN and 2nd-tier nodes. NIR fluorescence imaging allows non-ionizing detection of lymphatic tracers deeper into the tissue (up to 1 cm) and does not interfere with the surgical field. Moreover, as ICG binds to large proteins (such as albumin), this results in improved retention in the SLN. These favourable properties of NIR fluorescence imaging should therefore translate into improved detection of the SLN.

In previous preclinical studies, premixing of ICG with HSA showed clear advantages: it improved the retention of the dye in the SLN and increased the fluorescence brightness. **Chapter 2** aims to test this advantage in a clinical randomized setting, since lymph fluids consist of high protein levels, and ICG alone might rapidly bind to these endogenous proteins when draining in the lymphatic system. This could possible eliminate the need for premixing ICG with HSA. In vulvar cancer patients, no difference was found between groups injected with ICG with or without premixing with albumin in fluorescence contrast ($P = 0.65$) or number of fluorescent nodes detected

($P = 0.06$). Similar results were found in patients with cervical cancer and described in **Chapter 3**. This indicates that premixing of ICG with HSA can be omitted. This simplifies the clinical procedure and can facilitate the introduction of this technique in clinical practice.

Though NIR fluorescence imaging provides some depth penetration, studies showed the need for radioactive colloids for the detection of deeper located SLNs. Therefore, in **Chapter 4**, ICG was covalently bound to radioactive Nanocolloid (^{99m}Tc -Nanocolloid) to form the hybrid radioactive and NIR fluorescence tracer ICG- ^{99m}Tc -Nanocolloid tracer, which provides both preoperative imaging and intraoperative imaging. In breast cancer patients, this tracer permitted both fluorescence and radio-guidance of all SLNs. When the tracer is already injected for pre operative sentinel lymph node imaging, no additional injection prior to surgery is necessary and the intraoperative findings are comparable to those when using ICG alone. Moreover, NIR fluorescence staining outperformed blue dye staining as 100% of the SLNs were fluorescent and only 88% stained blue. Moreover, it was shown that increasing the particle density of ICG-Nanocolloid did not increase fluorescence brightness ($P = 0.590$), which indicates that a dose of $160\text{ }\mu\text{M}$ ICG- ^{99m}Tc -Nanocolloid (in $200\text{ }\mu\text{L}$) is optimal.

In addition to the clinical available NIR tracer ICG, novel fluorophores are developed, which have improved fluorescence properties and can be easily bound to tumour specific ligands or large proteins. In **Chapter 5** the novel fluorophore IRDye 800CW was bound to human serum albumin (complex: HSA800) and evaluated for SLN mapping. The procedure was performed ex vivo after resection in patients with colon cancer, as IRDye 800CW has not yet been approved by the FDA and EMA. HSA800 allowed clear fluorescent identification of the SLNs and was of added value to conventional blue dye, as NIR fluorescence allowed detection of additional SLNs and allowed easy detection of SLNs located deeper into the mesenteric fat. Moreover, NIR fluorescence cannot be confused with blue nodal staining resulting from preoperative tattooing of the tumour.

PART 2. Tumour detection

Chapter 6 describes the use of NIR light for tumour detection using tissue absorption and scattering characteristics of tumour tissue. This is used for longitudinal response measurements of breast cancer to neoadjuvant chemotherapy. Using diffuse optical spectroscopy in the NIR light spectrum, the Softscan can assess metabolic parameters such as Hb, HbO_2 , $\%\text{H}_2\text{O}$, and $\%\text{lipid}$. As tumour tissue has high tissue density (high H_2O content), contains less breast tissue (high lipid content) and has high metabolic activity, which requires high blood supply and high oxygen usage, tumour tissue can be clearly differentiated from normal breast tissue. As early as after the first chemotherapy

cycle a significant difference between responders and non-responders was found using the Softscan ($P = 0.023$).

In addition to SLN mapping, the use of ICG is also explored for tumour imaging as ICG is cleared by the liver and has been shown to passively accumulate around colorectal liver metastases. **Chapter 7** focuses on the clinical optimization of ICG dose and timing of injection for the detection of colorectal liver metastases and assess patient benefit. No difference in signal-to-background were found between the different treatment groups (10mg 24h, 10mg 48h, 20mg 24h, 20mg 48; $P = 0.70$). Therefore an injection of 10mg ICG at 24 h before surgery is considered desirable from a safety and logistical point of view. Importantly, in 5 of 40 patients (12.5%, 95% CI: 5.0-26.6), additional small and superficially located lesions were detected using NIR fluorescence, and were otherwise undetectable by preoperative computed tomography (CT), intraoperative ultrasound (IOUS), visual inspection, and palpation.

FUTURE PERSPECTIVES

Pre-operative imaging modalities such as HD-US, CT, MRI, PET and SPECT are rapidly improving. However, the occurrence of non-radical tumour resections and iatrogenic injuries during surgery is not uncommon. Therefore, the need for improved intraoperative imaging tools is imperative. Image-guided surgery using NIR fluorescence is real-time, can provide depth penetration and is highly specific, without altering the surgical field. For these reasons, NIR fluorescence imaging is currently attracting major interest world wide as new intra-operative imaging modality.¹

This thesis shows the use of NIR fluorescence imaging for identifying SLNs and tumour tissue and presents the advantages over other intra-operative imaging modalities using clinical available technologies. As the NIR fluorescence tracer ICG has already been used since the sixties with hardly any toxicity, safety is not an issue.² This has led to the exponential use of ICG in clinical trials for NIR fluorescence imaging. However, several hurdles will have to be conquered before the surgeon will use NIR fluorescence imaging in daily practice.

Cost-benefit analysis will have to show the additional benefit of NIR fluorescence imaging before it will be widely accepted as standard-of-care. This thesis and most current studies mainly focus on the feasibility and optimization of the technique. This is necessary before the start of large multi-center trials to provide the most efficient technique and allow for sample size calculations. Large multi-center studies are now in progress using already clinical available NIR probes, which will hopefully lead to wider implementation of NIR fluorescence imaging. Currently the costs of NIR fluorescence imaging mainly depend on the used imaging system, as costs of a vial of ICG are less than 100 Euro. Therefore, it is reasonable to suggest that with the benefit of NIR fluorescence imaging presented in the thesis, cost-benefit analysis will be favouring NIR fluorescence imaging in clinical practice.

Surgery is evolving to minimal invasive techniques. Both laparoscopic and robotic surgical techniques have shown to provide less morbidity and shorter hospital stays for multiple indications including large oncologic operations. Both techniques use camera systems to provide the surgeon with visual information of the operation field on a screen. Therefore, adding NIR fluorescence is relatively easy and only requires small adaptation of the camera sensor and light source. Already multiple commercial suppliers of laparoscopic and robotic surgical systems provide the option to use NIR fluorescence imaging. This will attribute to the fast introduction of intraoperative NIR fluorescence imaging.

Moreover, we are only at the start of this new imaging technology. Multiple research groups are developing new NIR fluorescent probes, which have improved properties for identification of tumour tissue or vital anatomical structures. Using intraoperative fluorescence imaging, cancer in the head and neck region can be clearly

visualized using cetuximab conjugated to a NIR fluorophore³ and folate-FITC allows for intraoperative detection of ovarian and lung cancer.^{4,5} The development of these new probes will further expand the use of NIR fluorescence image-guided surgery.

The development of these new tracers is not only focussed on the targeting part (e.g. HER2, EGFR) of the probe. Other aspects such as fluorescence brightness, particle size and particle charge are crucial for providing sufficient tumour-to-background signal.⁶ For example, during imaging of colorectal liver metastases, the tracer needs to be cleared preferably by the kidneys as liver take-up can result in a significant increase of the background signal, which subsequently decreases tumour-to-background signal.

The development of new FDA and EMA approved drugs require extensive research and validation. With the increasing interest of commercial partners, partly also as result of the successful use of currently available probes such as ICG, the introduction of new FDA and EMA fluorescent agents is coming closer.

Though, still for some indications, in which more depth penetration will be required, other solutions will have to be found. Several possibilities are currently investigated, such as opto-acoustic imaging and multimodal imaging combining fluorescence imaging with PET or SPECT.⁷ Combining fluorescence with PET or SPECT has the additional advantage of combining pre-operative imaging, which will further allow for improved surgical planning and could also provide a surgical roadmap for intraoperative navigation. This concept was recently demonstrated in patients with melanoma that underwent SLN biopsy.⁸ Using the same tracer pre- and intra-operative allows for real-time navigation after feeding SPECT/CT images to the intra-operative navigation system, and when approaching the targeted tissue, fluorescence imaging provides the real-time visual confirmation.

If the future of NIR fluorescence imaging will continue to develop as it currently is, in the near future not one NIR tracer but a combination of NIR fluorescent probes will be used to delineate the tumour and vital structures both pre-operative as provide real-time intra-operative navigation. All with the goal to reduce unnecessary tissue damage, which will reduce morbidity and reduce time of hospitalization and to improve oncological outcome by increasing the number of patients in whom a complete resection of tumour tissue will be achieved. This will reduce the need for re-interventions and improve disease free survival.

In addition to the use of NIR imaging during surgery, the use of NIR imaging as a non-invasive imaging modality has shown great potential. In this thesis, NIR imaging was successfully used to identify breast cancer patients who did not benefit from neoadjuvant chemotherapy and would therefore possibly benefit from a different chemotherapy regime or from direct surgery. With the increasing use of neoadjuvant chemotherapy in cancer in general (e.g. breast cancer, oesophageal cancer and rectal

cancer), NIR imaging could be of great benefit for monitoring tumour response to chemotherapy, thereby providing patient tailored medicine.

Not only the use of neoadjuvant chemotherapy is increasing. More medicinal tumour targeted treatment options are available every year. Tumour targeted treatments have shown improvement in the survival of cancer in for example stage IV melanoma and stage IV breast cancer.^{9,10} With the growing knowledge of pathways that are responsible for tumour progress, more treatment options will become available. This has already led to speculations that some cancers will not be the cause of death in patients with cancer, but will rather become a chronic illness.¹¹

With the improving options to treat the advanced stages of cancer, we simultaneously try less aggressive treatment strategies of in situ carcinoma or early stage cancer. This, to reduce morbidity from non-beneficial treatment. In for example patients with rectal cancer, patients with a clinical complete response to chemoradiotherapy did not undergo surgery. Instead, patients received intensive follow-up: “wait-and-see”, without effect on disease-free survival.¹² Moreover, in breast cancer patients it is debated to be less aggressive with surgery in ductal carcinoma in situ, which is currently evaluated in a clinical trial (EORTC 1401-BCG).

The field of oncology is evolving rapidly: earlier detection of small tumours, more advanced surgical techniques, and innovative medicinal treatment strategies. All of which are focused to reduce morbidity and improve survival. In all these developments clear visualisation of tumour is essential to correctly assess tumour extent and observe the effect of treatment. NIR imaging, as a novel imaging modality, will therefore make a significant contribution to the treatment of cancer.

REFERENCES

1. Vahrmeijer AL, Hutteman M, van der Vorst JR et al., Image-guided cancer surgery using near-infrared fluorescence. *Nat Rev Clin Oncol* 2013;10:507-18.
2. Alford R, Simpson HM, Duberman J et al., Toxicity of organic fluorophores used in molecular imaging: literature review. *Mol Imaging* 2009;6:341-54.
3. Rosenthal EL, Warram JM, de Boer E et al., Safety and tumor specificity of cetuximab-IRDye800 for surgical navigation in head and neck cancer. *Clinical Cancer Research* 2015;21:3658-66.
4. Okusanya OT, DeJesus EM, Jiang JX et al., Intraoperative molecular imaging can identify lung adenocarcinomas during pulmonary resection. *J Thor Car Surg* 2015;in press.
5. Van Dam GM, Themelis G, Crane LM et al., Intraoperative tumor-specific fluorescence imaging in ovarian cancer by folate receptor- α targeting: first inhuman results. *Nat Med* 2011;18:1315-9.
6. Choi HS, Gibbs SL, Lee JH et al., Targeted zwitterionic near-infrared fluorophores for improved optical imaging. *Nat Biotechnol* 2013;31:148-53.
7. De Boer E, Harlaar NJ, Taruttis A et al., Optical innovations in surgery. *Br J Surg* 2015;102:56-72.
8. Van den Berg NS, Brouwer OR, Schaafsma BE et al., Multimodal surgical guidance during sentinel node biopsy for melanoma: combined gamma tracing and fluorescence imaging of the sentinel node through use of the hybrid tracer indocyanine green-(99m)Tc-Nanocolloid. *Radiology* 2015;275:521-9.
9. Swain SM, Baselga J, Kim SB et al., Pertuzumab, Trastuzumab, and Docetaxel in HER2-positive metastatic breast cancer. *N Engl J Med* 2015;372:724-34.
10. Grob JJ, Long GV, Schadendorf D et al., Disease kinetics for decision-making in advanced melanoma: a call for scenario-driven strategy trials. *Lancet Oncol* 2015;16:522-6.
11. Voormolen S, De tumor even voor de gek houden, NRC 24-01-2015.
12. Beets GL, Figueiredo NL, Habr-Gama A, et al., A new paradigm for rectal cancer: Organ preservation introducing the International Watch & Wait Database (IWWD). *EJSO* 2015;41:1562-4.

NEDERLANDSE SAMENVATTING

Intraoperatieve beeldvorming middels nabij-infrarode (NIR) fluorescentie is een snel ontwikkelende technologie die de chirurg met real-time visuele informatie voorziet (**Hoofdstuk 1**). De mogelijkheid om lymfeklieren en tumoren te detecteren die chirurgisch verwijderd moeten worden kan de chirurg helpen de duur van de operatie te verkorten, onnodige weefselschade te beperken, en het verbeteren van radicale resecties. Dit proefschrift focust op het introduceren van NIR fluorescente beeldvorming in de kliniek. **Deel 1** van dit proefschrift beschrijft het optimaliseren van NIR fluorescente beeldvorming voor de schildwachtklierprocedure. Hierbij wordt met name gebruik gemaakt van de klinisch beschikbare NIR fluorescente tracer Indocyanine Groen (ICG) bij verschillende typen kanker. Daarbij worden bovendien de beperkingen en de klinisch voordelen van NIR fluorescente beeldvorming bij de schildwachtklierprocedure beschreven. **Deel 2** beschrijft het gebruik van NIR licht (700 – 900nm) voor het detecteren van tumorweefsel. Zo kunnen de optische eigenschappen van weefsel in het NIR lichtspectrum gebruikt worden voor het niet-invasief monitoren van tumor respons op neoadjuvante chemotherapie behandeling bij borstkankerpatiënten. Daarnaast kan NIR fluorescente beeldvorming gebruikt worden om tijdens de operatie tumorweefsel te identificeren, dat anders moeilijk of niet gevonden zou worden.

DEEL 1. Schildwachtklierprocedure

De schildwachtklierprocedure is voor verschillende type tumoren geïntroduceerd als standaard behandeling voor het voorkomen van een complete lymfeklierdissectie. Tevens kan de schildwachtklierprocedure gebruikt worden voor het selecteren van lymfeklieren voor additionele screening op tumorcellen door de patholoog om de lymfeklier stadiëring te verbeteren. Bij de huidige methode voor het detecteren van de schildwachtklier wordt met name gebruik gemaakt van een combinatie van radioactieve colloïden en een blauwe kleurstof. Echter, het gebruik van radioactieve deeltjes vereist de aanwezigheid van een Nucleair Geneeskundige. Daarbij kan het soms lastig zijn tijdens de operatie de schildwachtklier te localiseren met de gamma probe omdat er geen visuele feedback is en er verstoring kan zijn van het radioactieve signaal ter plaatse van de injectie plek. De blauwe kleurstof heeft als nadeel dat deze niet gezien kan worden door de huid of vetweefsel heen. Daarbij migreert de blauwe kleurstof snel voorbij de schildwachtklier naar de 2^e echelon klieren waardoor het differentiëren tussen de schildwachtklier(en) en 2^e echelon klieren bemoeilijkt wordt.

NIR fluorescente beeldvorming maakt het mogelijk om zonder radioactiviteit dieper in weefsel (tot 1 cm) te kijken zonder dat het interfereert met het chirurgisch veld. Daarbij bindt ICG aan grote eiwitten (zoals albumine) wat mogelijk resulteert in

een verbeterde retentie van ICG in de schildwachtklieren. Uit preklinische studies bleek dat het voor injectie mixen van ICG met humaan serum albumine zou leiden tot een toename van de retentie van ICG in de schildwachtklier en een verhoogd fluorescent signaal. In **hoofdstuk 2** en **hoofdstuk 3** wordt dit voordeel van het mixen van ICG met humaan albumine getest in een klinische gerandomiseerde setting. In patiënten met vulvakanker werd geen verschil gezien tussen de groepen die geïnjecteerd waren met ICG:HSA of ICG alleen wat betreft de mate van fluorescentie ($P = 0.65$) of het aantal gedetecteerde fluorescente schildwachtklieren ($P = 0.06$). Vergelijkbare resultaten werden gezien in patiënten met baarmoederhalskanker, waarbij ook geen verschil werd gezien tussen de 2 groepen wat betreft fluorescentie ($P = 0.72$) en aantal geïdentificeerd fluorescente schildwachtklieren ($P = 0.84$). Dit geeft aan dat het mixen van ICG met humaan serum albumine achterwege kan worden gelaten. Dit is waarschijnlijk het gevolg van dat ICG, zodra het de lymfbanen bereikt, snel bindt aan lichaamseigen eiwitten in de lymfebanen, waardoor deze stap voor injectie overbodig is. Het niet hoeven mixen van ICG met humaan serum albumine maakt de procedure simpeler en vergemakkelijkt de klinische introductie van deze techniek.

Toch heeft eerder onderzoek laten zien dat er een noodzaak is voor het gebruik van radioactieve colloïden voor het detecteren van dieper gelegen schildwachtklieren. Derhalve werd in **hoofdstuk 4** ICG gekoppeld aan het radioactieve Nanocolloid (99mTc-Nannocolloid) om de hybride fluorescente en radioactieve tracer ICG-99mTc-Nannocolloid tracer te vormen waarmee zowel preoperatieve als intraoperatieve beeldvorming mogelijk is. In patiënten met borstkanker kon de schildwachtklier in alle gevallen gedetecteerd worden door zowel fluorescente beeldvorming als radioactiviteit. Ook in deze studie was de identificatieratio van de schildwachtklier hoger middels fluorescentie (100%) dan met de blauwe kleurstof (83%). Een voordeel van deze gecombineerde injectie van ICG aan radioactief Nanocolloid is dat er geen aparte preoperatieve injectie van ICG meer nodig is. Tevens werd gezien dat het verhogen van de concentratie ICG-Nannocolloid partikels niet zorgt voor een verbetering van het fluorescente signaal ($P = 0.59$) of voor het kunnen vinden van meer schildwachtklieren. Op basis van deze resultaten was een dosis van 160 μM (in 200 μL) ICG-99mTc-Nannocolloid optimaal.

Naast de klinisch beschikbare NIR tracer ICG, zijn er meerdere fluorescente tracers in ontwikkeling die betere fluorescente eigenschappen hebben en makkelijker gekoppeld kunnen worden aan andere eiwitten. In **hoofdstuk 5** is de nieuwe fluorescente kleurstof IRDye 800CW, gekoppeld aan humaan serum albumine (complex: HSA800), geëvalueerd als tracer voor de schildwachtklierprocedure. Omdat IRDye 800CW nog niet goed gekeurd is voor klinisch gebruik door de FDA en EMA werd de procedure ex vivo uitgevoerd bij patiënten met darmkanker direct na de resectie hiervan. Na injectie van HSA800 rond de tumor was het mogelijk om middels fluorescente beeldvorming duidelijk de schildwachtklieren te detecteren in het mesenteriale vet en daarbij

was HSA800 van toegevoegde waarde in vergelijking tot de blauwe kleurstof. NIR fluorescente beeldvorming met HSA800 identificeerde meer schildwachtklieren die niet gevonden waren met de blauw kleurstof en het was mogelijk om lymfeklieren die dieper in het mesenteriaal vet lagen direct te detecteren. Daarnaast kan de fluorescente beeldvorming niet verward worden met de blauwe verkleuring van lymfeklieren die optreedt als gevolg van het preoperatief endoscopische markeren van darmtumoren.

DEEL 2. Tumor detectie

Deel II, hoofdstuk 6, beschrijft het gebruik van NIR licht voor de detectie van tumorweefsel waarbij gebruik wordt gemaakt van de optische eigenschappen (absorptie en scattering) van tumorweefsel. Dit kan worden gebruikt voor het meten van de tumor respons op neoadjuvante chemotherapie in patiënten met borstkanker tijdens de behandeling. Middels diffuse optische spectroscopie in het NIR lichtspectrum kan de Softscan weefselparameters berekenen, zoals Hb, HbO₂, %water en %vetweefsel. Omdat tumorweefsel een hoge weefseldichtheid kent (hoog percentage water), weinig normaal borstweefsel (hoog percentage vetweefsel) en een hoge metabolische activiteit heeft, welke veel bloedvoorziening nodig heeft en veel O₂ gebruikt, kan de tumor duidelijk worden onderscheiden van gezond weefsel. Daarbij was het mogelijk om al na 2 tot 3 weken na de eerste gift chemotherapie een accurate voorspelling te doen wat betreft de tumor respons op de therapie. Een goede voorspelling van patiënten die geen baat hebben bij de ingestelde therapie kun je op deze manier mogelijk vroegtijdig een andere therapie bieden, zoals bijvoorbeeld chirurgie. Daarbij kun je voorkomen dat deze patiënten onnodige toxische chemotherapie behandeling moeten ondergaan.

Naast de schildwachtklierprocedure wordt het gebruik van ICG voor NIR fluorescente beeldvorming ook onderzocht voor beeldvorming van solide tumoren. ICG wordt geklaard door de lever en recent onderzoek heeft laten zien dat ICG daarentegen juist accumuleert in de lever rondom colorectale metastasen. **Hoofdstuk 7** focust op het optimaliseren van de dosis en het moment van toediening voor het klinisch gebruik van ICG voor de detectie van colorectale levermetastasen. Daarbij wordt tevens gekeken naar de klinische toegevoegde waarde van deze nieuwe techniek. Er werd geen verschil in de ratio van het fluorescente signaal van de tumor en achtergrond gevonden voor de verschillende behandelgroepen (10 mg 24h, 10mg 48h, 20mg 24h, 20 mg 48h; P = 0.70). Daarom lijkt een dosis van 10mg, toegediend een dag voor de operatie, het meest voor de hand liggend vanuit logistieke redenen en veiligheidsaspecten. Een belangrijke bevinding was dat in 5 van de 40 patiënten (12.5%, 95% CI: 5.0-26.6) additionele kleine oppervlakkige tumoren gevonden werden middels NIR fluorescente beeldvorming, die initieel niet waren gevonden bij de preoperatieve CT, intraoperatieve echografie of door inspectie of palpatie.

Conclusie

NIR fluorescente beeldvorming is een veelbelovend techniek voor de intra-operatieve beeldvorming van tumoren en schildwachtklieren. Naast het proof-of-principle concept levert NIR fluorescente beeldvorming ook een duidelijk klinisch voordeel op ten opzichte van de conventionele technieken. Dit met name vanwege de zeer hoge specificiteit van NIR fluorescente contrastmiddelen en de hogere weefselpenetratie van NIR licht. Hierdoor kunnen met behulp van NIR fluorescente beeldvorming bij de schildwachtklierprocedure meer klieren gevonden worden in vergelijking tot blauwe kleurstof en zou de blauwe kleurstof ook achterwege kunnen worden gelaten. Echter, ondanks dat NIR licht dieper weefsel penetreert dan het licht dat voor de mens zichtbaar is (400nm – 700nm), is de huidige detectie diepte van de beschikbare intra-operatieve camerasystemen voor NIR licht beperkt tot ongeveer 1 cm. Derhalve blijven radioactieve tracers die tot veel dieper te traceren zijn pre- en peroperatief noodzakelijk. Het combineren van NIR fluorescente beeldvorming en radioactieve tracers is dan ook een logische volgende stap. Ook voor de intra-operatieve detectie van tumoren heeft NIR fluorescente beeldvorming evident meerwaarde. Zo is het mogelijk om middels ICG additionele colorectale levermetastasen te vinden die niet werden gezien op conventionele pre- en intra-operatieve beeldvorming. Met de komst van nieuwe tumorspecifieke NIR tracers en de verbetering van intra-operatieve camera systemen zal de meerwaarde alleen maar verder toenemen. Naast de toegevoegde waarde op het operatieve vlak, kan NIR beeldvorming ook gebruikt worden voor niet-invasieve beeldvorming bij het monitoren van de tumor respons op neoadjuvante chemotherapie bij bijvoorbeeld borstkankerpatiënten. Middels deze techniek kunnen patiënten worden geselecteerd die meer baat hebben bij een andere medicinale behandelstrategie, dan wel een vroege operatie.

Voordat deze techniek wijd verspreid geaccepteerd wordt, zullen grotere multicenter studies moeten uitwijzen of NIR fluorescente beeldvorming kosteneffectief is. De kosten voor het gebruik van ICG zijn laag (+/- 100E per patiënt). Derhalve is nu een groot gedeelte van de kosten het aanschaffen van een NIR camerasysteem. Momenteel worden steeds meer operaties middels minimaal invasieve technieken (bv. laparoscopie en robotchirurgie) verricht. Een groot aantal van de leveranciers van deze apparatuur biedt reeds NIR fluorescente systemen aan. De integratie van NIR fluorescente beeldvorming in reeds beschikbare apparatuur zal de introductie NIR fluorescente beeldvorming dan ook alleen maar versnellen.

De behandeling van kanker ontwikkelt snel, zowel op het gebied van nieuwe operatieve mogelijkheden, als medicamenteuze tumorspecifieke therapieën. Deze ontwikkelingen zullen leiden tot een vermindering van morbiditeit en een verbetering van de overleving van kanker. Het goed kunnen visualiseren van de tumor blijft essentieel om de uitgebreidheid van de tumor en/of het effect van de behandeling

te kunnen beoordelen. Het is ook te verwachten dat NIR fluorescente beeldvorming derhalve een belangrijke bijdrage zal leveren aan de behandeling van kanker.

LIST OF PUBLICATIONS

Boonstra MC, Tolner B, **Schaafsma BE**, Boogerd LS, Prevoo HA, Bhavsar G, Kuppen PJ, Sier CF, Bonsing BA, Frangioni JV, van de Velde CJ, Chester KA, Vahrmeijer AL. Preclinical evaluation of a novel CEA-targeting near-infrared fluorescent tracer delineating colorectal and pancreatic tumors. *Int J Cancer*. 2015 Oct 15;1910-20

Verbeek FP, Tummers QR, Rietbergen DD, Peters AA, **Schaafsma BE**, van de Velde CJ, Frangioni JV, van Leeuwen FW, Gaarenstroom KN, Vahrmeijer AL. Sentinel Lymph Node Biopsy in Vulvar Cancer Using Combined Radioactive and Fluorescence Guidance. *Int J Gynecol Cancer*. 2015 Jul;25(6):1086-93

van den Berg NS, Brouwer OR, **Schaafsma BE**, Mathéron HM, Klop WM, Balm AJ, van Tinteren H, Nieweg OE, van Leeuwen FW, Valdés Olmos RA Multimodal Surgical Guidance during Sentinel Node Biopsy for Melanoma: Combined Gamma Tracing and Fluorescence Imaging of the Sentinel Node through Use of the Hybrid Tracer Indocyanine Green-(99m)Tc-Nanocolloid. *Radiology*. 2015 May;275(2):521-9

Schaafsma BE, van de Giessen M, Charehbili A, Smit VT, Kroep JR, Lelieveldt BP, Liefers GJ, Chan A, Löwik CW, Dijkstra J, van de Velde CJ, Wasser MN, Vahrmeijer AL. Optical mammography using diffuse optical spectroscopy for monitoring tumor response to neoadjuvant chemotherapy in women with locally advanced breast cancer. *Clin Cancer Res*. 2015 Feb 1;21(3):577-84

Schaafsma BE*, Verbeek FP*, Elzevier HW, Tummers QR, van der Vorst JR, Frangioni JV, van de Velde CJ, Pelger RC, Vahrmeijer AL. Optimization of sentinel lymph node mapping in bladder cancer using near-infrared fluorescence imaging. *J Surg Oncol*. 2014 Dec;110(7):845-50

Tummers QR, Verbeek FP, **Schaafsma BE**, Boonstra MC, van der Vorst JR, Liefers GJ, van de Velde CJ, Frangioni JV, Vahrmeijer AL. Real-time intraoperative detection of breast cancer using near-infrared fluorescence imaging and Methylene Blue. *Eur J Surg Oncol*. 2014 Jul;40(7):850-8

Verbeek FP, **Schaafsma BE**, Tummers QR, van der Vorst JR, van der Made WJ, Baeten CI, Bonsing BA, Frangioni JV, van de Velde CJ, Vahrmeijer AL, Swijnenburg RJ. Optimization of near-infrared fluorescence cholangiography for open and laparoscopic surgery. *Surg Endosc*. 2014 Apr;28(4):1076-82

van der Vorst JR*, **Schaafsma BE***, Hutteman M, Verbeek FP, Liefers GJ, Hartgrink HH, Smit VT, Löwik CW, van de Velde CJ, Frangioni JV, Vahrmeijer AL. Near-infrared fluorescence-guided resection of colorectal liver metastases. *Cancer*. 2013 Sep 15;119(18):3411-8

van der Vorst JR, **Schaafsma BE**, Verbeek FP, Swijnenburg RJ, Tummers QR, Hutteman M, Hamming JF, Kievit J, Frangioni JV, van de Velde CJ, Vahrmeijer AL. Intraoperative near-infrared fluorescence imaging of parathyroid adenomas with use of low-dose methylene blue. *Head Neck*. 2014 Jun;36(6):853-8

Schaafsma BE, Verbeek FP, Rietbergen DD, van der Hiel B, van der Vorst JR, Liefers GJ, Frangioni JV, van de Velde CJ, van Leeuwen FW, Vahrmeijer AL. Clinical trial of combined radio- and fluorescence-guided sentinel lymph node biopsy in breast cancer. *Br J Surg*. 2013 Jul;100(8):1037-44

Verbeek FP, van der Vorst JR, **Schaafsma BE**, Swijnenburg RJ, Gaarenstroom KN, Elzevier HW, van de Velde CJ, Frangioni JV, Vahrmeijer AL. Intraoperative near infrared fluorescence guided identification of the ureters using low dose methylene blue: a first in human experience. *J Urol*. 2013 Aug;190(2):574-9

Schaafsma BE*, Verbeek FP*, Peters AA, van der Vorst JR, de Kroon CD, van Poelgeest MI, Trimboos JB, van de Velde CJ, Frangioni JV, Vahrmeijer AL, Gaarenstroom KN. Near-infrared fluorescence sentinel lymph node biopsy in vulvar cancer: a randomised comparison of lymphatic tracers. *BJOG*. 2013 May;120(6):758-64

Schaafsma BE, Verbeek FP, van der Vorst JR, Hutteman M, Kuppen PJ, Frangioni JV, van de Velde CJ, Vahrmeijer AL. Ex vivo sentinel node mapping in colon cancer combining blue dye staining and fluorescence imaging. *J Surg Res*. 2013 Jul;183(1):253-7

van der Vorst JR*, **Schaafsma BE***, Verbeek FP, Swijnenburg RJ, Hutteman M, Liefers GJ, van de Velde CJ, Frangioni JV, Vahrmeijer AL. Dose optimization for near-infrared fluorescence sentinel lymph node mapping in patients with melanoma. *Br J Dermatol*. 2013 Jan;168(1):93-8

van der Vorst JR*, **Schaafsma BE***, Verbeek FP, Keereweer S, Jansen JC, van der Velden LA, Langeveld AP, Hutteman M, Löwik CW, van de Velde CJ, Frangioni JV, Vahrmeijer AL. Near-infrared fluorescence sentinel lymph node mapping of the oral cavity in head and neck cancer patients. *Oral Oncol*. 2013 Jan;49(1):15-9

Schaafsma BE*, van der Vorst JR*, Gaarenstroom KN, Peters AA, Verbeek FP, de Kroon CD, Trimbos JB, van Poelgeest MI, Frangioni JV, van de Velde CJ, Vahrmeijer AL. Randomized comparison of near-infrared fluorescence lymphatic tracers for sentinel lymph node mapping of cervical cancer. *Gynecol Oncol.* 2012 Oct;127(1):126-30

Verbeek FP, van der Vorst JR, **Schaafsma BE**, Hutteman M, Bonsing BA, van Leeuwen FW, Frangioni JV, van de Velde CJ, Swijnenburg RJ, Vahrmeijer AL. Image-guided hepatopancreatobiliary surgery using near-infrared fluorescent light. *J Hepatobiliary Pancreat Sci.* 2012 Nov;19(6):626-37

van der Vorst JR, **Schaafsma BE**, Verbeek FP, Hutteman M, Mieog JS, Lowik CW, Liefers GJ, Frangioni JV, van de Velde CJ, Vahrmeijer AL. Randomized comparison of near-infrared fluorescence imaging using indocyanine green and 99(m) technetium with or without patent blue for the sentinel lymph node procedure in breast cancer patients. *Ann Surg Oncol.* 2012 Dec;19(13):4104-11

van der Vorst JR, Hutteman M, Gaarenstroom KN, Peters AA, Mieog JS, **Schaafsma BE**, Kuppen PJ, Frangioni JV, van de Velde CJ, Vahrmeijer AL. Optimization of near-infrared fluorescent sentinel lymph node mapping in cervical cancer patients. *Int J Gynecol Cancer.* 2011 Nov;21(8):1472-8

Hutteman M, van der Vorst JR, Gaarenstroom KN, Peters AA, Mieog JS, **Schaafsma BE**, Löwik CW, Frangioni JV, van de Velde CJ, Vahrmeijer AL. Optimization of near-infrared fluorescent sentinel lymph node mapping for vulvar cancer. *Am J Obstet Gynecol.* 2012 Jan;206(1):89.e1-5

Schaafsma BE, Image-Guided Surgery, in: *Handboek Colorectaal Carcinoom*, Punt C.J.A. (ed.), De Tijdstroom uitgeverij BV, Utrecht (2011)

Schaafsma BE, Mieog JS, Hutteman M, van der Vorst JR, Kuppen PJ, Löwik CW, Frangioni JV, van de Velde CJ, Vahrmeijer AL. The clinical use of indocyanine green as a near-infrared fluorescent contrast agent for image-guided oncologic surgery. *J Surg Oncol.* 2011 Sep 1;104(3):323-32

Schaafsma BE, Hiemstra E, Dankelman J, Jansen FW. Feedback in laparoscopic skills acquisition: an observational study during a basic skills training course. *Gynecol Surg.* 2009 Nov;6(4):339-343

* shared first authorship

CURRICULUM VITAE

Bob Schaafsma werd geboren op 8 mei 1985 te Leiden. Na het behalen van het vwo-diploma in 2003 aan het Stedelijk Gymnasium Nijmegen startte hij met de studie geneeskunde aan de Universiteit Leiden. Gedurende deze studie was hij tevens actief bij studentenvereniging Minerva en organiseerde hij in 2007 het Medisch Interfacultair Congres. Zijn coassistentenschappen deed hij onder meer bij de afdeling Gynaecologie in het Diaconessenhuis in Paramaribo, Suriname en bij de afdeling Heelkunde in het Tygerberg Hospital in Kaapstad, Zuid Afrika. Voor zijn wetenschapsstage startte hij in 2009 met een onderzoeksproject bij de “Image-Guided Surgery” bij de afdeling Heelkunde onder leiding van Dr. A.L. Vahrmeijer. Na zijn afstuderen in 2010 werd dit onderzoek vervolgd als promotieonderzoek (promotor: Prof. dr. C.J.H. van de Velde, co-promotor Dr. A.L. Vahrmeijer), waarvan de resultaten in dit proefschrift zijn beschreven. In 2013 startte hij bij de afdeling Heelkunde (ANIO) in het Groene Hart Ziekenhuis te Gouda en aansluitend in 2014 bij de afdeling Heelkunde (ANIO) in het St. Elisabeth Hospitaal te Curacao. Hij begon in 2015 met de opleiding tot Chirurg in het Leids Universitair Medisch Centrum onder Prof. dr. J.F. Hamming, waarna hij zijn opleiding nu continueert in het Groene Hart Ziekenhuis onder Dr. R.J. Schmitz.

DANKWOORD

Een proefschrift maak je niet alleen. “There is no I in we” en “nummer één wordt je niet alleen” zijn uitspraken die bijna dagelijks langskwamen de afgelopen jaren. De samenwerking met en steun van collegae, vrienden en familie hebben geleid tot de totstandkoming van dit proefschrift. Daarom wil ik graag iedereen die heeft bijgedragen hartelijk danken!